



## Review

## Uranium removal from environmental water and nuclear waste: Nanomaterial solutions and their environmental sustainability

Ahmed S. Helal<sup>a,b,\*</sup>, Miryana Hémadi<sup>c,\*</sup>, John S. Lomas<sup>c</sup>, Souad Ammar<sup>c</sup>,  
Ali Abdelhafiz<sup>a</sup>, Said M. El-Sheikh<sup>d</sup>, Sheta M. Sheta<sup>e</sup>, Mitchell Galanek<sup>f</sup>,  
Mohamed H. Hassan<sup>g</sup>, Jeng-Kuei Chang<sup>h</sup>, Ju Li<sup>a,\*</sup>

<sup>a</sup> Department of Nuclear Science and Engineering and Department of Materials Science and Engineering, Massachusetts Institute of Technology, 77 Massachusetts Avenue, Cambridge, MA 02139, USA

<sup>b</sup> Nanotechnology and Advanced Materials Laboratory, Nuclear Materials Authority, 3rd settlement 11936, Egypt

<sup>c</sup> Université Paris Cité, ITODYS, CNRS-UMR 7086, F-75013 Paris, France

<sup>d</sup> Nanomaterials and Nanotechnology Department, Central Metallurgical R & D Institute, Cairo 11421, Egypt

<sup>e</sup> Department of Inorganic Chemistry, National Research Centre, 33 El-Behouth Street, Dokki, Giza 12622, Egypt

<sup>f</sup> Office of Environment, Health & Safety, Massachusetts Institute of Technology, Cambridge, MA 02139, USA

<sup>g</sup> Department of Materials Science & Engineering, University of Pennsylvania, Philadelphia, PA 19104, USA

<sup>h</sup> Department of Materials Science and Engineering, National Chiao Tung University, Hsinchu 30010, Taiwan

## A B S T R A C T

The separation and extraction of uranium from mining waste water, contaminated surface water and groundwater, and even from seawater hold significant importance in various applications. Nanomaterial-based extraction methods have been quickly developing and offer a promising means of removing and recovering uranium from a variety of aqueous streams. Nanomaterials possess distinct advantages such as high adsorption capacity, dense active sites, ease of reuse, and excellent selectivity. In this comprehensive review, we conduct an in-depth examination of a wide range of nanomaterials, including carbonaceous, magnetic, functionalized, silicon-based, and metallic oxide/hydroxide nanomaterials, each exhibiting diverse morphologies. Additionally, we offer detailed discussions on mixed oxides and bio-nanocomposites. Carbonaceous nanomaterials demonstrate superior chemical stability in strongly acidic nuclear wastewaters than common inorganic sorbents like hydroxyapatite and hydrous oxides. Furthermore, they are more resilient to radiation and thermal conditions than organic exchange resins. Extraction using recyclable functionalized magnetic nanomaterials offers high selectivity and reduces the complexity of the required equipment. We delve into the challenges and opportunities associated with employing nanomaterials for uranium separation, discussing them in detail. The control of their structures and the stability (chemical, thermal, and mechanical) and toxicity of nanomaterials are important concerns. Finally, we perform an in-depth analysis of the environmental sustainability of nanomaterials. These materials can enter aquatic and terrestrial environments through direct industrial discharges, wastewater effluents, surface runoff, and indirectly via land-applied products like sludges or biosolids. Once in the environment, nanomaterials undergo transformations influenced by their properties and the surrounding medium, involving processes like aggregation, dissolution, and redox reactions.

### 1. Introduction

Finding sustainable energy supplies poses a significant challenge for human development [1–6]. Nuclear energy, as a clean and scalable source, offers a solution to the global energy problem [7,8]. The urgency of addressing global warming has prompted certain countries to develop their nuclear industries [9], thus highlighting the potential for nuclear energy to revolutionize the global energy structure [10–12].

Scientists and Scholars on Nuclear for Climate Change, in their Open Letter to Heads of Governments of G-20 countries [13], emphasize the pressing need for rapid nuclear infrastructure development in the next

20–30 years to meet the demands of our “burning” planet. Presently, there are over 430 nuclear reactors worldwide, generating 400 GWe (Gigawatt Electrical), which accounts for 11 % of global electricity output. By 2040, it is projected that nuclear capacity will reach 516 GWe [14–16]. For instance, China has set ambitious plans to construct 80 nuclear reactors by 2030 and a total of 230 reactors by 2050 [17].

Uranium plays a crucial role in nuclear energy. Fig. 1 illustrates the fluctuation of uranium prices from 1968 to 2020 [18]. In 2007, due to increasing demand, particularly from emerging economies like India and China, uranium reached its highest recorded spot price of \$140 per pound. However, the global economic crisis in 2008 resulted in a

\* Corresponding authors.

E-mail addresses: [ashelal@mit.edu](mailto:ashelal@mit.edu) (A.S. Helal), [hemadi@u-paris.fr](mailto:hemadi@u-paris.fr) (M. Hémadi), [liju@mit.edu](mailto:liju@mit.edu) (J. Li).

<https://doi.org/10.1016/j.cej.2025.160298>

Received 30 December 2024; Received in revised form 3 February 2025; Accepted 3 February 2025

Available online 13 February 2025

1385-8947/© 2025 The Author(s). Published by Elsevier B.V. This is an open access article under the CC BY license (<http://creativecommons.org/licenses/by/4.0/>).

significant drop in uranium prices to below \$50 per pound. In early 2011, as the world economy recovered from the financial crisis, uranium prices experienced a notable increase, reaching \$75 per pound. However, following the Fukushima Daiichi incident in the same year, the shutdown of all 54 Japanese nuclear power plants caused a global collapse in uranium prices. This led to a 13 % reduction in global uranium demand. Moreover, the sale of uranium from offline Japanese nuclear power plants' inventory had a substantial impact on the uranium market, causing prices to plummet from \$75 to \$21 per pound. The COVID-19 pandemic in 2020 further disrupted the uranium supply from mining companies, resulting in a price surge to \$34 per pound, marking the highest price in the past four years.

The International Atomic Energy Agency (IAEA) categorizes uranium resources as conventional and unconventional. Conventional resources refer to those from which uranium is extracted as the primary product, co-product, or significant by-product. Within this category, there are two main types: Reasonably Assured Resources (RAR) and Inferred Resources (IR), which can be recovered at a cost of less than \$260 per kilogram of uranium (kgU). Unconventional uranium resources encompass those from which uranium is recoverable as a minor by-product. The primary unconventional source of uranium resources is phosphate rock, while other sources such as black shale, non-ferrous ore, carbonate, lignite, and seawater are less significant [14].

The Republic of Kazakhstan is the world's leading producer of uranium. In 2015 Kazakhstan produced 23,800 tons of uranium (tU), accounting for 39 % of global uranium production. This surpassed the combined production of the second and third largest uranium producers, Canada and Australia. It is projected that the global annual uranium requirement will increase from 67,000 to 105,000 tU by 2035 [14]. Fig. 2 provides a visual representation of global uranium production and reactor requirements from 1946 to 2015 [19].

The worldwide demand for uranium has exceeded global production from 1990 to 2015. The scarcity of uranium supply necessitates fast and effective solutions to increase production from low-grade ores and unconventional sources like seawater. The nuclear fuel cycle begins with the extraction of uranium from ores and ends with the geological disposal of used fuel or high-level waste (Fig. 3) [20]. During the mining, recovery, and processing of uranium ores, certain amounts of U(VI) are

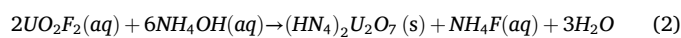
inevitably released into the environment [21–24]. The nuclear incident at Fukushima further heightened concerns regarding the safe disposal of radioactive substances [25]. Therefore, efficient separation and extraction of uranium are crucial for the sustainable utilization of uranium resources and environmental protection [26–30].

Common uranium minerals include carbonates, phosphates, oxides, vanadates, and silicates. Uranium recovery can be achieved by leaching the ore with the addition of an oxidizing agent, sulfuric acid, nitric acid, or sodium carbonate after the ore has been crushed and ground. Following the leaching process, uranium is extracted from the resulting leach liquor using organic extractants like tri-alkylamine, tributylphosphate, or tri-octylphosphine oxide through solvent extraction. In some cases, certain elements may be co-extracted along with uranium, depending on the composition of the leached ore. Consequently, a stripping process is employed to further purify uranium if necessary and facilitate the recyclability of the extractant. Stripping can be easily accomplished by contacting the uranium-loaded organic phase with a dilute nitric acid or a mixture of ammonium hydroxide and ammonium carbonate. Recovery of uranium from phosphate ores typically involves a multi-step solvent extraction process due to the high concentration of interfering metal ions such as iron, aluminum, calcium, and magnesium [31].

The extracted precursor undergoes additional processing to convert it into  $U_3O_8$ . Oxidation of  $U_3O_8$  is necessary before it can be converted to the fluoride species  $UF_6$ , enabling the isotope enrichment process. After enrichment, the enriched uranium stream is sent for fuel fabrication. To prepare the fuel, the enriched  $UF_6$  is first hydrolyzed according to the following reaction:



followed by ammonia precipitation process,



The ammonium-diuranate product obtained is further processed through reduction to convert it into  $UO_2$ . This reduction process is performed at a temperature of 1700 °C in a dry  $H_2$  atmosphere. The resulting  $UO_2$  compound is pressed and sintered to form a ceramic

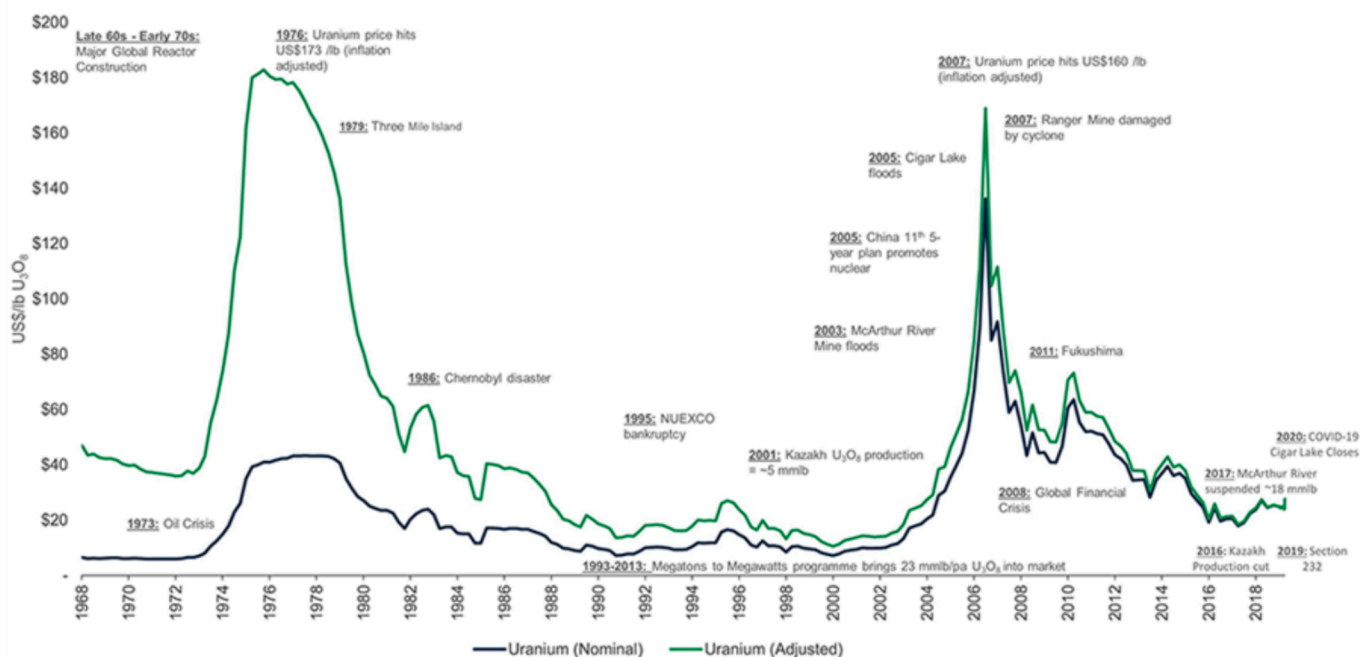


Fig. 1. Uranium price chart from 1968 to 2020 (Reprinted with permission from [18]).

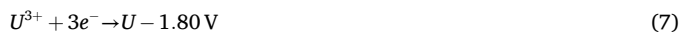
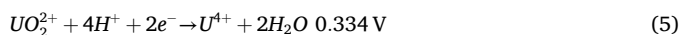


environments. Pentavalent uranium (U(V)) is highly sensitive to water and air, easily converting to U(VI) in the presence of trace amounts of water or oxygen. Unstable oxidation states can occur as transient species generated in solution by pulsed radiolysis [40]. In addition, they can achieve high stability in strong uranium coordination compounds due to geometrical structural constraints [41]. The chemistry of uranium extraction and recovery is highly complex, involving various aspects of fundamental physical and inorganic chemistry, such as complexation, hydrolysis, acid-base equilibria, and the type of ligands involved. In the following sections, we will provide a brief overview of the key factors that control uranium separation.

### 2.1. Acid-base equilibria, Complexation, and the type of ligands

The oxidation states of uranium in aqueous solutions can range from 2+ to 6+, but only the 4+ and 6+ oxidation states are stable in this environment. Uranyl ions,  $UO_2^{2+}$ , tend to coordinate with strong ligands in the plane orthogonal to the O=U=O axis. The potentials for the interconversion between different oxidation states of uranium in acidic and basic aqueous solutions can be represented by the following equations [42]:

In acidic solutions:



In basic solutions:



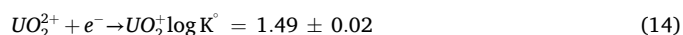
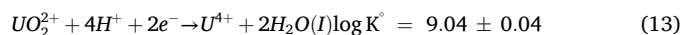
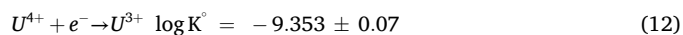
In environmental water, uranium has a strong tendency to react with various anions such as  $NO_3^-$ ,  $Cl^-$ ,  $CO_3^{2-}$ , and  $SO_4^{2-}$  to form various complexes [43]. The specific complexes formed by uranium depend on the pH of the solution. Here are some examples of uranium complexes at different pH values. At pH  $\leq 4.5$ , uranium can exist as  $UO_2^{2+}$ ,  $(UO_2)_2(OH)^{2+}$ , or  $(UO_2)_3(OH)^{5+}$  [44]. At pH 6,  $UO_2(OH)_2$  is formed. In the pH range of 6.5–7.5, the predominant species is the polynuclear complex  $(UO_2)_2CO_3(OH)^{3-}$ . In natural water containing dissolved  $CO_2$ , carbonate complexes play a significant role in uranium speciation. The triscarbonato complex ion  $(UO_2(CO_3)_3)^{4-}$  is the dominant species. At pH 7.1, the most abundant uranium species is  $(UO_2(CO_3)_3)^{2-}$ . In seawater with a pH  $\geq 8$ , uranium primarily exists as  $(UO_2(CO_3)_3)^{4-}$ ,  $(CaUO_2(CO_3)_3)^{2-}$ , and  $Mg(UO_2(CO_3)_3)^{2-}$  [45]. Carbonate complexes may compete with ligands or functional groups utilized for uranyl ion binding. This competition can influence the selectivity of the separation process, potentially resulting in fluctuations in uranium recovery efficiency. Competitive binding may not only reduce uranium uptake and diminish separation efficiency but also prolong extraction times or decrease throughput in industrial-scale operations. Selectivity plays a crucial role in the extraction of uranium from various sources such as mining solutions, contaminated groundwater, radioactive waste, and seawater. Each medium presents its own challenges from specific interfering metal ions and environmental conditions. For uranium extraction from mining solutions, the liquor can be highly acidic or

alkaline, and there may be interfering metal ions like  $Fe^{3+}$ ,  $Cu^{2+}$ ,  $Ni^{2+}$ , and  $Co^{2+}$ . On the other hand, seawater has a pH of around 8, and the main interfering ions are  $Na^+$ ,  $K^+$ ,  $Ca^{2+}$ ,  $Mg^{2+}$ ,  $Cl^-$ , and  $CO_3^{2-}$ . To achieve selective extraction, different ligands can be used, including those with oxime, ether, and phosphoryl functional groups, and diethylenetriamine pentaacetate (DTPA) [46]. The chemical speciation of uranyl ions, medium pH, and interfering metal ions greatly influence the rate of complex formation and the thermodynamic stability of the uranium complexes. In the case of uranium extraction using the glutarimide-dioxime ligand under seawater conditions, the reaction mechanism for the formation of U(VI)-glutarimide-dioxime complexes is complicated by the fact that the carbonate concentration and acidity cannot be changed independently. The effect of carbonate concentration on the formation of U(VI)-glutarimide-dioxime complexes is not straightforward and exhibits non-linear behavior. The rate of formation and the thermodynamic equilibrium of these complexes depend not only on the concentrations of uranyl ion and of the glutarimide-dioxime ligand but also on the carbonate concentration and those of other interfering metal ions [47]. To fabricate a highly selective material for uranium extraction, it is essential to have a comprehensive understanding of the behavior of uranium and ligands under specific environmental conditions. The selectivity for uranium over other ions is a critical factor in achieving efficient separation [48,49]. Direct ligand design can address the limitations of traditional ligands and sorbents. In this approach, ligands are designed with selective binding pockets containing soft donor atoms that can form thermodynamically favorable and stable geometrical structures with uranium. However, these ligands can be elaborate, expensive, and unsuitable for large-scale synthesis and applications [50].

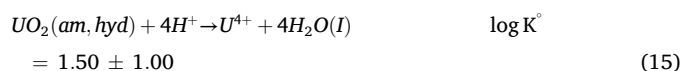
### 2.2. Hydrolytic, thermodynamic, and kinetics studies

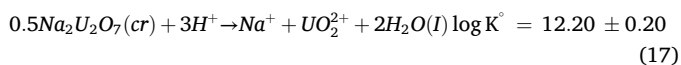
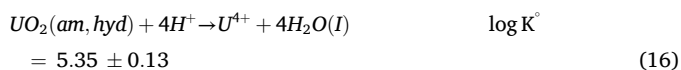
The migration and mobility of uranium in deep geological repositories or environmental water are influenced by factors such as its chemical speciation, solubility, and adsorption behavior. The oxidation state of uranium is particularly important as it directly affects these phenomena. Uranium exhibits diverse chemical behaviors in different oxidation states, making its hydrolytic behavior and coordination chemistry more complex and intricate than that of other elements. Under normal conditions, U(V) and U(VI) species exist as substitution-inert linear dioxocations, where coordination chemistry with secondary ligands is primarily restricted to the equatorial region. Uranium hexafluoride ( $UF_6$ ) is a solid at room temperature but easily sublimates at slightly higher temperatures.  $UF_6$  is utilized in isotope separation processes to enrich the  $^{235}U$  content for reactor fuel element production. U(IV) and U(VI) cations are moderately hydrated and strongly hydrolyzed, forming strong complexes with various chelating agents [32,51]. The equilibrium constants ( $\log K^\circ$ ) for  $U^{4+}$  and  $U^{6+}$  redox, solubility, and hydrolysis reactions are summarized in the following equations. These equations, with the equilibrium constants, provide an accurate view of non-specific redox processes for the boundary line of the U(VI)/U(IV) couple under alkaline conditions [52–55].

$U^{4+}$  and  $U^{6+}$  redox reactions

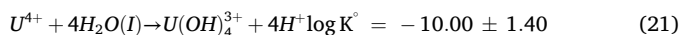
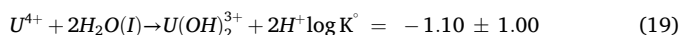
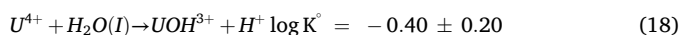


$U^{4+}$  and  $U^{6+}$  solubility reactions

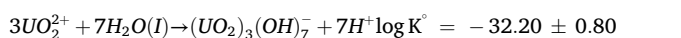
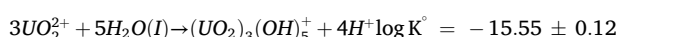
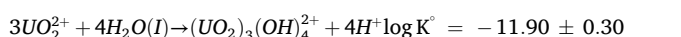
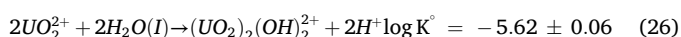
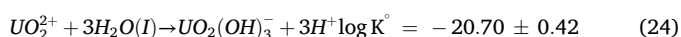
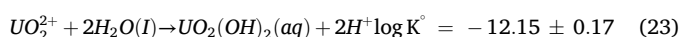




$U^{4+}$  hydrolysis reactions



$U^{6+}$  hydrolysis reactions



Nanoscale materials have become extremely important, having a significant impact in many scientific fields, including medicine, biology, electronics, materials science, and chemistry [56–60]. They are often very good for extracting metal ions at low concentrations. In addition, their morphologies and structures can be tuned to meet the requirements of a given application [61–64]. The utilization of nanomaterials for environmental remediation and radioactive waste management has attracted significant interest within the scientific community due to their unique physical and chemical characteristics [61,65–68]. Compared to traditional bulk materials, nanomaterials offer several advantages, such as high surface area, more active sites, high selectivity, high adsorption capacity, and fast adsorption of metals from water and waste effluents. The physical and chemical properties of the nanomaterial surfaces are the major factors that control the adsorption process. Engineering the surface of nanomaterials through grafting target ligands or functional groups to the surface can prevent agglomeration, enhance selectivity even in the presence of high concentrations of interfering metal ions, and increase their stability in harsh chemical environments [69–78]. Consequently, extraction by nanomaterials is the most promising technique for radionuclide- and heavy metal-contaminated water treatment technology.

This review focuses on the separation and extraction of uranium from various sources, including mining waste, contaminated water, and even seawater, using nanomaterials. Nanomaterials suitable for uranium extraction are reviewed in detail. The maximum adsorption capacities, based on the Langmuir isotherm ( $q_{max}$ ), of these materials are compared [69–78], and their extraction mechanisms are briefly summarized. Finally, research progress is summarized and future directions for

uranium separation technology are outlined.

### 3. Classification of Nanomaterials as Uranium Nano-adsorbents

Nanomaterials as uranium nano-adsorbents are classified based on their physical and chemical characteristics: carbonaceous, magnetic, functionalized, silicon-based, metallic oxide/hydroxide, nanostructured mixed oxide nanomaterials and bio-nanocomposites (Fig. 4).

#### 3.1. Carbonaceous nanomaterials

Carbonaceous nanomaterials combine the typical features of  $sp^2$ -hybridized carbon bonds with excellent mechanical, physical, and chemical properties. They have unusual properties that make them very attractive for applications in many fields, including medicine, micro/nano-electronics, molecular electronics, catalysis, and hydrogen power engineering. In the context of U extraction, mainly two categories of carbon nanostructures are used, namely carbon nanotubes (CNTs) and graphene nanosheets.

#### 3.2. Carbon nanotubes (CNTs)

CNTs were first disclosed in 1991 by Iijima [79]. They can be considered as cylindrical hollow microcrystals of graphene and are in one of two forms: single-walled SWCNTs or multi-walled CNTs (MWCNTs). CNT lengths range from 100 nm to 10  $\mu$ m. The CNT diameter depends on its number of layers (e.g. SWCNTs: 1–3 nm; MWCNTs: 5 to 100–200 nm) [80]. They have remarkable electronic properties, pore structures, specific surface areas, chemical stability, and mechanical characteristics. MWCNTs have been widely applied in many fields as catalyst supports, quantum nanowires, chemical sensors, electron field emitters, and hydrogen storage [81,82]. They have recently been applied as adsorbents for uranium [83–90].

Schierz and Zanker [83] studied the colloidal stability of CNTs, which affects their capacity to recover uranium. Treating CNTs with acid introduces defects and/or adds functional groups to the surface [87], which improves their colloidal stability and increases their adsorption capacity. Oxidation of MWCNTs opens the ends of the tubes, providing suitable openings for metal impregnation [91]. Sun et al. [85] used

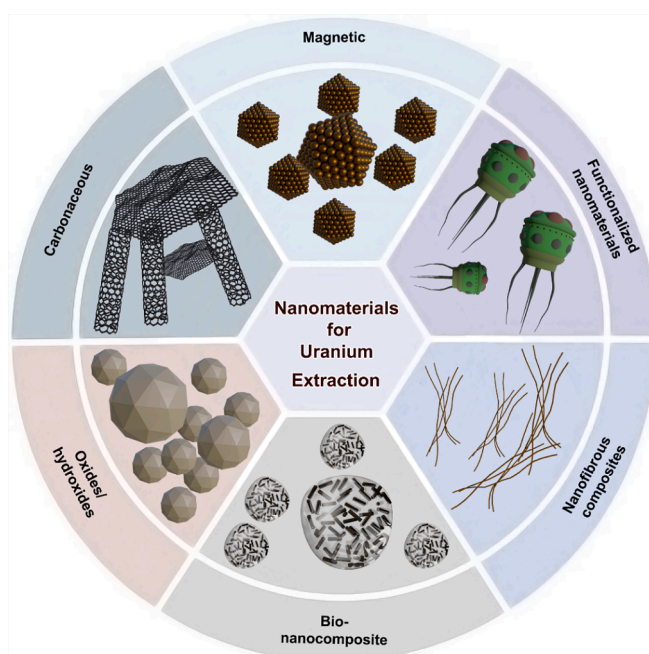


Fig. 4. Classification of nanomaterials as uranium nano-adsorbents.

oxidized MWCNTs for the recovery of U(VI) from an aqueous solution. The U(VI) extraction profile depends markedly on ionic strength and pH; a  $q_{\max}$  of  $33 \text{ mgU}\cdot\text{g}^{-1}$  was obtained. Fasfous and Dawoud [92] reported that the  $q_{\max}$  for U(VI) on MWCNTs increases with temperature (25 and  $39 \text{ mgU}\cdot\text{g}^{-1}$  at 25 and  $45^\circ\text{C}$ , respectively). The equilibrium between U(VI) and MWCNTs was achieved in 1 h with the removal of 69 % of the uranium. Zong and Gou [93] synthesized a magnetic iron oxide ( $\text{Fe}_3\text{O}_4$ )/MWCNT composite that was used for the preconcentration of U(VI) from a solution at pH 7, with a  $q_{\max}$  of  $24 \text{ mgU}\cdot\text{g}^{-1}$ . Zolfonoun and Yousefi [94] investigated an MWCNT- $\text{Fe}_3\text{O}_4$  nanocomposite as an adsorbent for the solid-phase extraction and preconcentration of uranium. Due to the high surface area of MWCNTs, a satisfactory concentration factor was achieved within 5 min. ( $q_{\max} = 36 \text{ mgU}\cdot\text{g}^{-1}$ ). Tan et al. [95] prepared a cobalt ferrite ( $\text{CoFe}_2\text{O}_4$ )/MWCNT composite for U(VI) extraction from an aqueous solution. The uranium adsorption capacity of  $\text{CoFe}_2\text{O}_4$ , MWCNTs, and  $\text{CoFe}_2\text{O}_4$ /MWCNTs as a function of pH is presented in Fig. 5a. The results confirmed that the uranium extraction process is pH-dependent, with a  $q_{\max}$  of  $213 \text{ mgU}\cdot\text{g}^{-1}$  as calculated from the Langmuir isotherm (Fig. 5b). The adsorption process was complete in 6 h and was an endothermic spontaneous reaction. Zare et al. [96] reported that the loading of silver hydroxide AgOH NPs onto MWCNTs provides a highly effective uranium adsorbent. Adsorption and mass transfer of uranium are enhanced by ultrasound. The AgOHNP/MWCNT composite is appropriate for the quantitative and qualitative recovery of  $\text{UO}_2^{2+}$  because it has a large surface area. The adsorption of the  $\text{UO}_2^{2+}$  ions followed a second-order rate equation combined with an intraparticle diffusion model. The obtained adsorption results are in good agreement with the Langmuir model, with a  $q_{\max}$  of  $234 \text{ mgU}\cdot\text{g}^{-1}$ .

### 3.2.1. Graphene oxide nanosheets

Graphene consists of a  $\text{sp}^2$ -bonded carbon layer that is only one atom thick. Its electrical properties were first reported in 2004 [97]. Graphene has attracted much interest due to its unique two-dimensional structure and exceptional physicochemical properties, such as excellent thermal conductivity, mechanical strength/weight ratio, and specific surface area ( $2620 \text{ m}^2\cdot\text{g}^{-1}$ ) [98,99]. Graphene oxide (GO) has a high surface area with an abundance of surface functional groups (e.g. hydroxyls, carboxyls, and epoxides) and a lower density than other inexpensive substances such as clays and oxides [100–102].

Li et al. [99] used GO nanosheets to extract uranium from aqueous solutions. The adsorption process was pH-dependent ( $q_{\max}$  at pH 4 =  $299 \text{ mgU}\cdot\text{g}^{-1}$ ) and ionic strength-independent, which indicates that inner-sphere complexes of uranium formed on the GO. Xinquan et al. [103] obtained a  $q_{\max}$  of  $139 \text{ mgU}\cdot\text{g}^{-1}$  for few-layered GO nanosheets. Zhao et al. [104] used a similar material ( $q_{\max} = 98 \text{ mgU}\cdot\text{g}^{-1}$ ) for the elimination of U(VI) ions from wastewater. Cheng et al. reported a  $q_{\max}$  of 161

$\text{mgU}\cdot\text{g}^{-1}$  for a GO-supported sepiolite composite [105]. Tan et al. [10] synthesized Layered Double Hydroxide (LDH)/GO hierarchical three-dimensional composites via the *in-situ* development of LDH nanosheet arrays on graphene. SEM and TEM characterizations of the synthesized LDH/GO are displayed in Fig. 6a,b. The uranium adsorption process follows a second-order rate equation (Fig. 6c) with a  $q_{\max}$  for U(VI) of  $278 \text{ mgU}\cdot\text{g}^{-1}$  (Fig. 6d). Gu et al. [106] combined GO and CNTs. The adsorption process fits well with the Langmuir isotherm ( $q_{\max} = 86 \text{ mgU}\cdot\text{g}^{-1}$ ) and a second-order rate equation.

The application of carbonaceous nanomaterials for uranium extraction does face certain challenges. One major drawback is the expensive and multistep fabrication methods required to produce these nanomaterials on a semi-pilot or pilot scale, resulting in low efficiency. Additionally, carbonaceous nanomaterials tend to agglomerate in aqueous media, leading to a decrease in the number of active sites available for adsorption, which reduces their adsorption capacity [107]. While many studies have been conducted under laboratory conditions, it is important to examine the performance of these materials using real contaminated water samples to assess their practical applicability. To overcome these challenges, it is necessary to develop economical and environmentally friendly synthesis methods for carbonaceous nanomaterials. Furthermore, surface functionalization techniques and the combination of these materials with other nanocomposites, particularly magnetic ones, should be explored to enhance their adsorption capabilities. These aspects will be discussed in more detail in the following sections. A summary of the maximum adsorption capacities ( $q_{\max}$ ) of carbonaceous nanomaterials is given in Table 2.

### 3.3. Magnetic nanomaterials

Magnetic sedimentation techniques offer a fast and effective approach for the separation of nanoparticles (NPs). The solid-liquid separation process under an applied magnetic field is simple and eliminates the need for additional centrifugation or filtration steps. Magnetic nanocomposites have been widely investigated as adsorbents for radionuclides, demonstrating good adsorption efficiency and selectivity [108–115].

Studies have explored the adsorption properties of magnetite  $\text{Fe}_3\text{O}_4$  NPs for U(VI), although the adsorption capacity was relatively small [116]. Silica-coated magnetite nanoparticles had a higher adsorption capacity with a  $q_{\max}$  of  $52 \text{ mgU}\cdot\text{g}^{-1}$  [117].  $\text{CoFe}_2\text{O}_4$  hollow spheres showed promise for U(VI) removal with a  $q_{\max}$  of  $170 \text{ mgU}\cdot\text{g}^{-1}$  at  $25^\circ\text{C}$ , reaching equilibrium in 3 h [118]. Engineered magnetic nanocomposites, such as  $\text{Fe}_3\text{O}_4$ @C/LDH,  $\text{Fe}_3\text{O}_4$ @C@Ni-Al LDH, and  $\text{Fe}_3\text{O}_4$ @C, have been synthesized for the magnetic separation of uranium [119]. Carbon-coated iron nanoparticles ( $\text{Fe}_3\text{O}_4$ @C) were

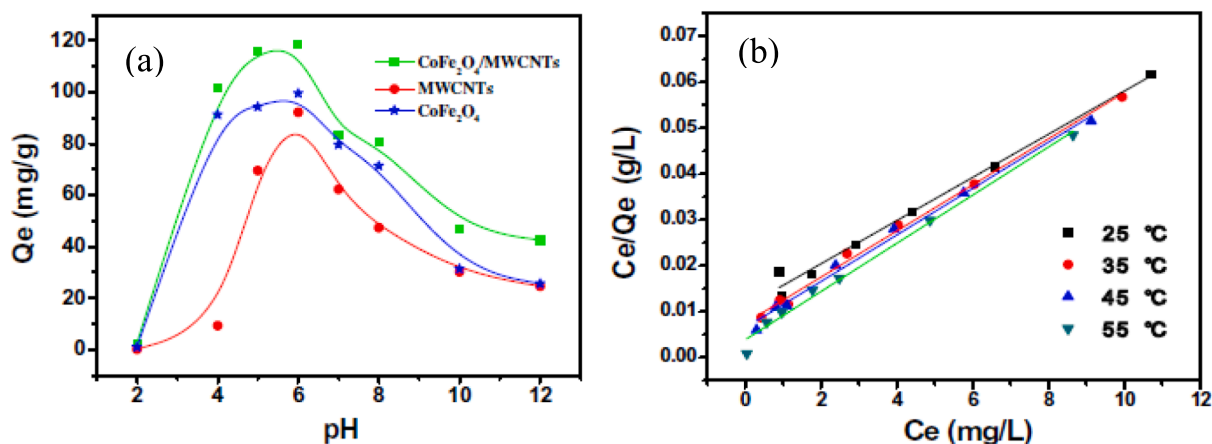


Fig. 5. (a) Effect of initial pH on adsorption properties of  $\text{CoFe}_2\text{O}_4$ , MWCNTs and  $\text{CoFe}_2\text{O}_4$ /MWCNTs. (b) Langmuir isotherm for the removal of U(VI) by  $\text{CoFe}_2\text{O}_4$ /MWCNTs (Reprinted with permission from ref. [95]. Copyright 2015, Elsevier).

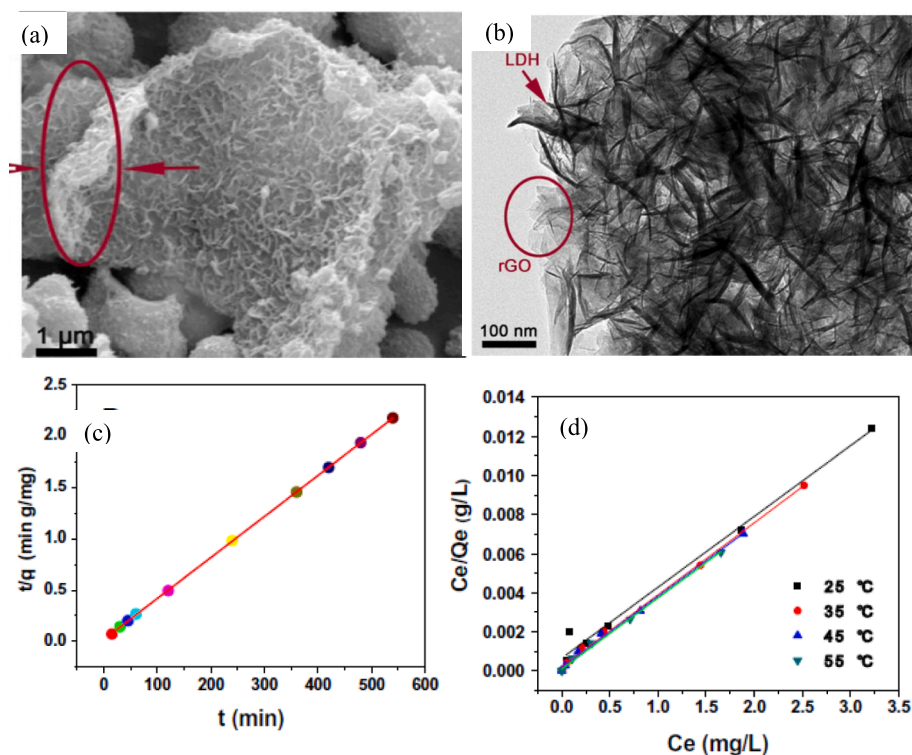


Fig. 6. (a) SEM images of GO/LDH composite. (b) TEM images of the GO/LDH composite. (c) Pseudo-second-order plot for the removal of U(VI) by GO/LDH. (d) Langmuir isotherm for the removal of U(VI) by GO/LDH (Reprinted with permission from ref. [10]. Copyright 2015, Elsevier).

Table 2

Adsorption capacities of carbonaceous nanomaterials.

Carbonaceous nanomaterial	Maximum adsorption capacity (mgU·g <sup>-1</sup> )	Reference
Pristine CNTs	4.3	[83]
Pristine CNTs treated with conc. HNO <sub>3</sub> and H <sub>2</sub> SO <sub>4</sub>	45.9	[83]
Untreated MWCNTs	14.3	[84]
MWCNTs-carboxymethyl cellulose	111.9	[84]
Oxidized MWCNTs	33.3	[85]
Oxidized MWCNTs	17.5	[87]
Plasma-functionalized MWCNTs	96.6	[88]
Untreated MWCNTs	39.2	[92]
Carbon NT/iron oxide composite	26.2	[93]
CoFe <sub>2</sub> O <sub>4</sub> /MWCNTs	212.7	[95]
AgOH-MWCNT NPs	234.0	[96]
GO nanosheet	299.0	[99]
GO nanosheet	330.8	[103]
GO nanosheet	97.2	[104]
GO@sepiolite	161.3	[105]
LDH@GO	227.8	[10]
GO-CNTs	86.1	[106]

combined with nanosheets of Ni-Al LDH using an *in-situ* growth method, resulting in a composite with a  $q_{\max}$  of 174 mgU·g<sup>-1</sup>. The adsorption process was rapid and followed pseudo-second-order kinetics [120,121]. Other composites, such as Fe<sub>3</sub>O<sub>4</sub>@GO ( $q_{\max}$  = 70 mgU·g<sup>-1</sup>) [121] and MnO<sub>2</sub>-Fe<sub>3</sub>O<sub>4</sub>-GO ( $q_{\max}$  = 109 mgU·g<sup>-1</sup>) [122], are also effective uranium adsorbents [121,122]. Additionally, U(VI)-loaded MnO<sub>2</sub>-Fe<sub>3</sub>O<sub>4</sub>-GO composites showed efficient regeneration capabilities.

Zerivalent Iron (ZVI) NPs have been extensively utilized for uranium extraction due to their high surface area and numerous active sites [123–127]. ZVI NPs can be injected directly into contaminated sediments and aquifers [128], benefitting from their colloidal size and easy diffusion through porous media [129–133]. However, remobilization of contaminants poses a technical challenge, as incomplete chemical

reduction and certain conditions can lead to re-release of uranium [87–90]. Efforts have been made to address this challenge and improve the stability of uranium immobilization on ZVI NPs. Crane et al. [134] evaluated the removal of uranium from dissolved oxygen-bearing groundwater, which contained high concentrations of dissolved bicarbonate (>500 mg·L<sup>-1</sup>). ZVI NPs were initially effective, more than 98 % of uranium being removed in 2 h. However, over longer periods (>7 days), more than 50 % of the uranium was re-released due to incomplete chemical reduction. The uranium is leached again at the same time as dissolved oxygen re-enters, and highly stable aqueous uranium complexes are subsequently reformed. In roughly neutral solutions, near-total chemical reduction of UO<sub>3</sub> to UO<sub>2</sub> can be achieved on the surface of ZVI NPs [135], whereas reduction is quenched in solutions containing carbonates [123,134]. Dickinson and Scott [136] used ZVI NPs as highly efficient remediators of uranium-containing waste effluent. Uranium was removed from the solution to <1.5 % of its initial concentration in both oxic and anoxic systems within the first hour of the reaction and remained stable on the surface of the ZVI NPs for 48 h. Uranium uptake is a coupled Fe-U redox reaction, as demonstrated by X-ray photoelectron spectroscopy analysis. ZVI NPs are very good materials for the permeable reactive barrier technique for remediating uranium-contaminated subsurfaces. Fig. 7 clarifies the uranium extraction mechanism by Fe/RGO composites at environmental water conditions. The rapid reductive precipitation of U(VI) to the sparingly soluble U(IV) species is responsible for uranium immobilization [137]. Solutions containing U(VI) (24 ppm) can be cleaned up completely using ZVI NPs, despite the presence of sodium bicarbonate, humic acid, and other groundwater constituents at pH 5–9. Up to an initial U concentration (C<sub>0</sub>) of 643 ppm, 100 % of the uranium was removed. A  $q_{\max}$  of 8170 mgU·g<sup>-1</sup> was obtained for ZVI NPs at a C<sub>0</sub> of 714 ppm.

The reductive removal of U(VI) by ZVI NPs can be significantly improved by using Na-bent (Na<sup>+</sup>-saturated bentonite) as a support material (Fig. 8). The presence of Na-bent enhances the removal efficiency of cationic U(VI) to a remarkable extent, with 99 % of the uranium removed. This value is higher than for ZVI NPs alone (48 %) or ZVI

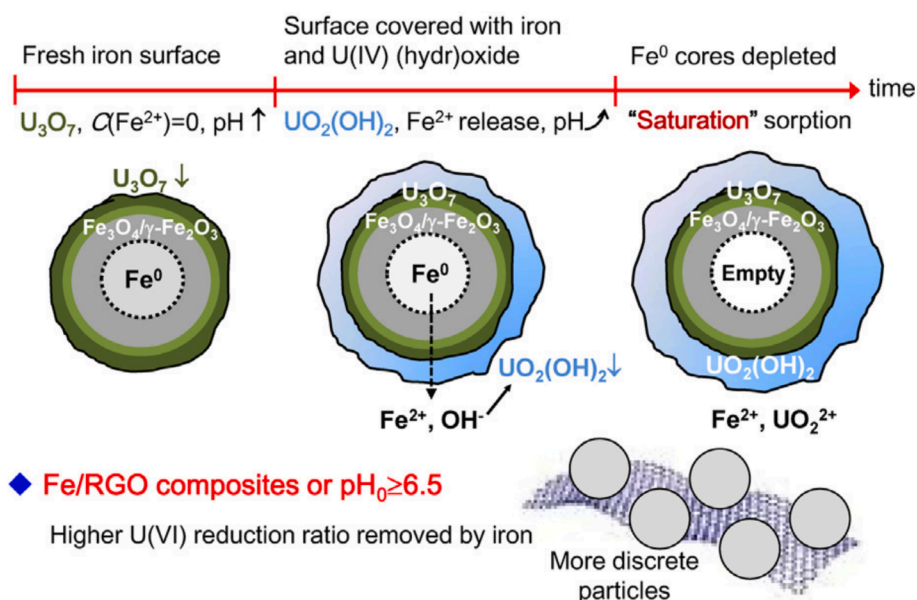


Fig. 7. Uranium separation strategy using ZVI-NPs and graphene composite (Reprinted with permission from ref. [137]. Copyright 2015, Elsevier).

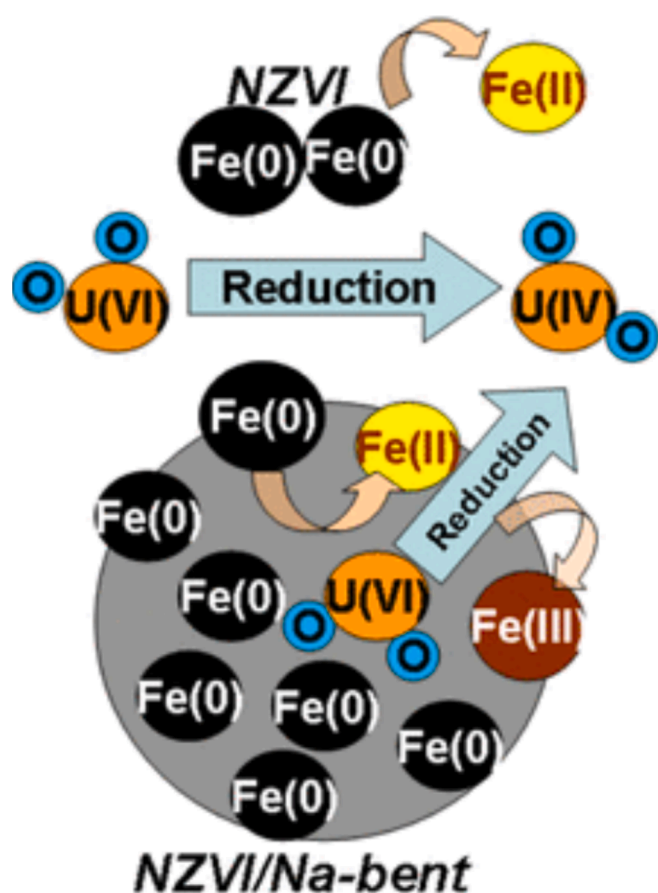


Fig. 8. Uranium separation strategy using ZVI-NPs supported on Na – bent (Reprinted with permission from ref. [138]. Copyright 2014, American Chemical Society).

NPs supported on positively charged bentonite (Al-bent) [138]. The utilization of Na-bent as a support material offers several advantages. Firstly, it enhances the reactivity and reusability of ZVI NPs. Secondly, it acts as a pH buffer, keeping the pH range optimal for U(VI) removal.

This buffering effect is essential to maintaining the efficiency of U(VI) removal by ZVI NPs. Thirdly, Na-bent facilitates the mass transfer of U(VI) from the solution to the surface of the nanoparticles. This improved mass transfer enhances the contact between U(VI) ions and ZVI NPs, leading to increased efficiency in U(VI) removal. Finally, it may also play a role in moving insoluble reduction products away from the surface of the nanoparticles, preventing their accumulation and potential interference with the removal process. Overall, the use of Na-bent as a support material for ZVI NPs provides multiple benefits, including enhanced removal efficiency, improved reusability, pH buffering, and facilitated mass transfer, making it a promising material for the reductive removal of U(VI).

Ling and Zhang [139] synthesized a unique structure using ZVI NPs, enabling quick separation and encapsulation of small amounts of uranium from water. The STEM-XEDS elemental mapping of Fe, U, and O for uranium extraction by Fe<sub>2</sub>O<sub>3</sub> and ZVI NPs is shown in Fig. 9. After 1 h of the uranium extraction experiment using ZVI NPs, the iron signal near the surface was significantly decreased (Fig. 9b), while oxygen was widely distributed (Fig. 9c). Uranium was found to be very well dispersed inside the nanoparticle (Fig. 9d,e). After 24 h, uranium accumulated at the center of the nanoparticle (Fig. 9i,j). In contrast, for the extraction experiment using Fe<sub>2</sub>O<sub>3</sub>, uranium was concentrated on the outer surface (Fig. 9k-o). This provided evidence that U(VI) is reduced to UO<sub>2</sub> and deposited in the core of ZVI NPs. Moreover, over 90 % of the uranium was recovered in less than 2 min. with a concentration of 1 g·L<sup>-1</sup> of ZVI NPs.

Magnetic nanocomposites are considered a viable option for the simple and effective separation of uranium from contaminated solutions. However, they tend to aggregate due to van der Waals forces and magnetic dipolar forces, which reduce the number of active sites and, consequently, the uranium adsorption capacity and selectivity. Additionally, small magnetic nanocomposites (less than 12 nm) require a strong magnetic field for effective separation. To overcome these challenges, the development of surface coatings for these composites is necessary. The adsorption capacities of uranium by magnetic nanomaterials are summarized (Table 3).

#### 3.4. Nanostructured oxides, hydroxides, and mixed composites

Titanium dioxide (TiO<sub>2</sub>) is a commonly used substrate in the treatment of various environmental contaminants. Different forms of TiO<sub>2</sub>

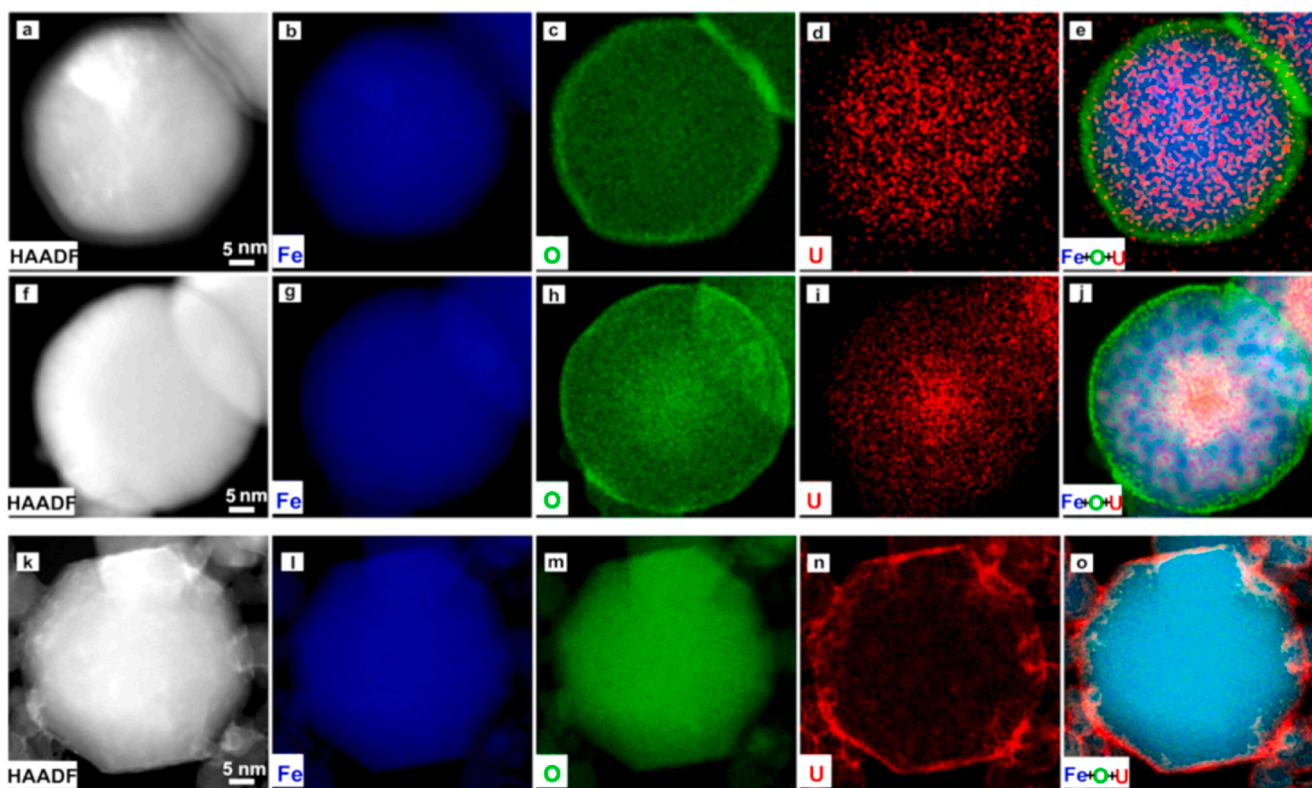


**Fig. 9.** STEM XEDS mapping of uranium reactions with hematite ( $\text{Fe}_2\text{O}_3$ ) and ZVI-NPs: (a – e) after 1 h with ZVI-NPs; (f – j) after 24 h; (k – o) after 24 h with hematite. (a,f,k) HAADF images; (b,g,l) Fe mapping; (c,h,m) O mapping; (d,i,n) U mapping; (e,j,o) Fe + O + U color overlays (Reprinted with permission from ref. [139] Copyright 2015, American Chemical Society).

**Table 3**

Adsorption capacities for uranium on magnetic nanomaterials.

Magnetic nanomaterial	Maximum Adsorption capacity ( $\text{mgU}\cdot\text{g}^{-1}$ )	Reference
Attapulgite/iron oxide	11.6	[110]
Arsenazo-III-modified maghemite NPs	285	[111]
Maghemite NPs	20.3	[112]
Magnetite NPs	3.8	[116]
$\text{Fe}_3\text{O}_4/\text{SiO}_2$ composite	52	[117]
$\text{CoFe}_2\text{O}_4$ hollow spheres	170.1	[118]
$\text{Fe}_3\text{O}_4/\text{C@LDH}$ composite	174.1	[120]
$\text{Fe}_3\text{O}_4/\text{GO}$	69.5	[121]
$\text{MnO}_2\text{-Fe}_3\text{O}_4\text{-GO}$	108.7	[122]
ZVI NPs and graphene composite	8173	[137]
ZVI NPs	2400	[139]

have been studied for their adsorption properties, but some parameters of these materials remain unexplored. Comarmond et al. [140] studied uranium adsorption on well-characterized  $\text{TiO}_2$  surfaces, focusing on parameters such as surface charge, surface area, and impurities. The differences in adsorption properties were primarily related to the morphology, crystallographic form, grain size, and surface area of  $\text{TiO}_2$ , rather than to surface charge or impurities. The crystal structure of  $\text{TiO}_2$  nanoparticles played a crucial role in determining uranium uptake. The study also revealed that samples consisting of a mixture of anatase and rutile phases of  $\text{TiO}_2$ , with varying percentages (composite = anatase<sub>(100-x)</sub> + rutile<sub>(x)</sub>), exhibited different uranium uptake behaviors. Increasing the fraction of anatase to rutile enhanced uranium uptake, at the same pH (Fig. 10). This enhancement can be attributed to the higher activity of anatase, which has a more open crystal structure than rutile (with corner-sharing and edge-sharing structures, respectively).

Nano-sized alumina, which is highly resistant to pH changes and

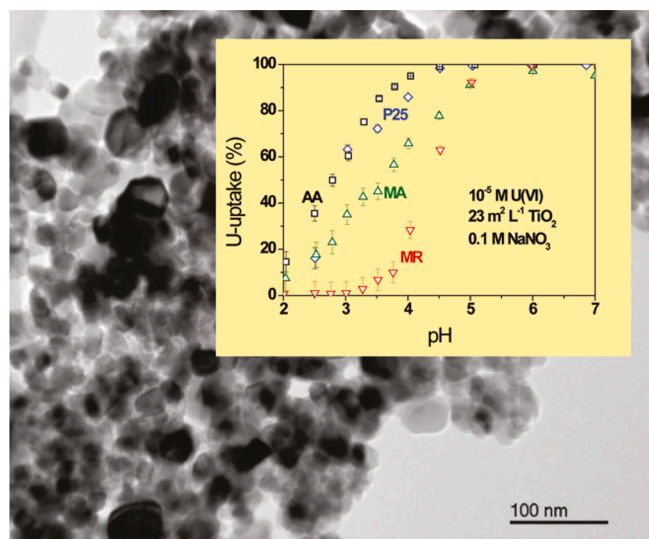


**Fig. 10.** Uptake of uranium by different  $\text{TiO}_2$  materials (P25: 86% anatase, 14% rutile; AA: 91% anatase, 9% rutile; MA: 100% anatase; MR: 99% rutile, 1% anatase) (Reprinted with permission from ref. [140]. Copyright 2011, American Chemical Society).

swelling when placed in organic solvents, has been applied for the separation and extraction of uranium [141,142]. Qian et al. [143] compared the adsorption and desorption behavior of uranium on nano-alumina and nano-goethite in aqueous solution. The maximum adsorption capacities ( $q_{\text{max}}$ ) were found to be  $151 \text{ mgU}\cdot\text{g}^{-1}$  for nano-alumina and  $79 \text{ mgU}\cdot\text{g}^{-1}$  for nano-goethite. Batch desorption experiments indicated that uranium bound more strongly to NPs than to other particles.

This observation aligns with surface complexation modeling, which assumes the presence of strong and weak adsorption sites on NPs, while only weak sites are present on  $\alpha$ -alumina and  $\alpha$ -FeO(OH). The high adsorption capacity and porosity of nano-sized alumina can be attributed to its low temperature sensitivity, excellent mechanical strength, high surface area, high surface reactivity, and absence of internal diffusion resistance. These factors contribute to the efficient extraction and separation of uranium [56]. Magnesium nanomaterials, specifically nano-magnesium hydroxide, ( $\text{Mg}(\text{OH})_2$ ), are another class of adsorbents with favorable properties for uranium adsorption.  $\text{Mg}(\text{OH})_2$  is environmentally friendly, non-toxic, and cost-effective [144]. It has a higher adsorption capacity for uranyl ions ( $\text{UO}_2^{2+}$ ) than many other adsorbents. Adsorption on the nano- $\text{Mg}(\text{OH})_2$  surface follows the Langmuir isotherm, where traces of uranyl ion form a monolayer on the surface [63,145]. As the uranyl ion concentration exceeds a certain threshold, the adsorption capacity continues to increase, indicating the formation of U-rich nanocrystals and uranyl ion crystallites dispersed over the surface (Fig. 11). These findings demonstrate the potential of nano-sized alumina and nano- $\text{Mg}(\text{OH})_2$  as efficient adsorbents for uranium extraction, offering high adsorption capacities, selectivity, and environmental compatibility.

Various nanostructured materials have been explored for uranium extraction and adsorption due to their unique properties. A  $\text{Fe}_3\text{O}_4@ \text{TiO}_2$  core-shell composite was prepared by Tan et al. [146] for uranium uptake from an aqueous solution. The adsorption process is described by the Langmuir isotherm ( $q_{\text{max}} = 119 \text{ mgU}\cdot\text{g}^{-1}$  at pH 6), and is spontaneous and endothermic. The removal of U(VI) by tin oxide was investigated by Nilchi [147]. The adsorption results are well fitted by the Freundlich and Langmuir isotherms ( $q_{\text{max}} = 67 \text{ mg}\cdot\text{U}\cdot\text{g}^{-1}$ ). Yusan and Erenturk [148] used goethite as a uranium adsorbent; equilibrium was attained in 2 h. The adsorption isotherm is best fitted with the Langmuir model, which indicates that the process is homogeneous. Adsorption is endothermic ( $+40 \text{ kJ}\cdot\text{mol}^{-1}$ ). Cerium molybdate [149] and vanadate [150] have been used for the extraction of uranium ( $q_{\text{max}}$  for cerium vanadate =  $19 \text{ mgU}\cdot\text{g}^{-1}$ ).

Kaynar et al. [151] used nanoporous ZnO powders for uranium extraction. The degree of adsorption and the distribution coefficient are 98.6 % and  $7.3 \text{ mL}\cdot\text{g}^{-1}$ , respectively, at pH 5 and  $30^\circ\text{C}$ , for a contact time of 1 h and 20 ppm of U(VI). The  $q_{\text{max}}$  value based on the Freundlich isotherm is  $10.5 \text{ mgU}\cdot\text{g}^{-1}$  at  $40^\circ\text{C}$ . Abdi et al. [152] fabricated different types of copper oxide  $\text{CuO}/\text{NaX}$  nanocomposites by exchanging different cations ( $\text{Ag}^+$ ,  $\text{K}^+$ ,  $\text{Mg}^{2+}$ , and  $\text{Ca}^{2+}$ ) with  $\text{Na}^+$  in NaX zeolite for uranium extraction under drinking water conditions. The efficiency for U(VI) removal and the distribution coefficient of original NaX zeolite were

decreased by the presence of competing anions and/or cations. However, the incorporation of  $\text{CuO}$  NPs and various cations into NaX zeolite strongly enhanced the ability of the nanocomposite to remove uranium from contaminated drinking water. Another type of NaX-nanozeolite was prepared by modifying the structure with silver cations and zinc oxide NPs to improve their uranium adsorption capacity [153]. The nanocomposites showed excellent selectivity for uranium ions in the presence of other competing anions and cations in the contaminated waters. Mortada et al. [154] decorated titanium oxide nanotubes ( $\text{DTiO}_x\text{NTs}$ ) with copper ferrite  $\text{CuFe}_2\text{O}_4$  quantum dots. The  $q_{\text{max}}$ , obtained from the Langmuir isotherm, for  $\text{DTiO}_x\text{NT}$  adsorption of U(VI) is  $366 \text{ mgU}\cdot\text{g}^{-1}$ , which is better than that for  $\text{TiO}_x\text{NTs}$  alone ( $277 \text{ mgU}\cdot\text{g}^{-1}$ ). Moreover, Chen et al. [155] reported that the nanocomposite  $\text{Ag}_2\text{O}@ \text{Mg}(\text{OH})_2$  is a highly effective scavenger for iodine and uranium from water.

ZVI NPs were immobilized on negatively charged diatomite (D) to create a novel composite (ZVI-D) to improve the sequestration of U(VI) from water [156]. Batch results showed that the as-synthesized ZVI NPs are less efficient in uranium sequestration than ZVI-D NPs. Diatomite plays multiple roles in enhancing uranium extraction: as a pH-buffering agent, as an adsorbent of U(VI), and as a scavenger for insoluble reaction products. The removal of U(VI) by a  $\text{Fe}_3\text{O}_4@ \text{gelatin}$  composite was described by Tang et al. [157]. The process is endothermic and spontaneous ( $q_{\text{max}} = 65 \text{ mgU}\cdot\text{g}^{-1}$ ). Wang et al. [158] prepared a series of nanostructured zirconium titanium pyrophosphates,  $\text{Zr}_{1-x}\text{Ti}_x\text{P}_2\text{O}_7$ . The  $q_{\text{max}}$  of  $\text{TiP}_2\text{O}_7$  for U(VI) is  $310 \text{ mgU}\cdot\text{g}^{-1}$  at pH 5 and  $30^\circ\text{C}$  for a time of 1 h. Kinetic analysis of the extraction process suggested that chemisorption is the rate-controlling step. Chouyyok et al. [159] fabricated unique nanostructured metal oxide sorbents, a  $\text{Fe-MnO}_2\text{-NP}$  composite and 8 nm  $\text{Mn-Fe}_3\text{O}_4$  magnetic NPs, for uranium recovery and separation from seawater. These materials adsorb U(VI) rapidly, adsorbing up to  $3 \text{ mgU}\cdot\text{g}^{-1}$  after 4 h of contact with natural seawater. Sodium carbonate was used as an effective, simple, non-toxic, and inexpensive agent for stripping uranium from adsorbents. Table 4 summarizes the adsorption capacities of nanostructured oxides, hydroxides, and mixed composites for uranium.

Nanosized metal oxides and hydroxides show great extraction efficiency for the removal of uranium from aqueous solution due to their high surface areas and numerous active sites. The smaller their particle size, the greater is their tendency to agglomerate because of van der Waals and other interactions. Moreover, a smaller particle size requires more expensive filtration systems. To overcome these problems, the scaling up of fabrication methods, surface functionalization, and risk assessment of these types of nanomaterials are required.

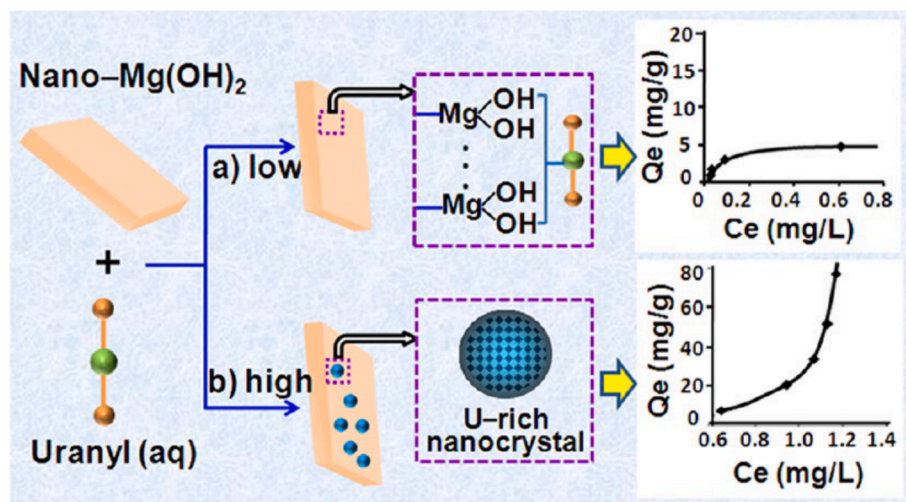


Fig. 11. Mechanism of the interaction between nano- $\text{Mg}(\text{OH})_2$  and uranyl ion in water (Reprinted with permission from ref. [145]. Copyright 2013, American Chemical Society).

**Table 4**

Adsorption capacities of uranium on nanostructured oxides, hydroxides, and mixed composites.

Nanostructured oxides, hydroxides, and mixed composites	Maximum adsorption capacity (mgU·g <sup>-1</sup> )	Reference
ZnS-AACF	359.72	[70]
MnO <sub>2</sub> @chitosan	326.54	[72]
Co-Mo-Ni ternary hydroxide	585.6	[77]
Nanoporous alumina	11.6	[141]
Nano alumina	151	[143]
MgO	81.4	[144]
Mg(OH) <sub>2</sub>	12.1	[63]
Mg(OH) <sub>2</sub>	73	[145]
Fe <sub>3</sub> O <sub>4</sub> @TiO <sub>2</sub> core-shell	118.8	[146]
Tin oxide NPs	66.7	[147]
α-FeOOH	144.5	[148]
Nano-cerium vanadate	19.0	[150]
Nanoporous ZnO	10.5	[151]
CuO/X zeolite-based nanocomposites	6.8	[152]
MWCNTs-Fe <sub>3</sub> O <sub>4</sub>	36.1	[94]
NaX nanozeolites	4.6	[153]
TiO <sub>2</sub> NPs	277	[154]
CuFe <sub>2</sub> O <sub>4</sub> -TiO <sub>2</sub> NPs	366	[154]
Fe <sub>3</sub> O <sub>4</sub> @gelatin	65.2	[157]
TiP <sub>2</sub> O <sub>7</sub>	309.8	[158]
Mn-Fe <sub>3</sub> O <sub>4</sub>	3	[159]

### 3.5. Nanofibrous and silicate composites

Due to its reliability and simplicity, electrospinning is a widely used technique for producing nanofibers [160,161]. Fe<sub>3</sub>O<sub>4</sub>/polyvinyl alcohol (PVA) magnetic fiber scaffolds were synthesized by electrospinning [162]. Mirzabe and Keshtkar [163] synthesized electrospun Fe<sub>3</sub>O<sub>4</sub>@-SiO<sub>2</sub>@APTES/PVA nanofibers for U(VI) adsorption (Fig. 12). The kinetics and isotherm data were well fitted by the Langmuir model, with a  $q_{\max}$  of 69 mgU·g<sup>-1</sup> at pH 5. Polyacrylonitrile (PAN)/SiO<sub>2</sub>/APTES composite nanofiber adsorbents were prepared by Dastbaz and Keshtkar [164]. The U(VI) adsorption process is endothermic and follows the Langmuir model ( $q_{\max} = 193$  mgU·g<sup>-1</sup> at 45 °C). Singh and Balasubramanian [165] used cellulose-camphor soot nanofibers for U(VI) recovery from nuclear wastewater. The  $q_{\max}$  at pH 6 is 410 mgU·g<sup>-1</sup> in 1 h with 96 % efficiency. Adsorption kinetics follow the pseudo-first-order and Elovich models. Xie et al. [166] employ a two-nozzle electrospinning process to synthesize a unique nanofibrous adsorbent that combines the high affinity of amidoxime groups and the small size effect of nanomaterials. The  $q_{\max}$  for uranium extraction in simulated seawater is 1.6 mgU·g<sup>-1</sup> even in the presence of high concentrations of interfering ions. Wang et al. [167] prepared mesoporous amidoxime-functionalized silica nanospheres from coal fly ash in an alkane aqueous system. The nanocomposite efficiently separated uranium from an aqueous solution, achieving 98.9 % removal of 50 mg L<sup>-1</sup> U(VI). Uranium adsorption was significantly pH-dependent.

Magnesium silicate nanotubes were synthesized by Qu et al. [168] as super-adsorbents of UO<sub>2</sub><sup>2+</sup> from water. These materials retain the tubular structure of the templates, which results in surface areas as high as 649 m<sup>2</sup>·g<sup>-1</sup>. Magnesium silicates show a  $q_{\max}$  for uranyl ions of 929 mgU·g<sup>-1</sup>. Nano-porous silica has a  $q_{\max}$  for uranium of 36 mgU·g<sup>-1</sup> in the absence of anions and 18 mgU·g<sup>-1</sup> in the presence of sulfate anion [169]. Batch experiments show that high concentrations of phosphate, nitrate, and chloride anions alone do not affect uranium recovery. Silica NPs modified with salicylaldehyde are efficient adsorbents for the removal of uranium from an aqueous solution [170]. The uptake of uranyl ions by modified NPs is significantly better than that by unmodified ones. The experimental data are fitted by a Langmuir isotherm ( $q_{\max} = 53$  mgU·g<sup>-1</sup> at pH 5.5). The thermodynamic results indicate that the uranium adsorption is entropy-driven with a positive enthalpy change. Zhang et al. [171] fabricated magnesium silicate nanostructures

from natural rice husks. They appear as twisted nanosheets about 20 nm-thick, and self-assembly leads to a three-dimensional hierarchical flower-like structure as shown by SEM (Fig. 13). The  $q_{\max}$  for uranium is 483 mgU·g<sup>-1</sup>.

Table 5 lists the adsorption capacities of uranium on nanofibrous and silicate composites, which show great performance and selectivity for uranium separation and extraction. The main drawbacks of these nanomaterials include synthesis challenges and the scaling-up of the fabrication method.

### 3.6. Functionalized nanomaterials

Engineering the nanomaterial surface is a key challenge. Generally, surface modification can be achieved by chemical/physical adsorption or surface coating with appropriate molecules based on a specific application. Functionalization of NPs improves the surface and optical properties, prevents magnetic agglomeration, enhances selectivity [172,173], and increases adsorption capacity [10,61]. Functionalized nanomaterials have been widely reported for uranium extraction [84,174–179]. Shao et al. [84] reported carboxymethyl cellulose grafted onto MWCNTs using plasma techniques ( $q_{\max} = 112$  mgU·g<sup>-1</sup>). However, these plasma-treated CNTs show poor selectivity. Amidoxime-grafted MWCNTs (AO-g-MWCNTs), also prepared by plasma techniques, were used to separate U(VI) from nuclear industrial effluents with high selectivity [180]. The optimum U(VI) adsorption is 145 mgU·g<sup>-1</sup> at pH 4.5. The adsorption process is fast, spontaneous and endothermic, and follows the Langmuir isotherm.

Abdeen and Akl [180] reported that a hydrogel composite of poly (vinyl alcohol)/carbon nanotube extracts and removes uranium ions better than poly(vinyl alcohol) alone ( $q_{\max} = 233$  mgU·g<sup>-1</sup>). Nano-diamond (ND) particles were functionalized with a single-armed ligand (SA) and a double-armed ligand (DA), with amide-thiourea (having the same coordination unit), then applied for the adsorption of uranium [181]. Batch adsorption experiments showed that ND-SA and ND-DA have high  $q_{\max}$  (200 mgU·g<sup>-1</sup>), very high adsorption rates (2 min. to reach equilibrium), and good selectivity (up to 82 % and 72 %, respectively) for uranium. Nanosheets of cyclodextrin-modified (CD) GO were prepared by *in-situ* polymerization. The mutual effects of uranium (VI) and humic acid adsorption onto CD/GO in an aqueous system are significantly affected by ionic strength and pH. The presence of humic acid enhances U(VI) adsorption at low pH values and reduces it at high pH, whereas the presence of U(VI) enhances humic acid adsorption [182].

Functionalized magnetic nanocomposites have emerged as powerful materials for selective extraction of trace metals from soil, industrial effluents, or wastewater streams. These advanced adsorbents, acting as “nanosponges” toward metal ions, can be easily retrieved from the solution by means of a magnet and reused, offering a promising sustainable and green technology [10,61,183]. Wang et al. [184] utilized bisphosphonate-modified magnetite nanoparticles for the removal of UO<sub>2</sub><sup>2+</sup> from water and blood with efficiencies of 99 % and 69 %, respectively. Mahfouz et al. [185] investigated the extraction of uranium by magnetic NPs of diethylenetriamine-functionalized chitosan ( $q_{\max} = 178$  mgU·g<sup>-1</sup> at pH 3.6). The kinetics of uranium uptake follow a second-order rate equation. Sadeghi et al. [186] reported the use of quercetin-modified magnetic NPs ( $q_{\max} = 13$  mgU·g<sup>-1</sup>) as an adsorbent for the removal of U(VI) from environmental waters.

In our group, we have grafted diamidoxime (dAMD) on the surface of magnetic nanocomposites [61]. The nanocomposite exhibited a strong affinity for uranium ( $K_a = 10^5$  M<sup>-1</sup>, measured by nano-Isothermal Titration Calorimetry). Compared to linear ligands or multi-armed ligands, the cyclic chelating ligand exhibits the highest selectivity and binding affinities due to it forming a more thermodynamically stable complex with the metal ions. Therefore, we grafted succinyl-β-cyclodextrin (SβCD) onto maghemite nanoparticles using the sol-gel method [109]. Fig. 14 illustrates the uranium extraction mechanism by the

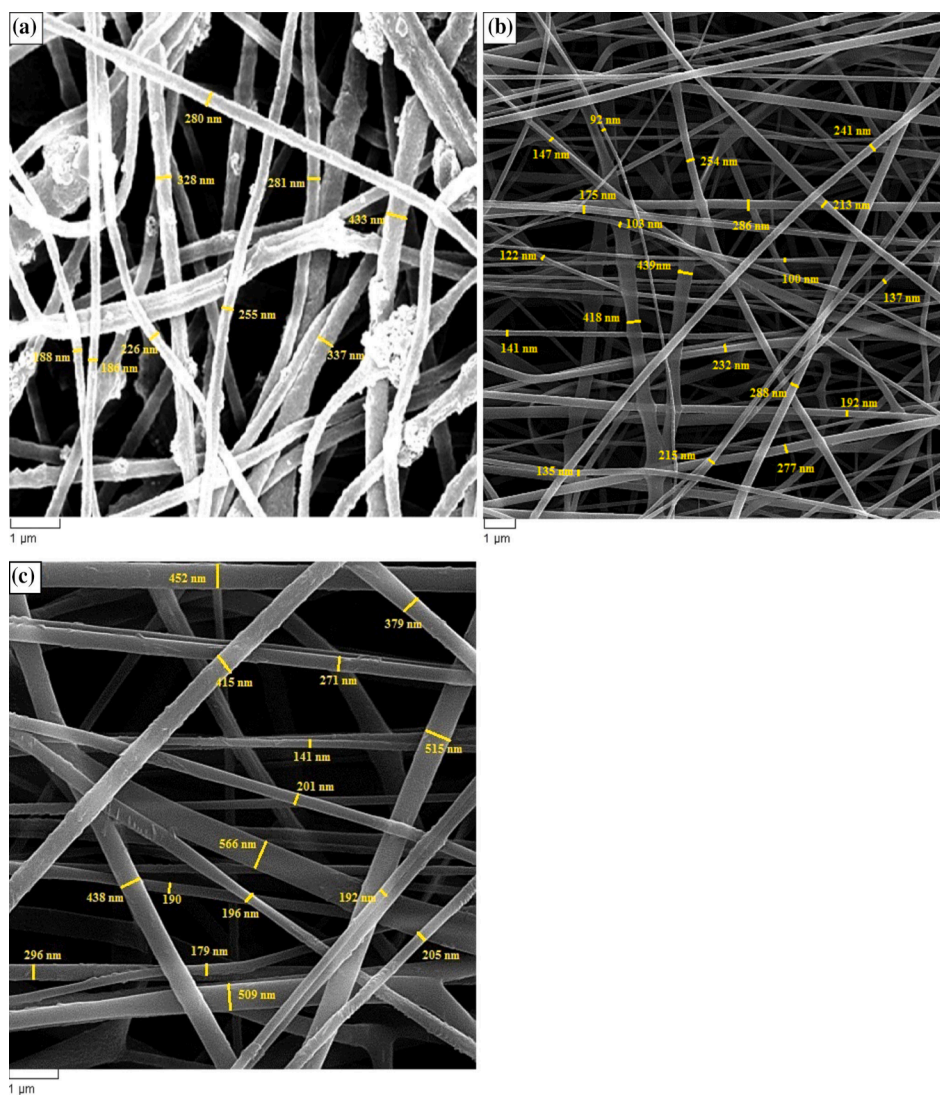


**Fig. 12.** SEM images of  $\text{Fe}_3\text{O}_4@\text{SiO}_2@\text{APTES}(15\%)/\text{PVA}$  (a)  $\text{Fe}_3\text{O}_4@\text{SiO}_2@\text{APTES}(20\%)/\text{PVA}$  (b) and  $\text{Fe}_3\text{O}_4@\text{SiO}_2@\text{APTES}(25\%)/\text{PVA}$  (c) nanofibers (Reprinted with permission from ref. [163]).

magnetic nanocomposite. The adsorption capacity of U(VI) is pH-dependent ( $q_{\max} = 286 \text{ mgU}\cdot\text{g}^{-1}$  at pH 6). The extraction occurs via chemisorption and exhibits excellent selectivity for U(VI) over other competing metal ions such as  $\text{Na}^+$ ,  $\text{K}^+$ ,  $\text{Cs}^+$ ,  $\text{Mg}^{2+}$ , and  $\text{Al}^{3+}$ . Furthermore, this nanocomposite has a long service life, as it can be recycled up to 10 times without a noticeable change in adsorption capacity or leaching of the magnetic core.

In a recent breakthrough, we have achieved a significant milestone in the separation and extraction of uranium from contaminated environmental water [187]. By utilizing an electrified multifunctional graphene foam electrode, we were able to reduce the uranium concentration in spiked seawater from 3 ppm to below the drinking water limit set by the Environmental Protection Agency (EPA) of 30 ppb. This new technology addresses the major drawbacks of traditional processes by employing an electrochemical potential to guide the movement of uranyl ions in the solution, resulting in enhanced kinetics, higher electrosorption capacity, scalability, and high selectivity facilitated by specifically grafted ligands.

This functionalized graphene foam electrode plays a critical role in the uranium extraction process. The functional groups of the foam attract uranium cations from the solution, while the graphene itself acts as a catalyst for the hydrogen evolution reaction (HER). The HER is crucial for increasing the local pH on the electrode surface, which is

essential for the electrolytic uranium deposition process. The increased local pH leads to the production of bridging hydroxy anions on the electrode surface, promoting the polymerization of uranyl cations. When a negative potential of  $-0.9 \text{ V}$  vs SCE is applied to the working electrode, uranyl ions in the solution migrate towards the electrode, where they are complexed by the functional groups of the graphene foam. The HER of water at this potential increases the local pH value on the electrode surface. Fig. 15a and 15b provide an explanation of the electrolytic uranium deposition process, while Fig. 15c shows a scanning electron microscopy (SEM) image of the graphene foam electrode after uranium deposition, revealing a dense growth of uranium deposits on the electrode surface. Additionally, the transmission electron microscopy (TEM) image of the uranium deposit reveals the quasi-2D hexagonal shape of  $\text{UO}_2(\text{OH})_2$  (Fig. 15d).

We achieved a remarkable electrosorption capacity of  $4650 \text{ mgU}\cdot\text{g}^{-1}$  without reaching saturation. Furthermore, our electrode demonstrated reusability, as it could be recycled at least 7 times in uranium solutions with concentrations 40 times higher than the initial concentration (Fig. 15e). This was achieved by applying a positive potential of 2 V for 2 h, resulting in the oxidation of water to oxygen gas on the electrode surface and reducing the local pH, which leads to the dissolution of the uranium deposit. Throughout the reusability experiments, no cracking or exfoliation of the electrode was observed, indicating the high stability

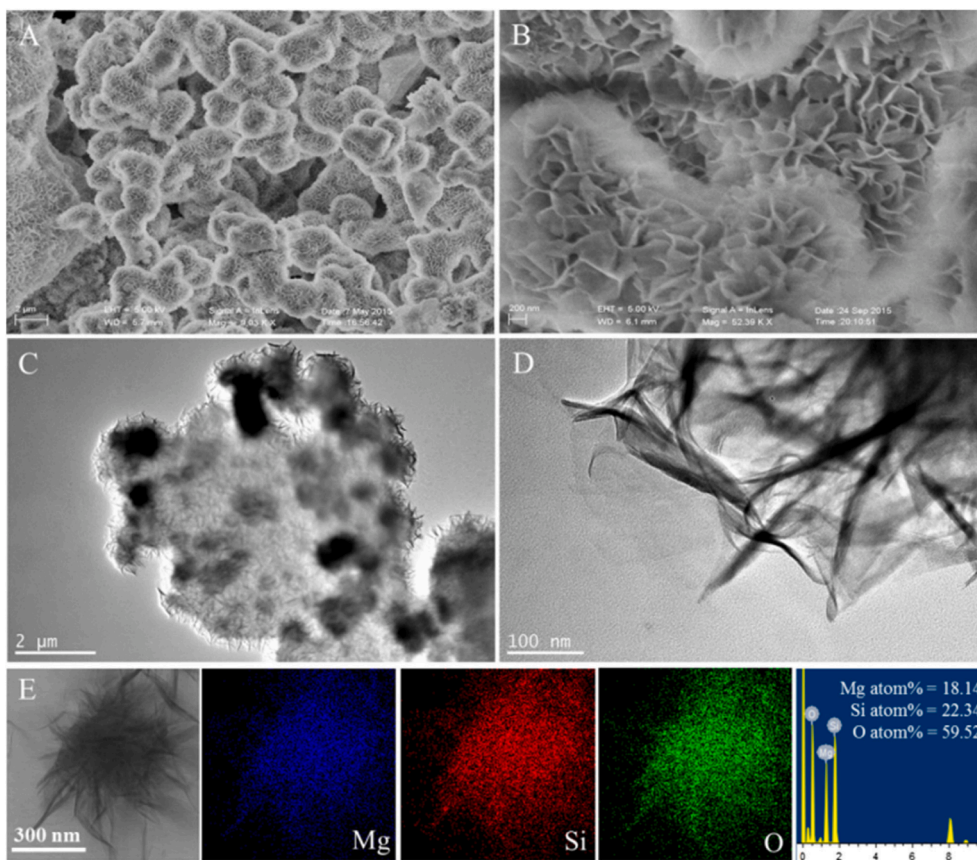


Fig. 13. SEM (A and B), TEM (C and D), mapping images and EDS analysis (E) of flower-like MgSi (Reprinted with permission from ref. [171]. Copyright 2017, Elsevier).

Table 5

Adsorption capacities of uranium on nanofibrous and silicate composites.

Nanofibrous and silicate composites	Maximum adsorption capacity (mgU·g <sup>-1</sup> )	Reference
SiO <sub>2</sub> nanomeshes	822	[71]
SiO <sub>2</sub> @Zn <sub>2</sub> SiO <sub>4</sub> nanotubes	250	[78]
Fe <sub>3</sub> O <sub>4</sub> @SiO <sub>2</sub> /PVA nanofiber	69.0	[163]
Polyacrylonitrile composite nanofiber	193.1	[164]
Cellulose-camphor soot nanofibers	410	[165]
PAO/PVDF composite nanofiber	12.1	[166]
Magnesium silicate NTs	929	[168]
Nanoporous silica	36.0	[169]
Silica NPs-salicylalimine	52.6	[170]
MgSi hierarchical flower-like structure	482.8	[236]

of the functionalized graphene foam under both reduction and oxidation conditions. The decrease in uranium extraction capacity observed after 7 cycles can be attributed to the loss of functional groups from the foam.

This technology opens up new possibilities for utilizing multifunctional graphene foam freestanding electrodes as a platform for the clean-up of other dangerous radionuclides and heavy metals from contaminated environmental water, presenting a promising approach for environmental remediation.

Tan et al. [188] developed oxine-functionalized magnetic Fe<sub>3</sub>O<sub>4</sub> particles to enhance the extraction of U(VI). The adsorption process is influenced by pH and is independent of ionic strength, suggesting that inner-sphere surface complexation dominates the extraction mechanism. The adsorption results follow the Langmuir isotherm ( $q_{\max} = 125 \text{ mgU}\cdot\text{g}^{-1}$ ) and the second-order rate equation. Thermodynamic data indicate that the process is endothermic and spontaneous. Popescu et al.

[189] grafted carboxymethyl-cellulose (CMC) onto the surface of ZVI, resulting in enhanced uranium removal ( $q_{\max} = 323 \text{ mgU}\cdot\text{g}^{-1}$ ). The adsorption mechanism involves redox precipitation, chemisorption, and physical adsorption, and the Langmuir and Freundlich isotherms describe the adsorption of uranyl ions [190]. Huang et al. [191] designed polystyrene nanoparticles coated with polyamidoxime for U(VI) removal, showing favorable performance at near-neutral pH (6.5). Equilibrium adsorption was achieved in 6 h, with a  $q_{\max}$  of  $247 \text{ mgU}\cdot\text{g}^{-1}$ . Li et al. [192] prepared a crown ether/Fe<sub>3</sub>O<sub>4</sub> nanocomposite for uranium extraction, with pH-dependent extraction and a  $q_{\max}$  of  $91 \text{ mgU}\cdot\text{g}^{-1}$  at pH 5.5 and 45 °C. The Freundlich isotherm described the adsorption process.  $\beta$ -Cyclodextrin ( $\beta$ -CD) chemically grafted onto halloysite NT/iron oxides gave optimal separation at pH 7 ( $q_{\max} = 108 \text{ mgU}\cdot\text{g}^{-1}$ ), and adsorption was irreversible at pH 5.5 [193]. Zong et al [194] showed that the extraction of uranium by a carboxymethyl- $\beta$ -cyclodextrin-functionalized magnetic nanocomposite is controlled by an outer-sphere surface complexation mechanism and/or cation exchange at lower pH values and inner-sphere complexation and surface co-precipitation at higher pH values.

Amino acids have shown promise as chelating agents for uranyl ions. Galhoum et al. [195,196] synthesized alanine, cystine, and serine-based functionalized chitosan magnetic nanoparticles for uranium extraction. The Langmuir isotherm described the adsorption process, with  $q_{\max}$  values near 85, 97, and  $116 \text{ mgU}\cdot\text{g}^{-1}$  for alanine-, cysteine-, and serine-based adsorbents, respectively. Adsorption was spontaneous, exothermic, and increased the entropy of the system. Shehzad et al. [197] developed a magnetic chitosan nanosorbent grafted with maleic anhydride (MCN-MA) for U(VI) extraction, achieving a  $q_{\max}$  of  $188 \text{ mgU}\cdot\text{g}^{-1}$  from wastewater. Engineered manganese ferrite MnFe<sub>2</sub>O<sub>4</sub> nanocrystals, stabilized by oleyl-based surface bilayers, had excellent uranium-binding capacity and stability under relevant environmental

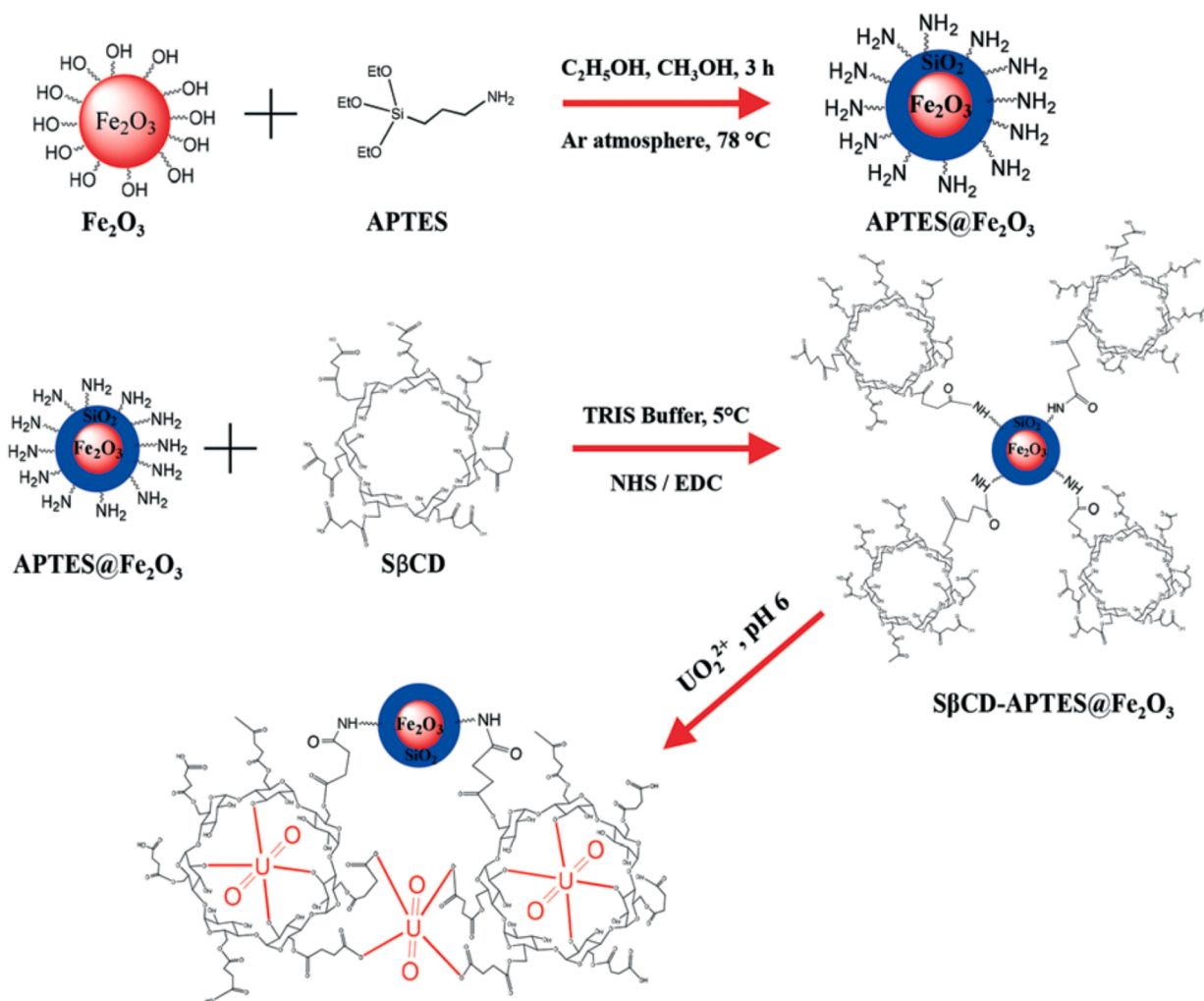


Fig. 14. Grafting of  $\beta\text{CD}$  onto maghemite NPs and uranium extraction strategy. (Reprinted with permission from ref. [109]. Copyright 2018, Royal Society of Chemistry).

conditions [198,199]. Particularly,  $\text{MnFe}_2\text{O}_4$  cores with oleyl phosphate bilayers bound uranium preferentially and were highly water-stable at high pH and ionic strength (up to 235 ppm sodium chloride, 51 ppm calcium chloride, and 60 ppm uranyl at pH 5–9).  $\text{MnFe}_2\text{O}_4$  cores have a higher binding capacity,  $667 \text{ mgU}\cdot\text{g}^{-1}$ , than  $\text{Mn}_2\text{FeO}_4$ ,  $\text{Mn}_x\text{O}_y$ , and  $\text{Fe}_3\text{O}_4$  (313, 270, and  $345 \text{ mgU}\cdot\text{g}^{-1}$ , respectively). The improved uranium adsorption capacity of  $\text{MnFe}_2\text{O}_4$  is due to the enhanced reduction of U(VI) to  $\text{UO}_2$  at the interface between the uranyl ion and the nanocrystal [199].

Chen et al. [200] synthesized a bi-functionalized magnetic iron oxide composite, covalently bound by phosphonate and ammonium groups, for U(VI) adsorption in alkaline media ( $q_{\text{max}} = 71 \text{ mgU}\cdot\text{g}^{-1}$  at pH 9). The adsorption process was endothermic and described by the Freundlich isotherm. A functionalized magnetic  $\text{Fe}_3\text{O}_4@\text{SiO}_2$  composite was prepared by embedding iron oxide NPs into MCM-41 in a one-step process, followed by aminopropyl grafting on the mesopore channels [201]. The composite not only reached a  $q_{\text{max}}$  of  $160 \text{ mgU}\cdot\text{g}^{-1}$  at pH 5.0 in 2 h but also showed good selectivity for U(VI) ions in the presence of different competing metal ions. The adsorbed U(VI) could be stripped easily by  $1 \times 10^{-2} \text{ M HNO}_3$  solution, the recovered adsorbent was recycled for up to four cycles without any change in adsorption capacity. Mahmoud [202] developed a multifunctional silica magnetic nanocomposite for uranium extraction, with an ion exchange mechanism and a  $q_{\text{max}}$  of  $66 \text{ mgU}\cdot\text{g}^{-1}$ .

Calixarene derivatives have been explored as promising ligands for uranium extraction. Xu et al. [203] used diazotization-coupling and

substitution reactions to synthesize magnetic nanocomposite functionalized m-carboxyphenylzocalix[4]arene-amine-oxime. The nanocomposite exhibited remarkable selectivity and reusability. Luo et al. [204] introduced a heteroatom, sulfur, into the calixarene to fabricate a magnetic nanocomposite functionalized with m-carboxyphenylzocalix[4]arenesulfide, showing efficient uranium extraction even at low concentrations. Thermodynamic analysis indicated that the uranium adsorption was a spontaneous, endothermic process, with a  $q_{\text{max}}$  of  $125 \text{ mgU}\cdot\text{g}^{-1}$ . Wang et al. [205] developed triethylenetetramine-functionalized SW carbon nanohorns (SWCNH-TETA) for uranium extraction from wastewater, with a high adsorption capacity of  $333 \text{ mgU}\cdot\text{g}^{-1}$  due to their nitrogen-rich structure. The adsorption results showed that the acidity and temperature of the solution play critical roles in uranium extraction efficiency. Zhang et al. [206] synthesized water-stable carboxyl-functionalized  $\text{Ti}_3\text{C}_2\text{T}_x$  MXene nanosheets for uranium extraction from aqueous solutions. The extraction followed an inner-sphere complexation mechanism, with a  $q_{\text{max}}$  of  $345 \text{ mgU}\cdot\text{g}^{-1}$ .

Functionalized magnetic nanomaterials have limitations, particularly in harsh environmental conditions like the low pH and high temperatures encountered in nuclear waste scenarios. These conditions can lead to leaching of the magnetic core and degradation of functional groups. Regenerating functionalized magnetic nanomaterials requires specialized protocols due to the strong bonds formed between uranium and functional groups. Additionally, scaling up the synthesis and production of these nanomaterials for large-scale uranium extraction

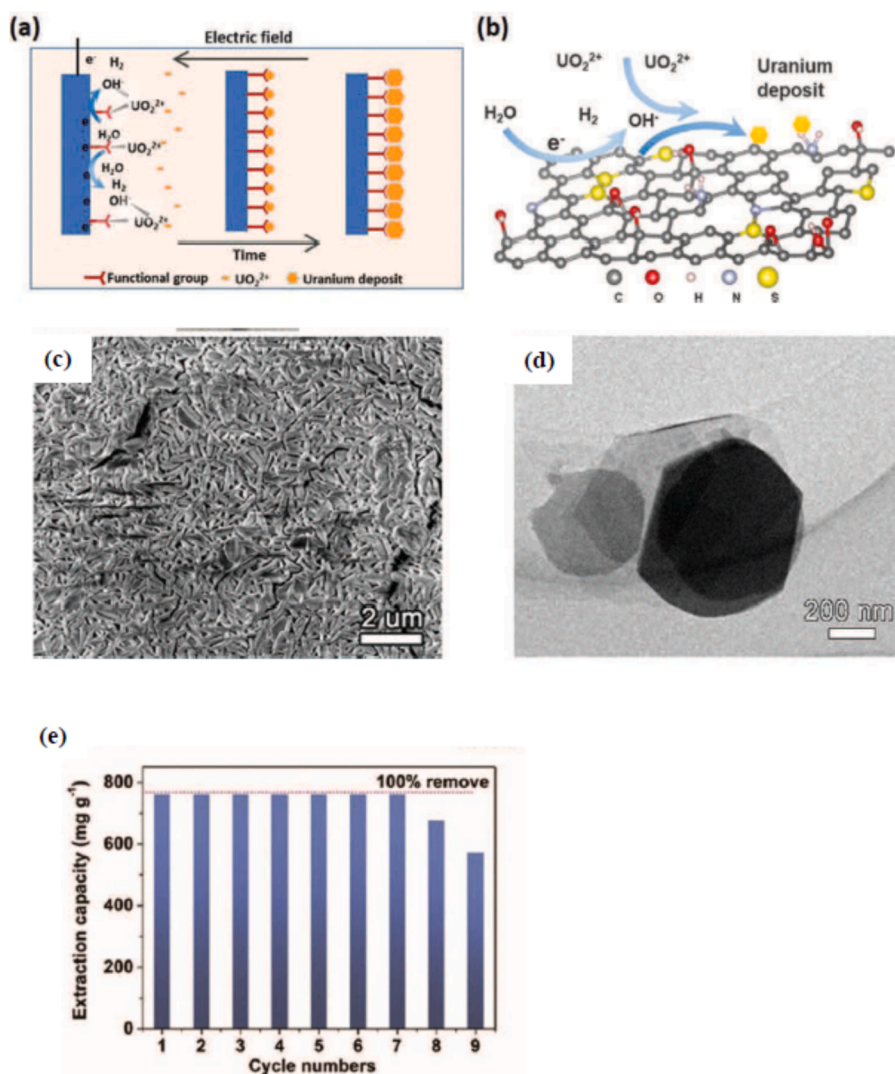


Fig. 15. a,b) Electrolytic deposition of uranium. c) SEM of functionalized graphene foam after electrodeposition. d) TEM image of uranium deposit. e) Cycling performance of uranium extraction at  $50 \text{ mg L}^{-1}$ . (Reprinted with permission from ref. [187]. Copyright 2021, Wiley).

applications poses challenges and may yield batch-to-batch variability in performance. Table 6 shows the maximum adsorption capacities of functionalized nanomaterials for uranium.

### 3.7. Bio-nanocomposites

Lovely et al. reported that bio-nanocomposites can reduce  $\text{UO}_3$  to  $\text{UO}_2$  with high efficiency and low cost [207]. Besides the ability of microorganisms to extract, remove, and recover radioactive ions from water, as living templates they can be used to extend the scale of inorganic material patterning [208,209]. Based on this ability, the design of materials with the advantages of both nanomaterials and microorganisms can meet the rigorous requirements for adsorbing uranium ions from different aqueous solutions [210]. Fungus- $\text{Fe}_3\text{O}_4$  NP bio-nanocomposites were synthesized by Li et al. [211] using a simple co-culture method. The fabrication scheme and the microstructural analysis of the bio-nanocomposite are shown in Fig. 16f and Fig. 16a-e, respectively. Adsorption tests show that the material can preconcentrate trace uranyl ions from nuclear wastewater with a  $q_{\text{max}}$  of  $171 \text{ mgU}\cdot\text{g}^{-1}$ .

The bacterium *Serratia sp.* produces amorphous calcium phosphate nanominerals (BHAP), which have a high adsorption capacity for uranium when subjected to calcination at  $450^\circ\text{C}$  or higher. The cell biomass is removed, and the bio-minerals are transformed into hydroxyapatite

(HAP), where uranium is specifically surface-complexed [212]. In another study, a microstructure of silica NPs was assembled with *Streptococcus lactis* cells through evaporation-induced self-assembly. The SEM analysis for  $\text{SiO}_2@ \text{Streptococcus lactis}$  is shown in Fig. 17. The bio-composite is used in a uranium bioremediation application [213].

The uranium removal process using the bio-nanocomposite was found to be highly efficient, with more than  $85 \pm 2\%$  of total uptake achieved in 10 min. The  $q_{\text{max}}$  for the spray-dried doughnut-shaped microstructures was  $170 \text{ mgU}\cdot\text{g}^{-1}$  at pH 5 and  $25^\circ\text{C}$ . Kinetic analysis indicated that the adsorption process followed a second-order rate model, and the extraction was endothermic and spontaneous.

The reduction of soluble U(VI) to the insoluble U(IV) phase in order to remediate uranium-contaminated effluent was investigated using an integrated system combining abiotic and biotic processes [214]. In the presence of lactate supported on active carbon, autochthonous microorganism growth was stimulated, resulting in the removal of 77 % of uranium (VI) in four days. Additionally, the use of 50 nm-diameter iron NPs alone led to a 60 % reduction of U(VI) in 4 h. However, when lactate and iron NPs immobilized on active carbon were combined, the efficiency of U(VI) removal increased to 96 % in 30 min. Uranium-reducing bacteria were immobilized in beads using sodium alginate, anthraquinone-2,6-disulfonate (AQDS), and carbon nanotubes (CNTs) [215]. Beads containing 0.7 % AQDS-CNTs achieved over 97.5 %

**Table 6**  
Adsorption capacities of uranium on functionalized nanomaterials.

Functionalized nanomaterial	Maximum adsorption capacity (mgU·g <sup>-1</sup> )	Reference
Electrospun polyvinyl alcohol/titanium oxide nanofiber	196.1	[175]
Amberlite-7HP@Fe <sub>3</sub> O <sub>4</sub>	47.7	[177]
Succinyl-β-cyclodextrin – APTES@Fe <sub>2</sub> O <sub>3</sub>	286	[109]
DTPA – APTES@Fe <sub>2</sub> O <sub>3</sub>	249	[46]
Ti <sub>3</sub> C <sub>2</sub> Tx MXene /PAO	625	[69]
MWCNT@PDA@TNS	283.29	[73]
Phytic acid@CNM	552.49	[76]
Carboxymethylcellulose-MWCNTs	111.9	[84]
Amidoxime-grafted MWCNTs	145	[180]
PVA/MWCNTs	233.6	[180]
Amide-thiourea-functionalized ND	200	[181]
Cyclodextrin-modified GO nanosheets	43.2	[183]
Diethylenetriamine-functionalized magnetic chitosan	178	[185]
Quercetin-modified magnetic NPs	12.3	[186]
Oxine@Fe <sub>3</sub> O <sub>4</sub>	125	[188]
CMC-ZVI	322.6	[189]
Fe <sub>3</sub> O <sub>4</sub> – NH <sub>2</sub>	268.5	[190]
Polyamidoxime@polystyrene NPs	246.9	[191]
18-crown-6@Fe <sub>3</sub> O <sub>4</sub>	91.1	[192]
CD/HNT/iron oxide	107.6	[193]
Carboxymethyl-β-cyclodextrin@Fe <sub>3</sub> O <sub>4</sub>	136.85	[194]
Alanine/chitosan/magnetic NPs	85	[195]
Cysteine/chitosan/magnetic NPs	97	[196]
Serine/chitosan/magnetic NPs	116	[195]
Engineered MnFe <sub>2</sub> O <sub>4</sub>	600	[198]
Oleyl phosphate/MnFe <sub>2</sub> O <sub>4</sub>	666.7	[199]
Ammonium-phosphonate/iron oxide	70.7	[200]
Aminopropyls@ Fe <sub>3</sub> O <sub>4</sub> @SiO <sub>2</sub>	160	[201]
Fe <sub>2</sub> O <sub>3</sub> -di(amidoxime)	120	[61]
SβCD-APTES@Fe <sub>2</sub> O <sub>3</sub>	286	[109]
Carboxymethyl-β-cyclodextrin@Fe <sub>3</sub> O <sub>4</sub>	136.85	[194]
Fe <sub>3</sub> O <sub>4</sub> @SiO <sub>2</sub>	66.43	[202]
Magnetic functionalized m-carboxyphenyl azocalix[4]arene-amine-oxime derivatives	149.25	[203]
Magnetic functionalized carboxyphenyl-azocalix[4]arene symmetrical sulfide	125.37	[204]
Triethylenetetramine-functionalized single-walled carbon nanohorns	333.13	[205]
Carboxyl-functionalized Ti <sub>3</sub> C <sub>2</sub> Tx MXene nanosheets	344.8	[206]

removal of U(VI) (20 mgU·L<sup>-1</sup>) in 8 h, being more efficient than systems without AQDS-CNTs. This improvement is attributed to enhanced electron transfer facilitated by CNTs and AQDS. The presence of Cu(II), Mn(II), and Fe(III) slightly favors U(VI) reduction, while Zn(II), Cr(II), Ni(II), and Pb(II) strongly inhibit the process.

The biosorption of uranium from an aqueous solution onto *Rhodotorula glutinis* and magnetically modified yeast cells was studied by Bai et al. [216] in a batch system. Bio-nanocomposites of fungus-Fe<sub>3</sub>O<sub>4</sub> were prepared using a self-assembly technique [217]. SEM images revealed uniform decoration of Fe<sub>3</sub>O<sub>4</sub> nanoparticles on the fungus surface (Fig. 18). X-Ray photoelectron spectroscopy (XPS) analysis confirmed the formation of inner-sphere radionuclide complexes through bonding with oxygen-containing functional groups (acetal, carboxyl, and alcohol) of fungus-Fe<sub>3</sub>O<sub>4</sub>. The  $q_{\max}$ , as determined from the Langmuir isotherm, was 224 mgU·g<sup>-1</sup> at pH 5 and 30 °C. The adsorption of uranium on fungus-Fe<sub>3</sub>O<sub>4</sub> was endothermic and spontaneous. Colomina et al. [218] reported that *Sphaerotilus natans* filamentous bacteria bonded to amorphous iron phosphate can effectively adsorb U(VI). Various biomaterial-FeS NPs have been developed for *in-situ* immobilization of U(VI) from radioactive wastes [219]. TEM images indicated that the aggregation of FeS NPs in aqueous suspension can be suppressed by gelatin and sodium carboxymethyl cellulose (CMC). The resulting composites, gelatin-FeS and CMC-FeS, were stable and had high

adsorption capacities for uranium. The  $q_{\max}$  values for U(VI) on CMC-FeS and gelatin-FeS at pH 5 and 20 °C were approximately 430 and 556 mgU·g<sup>-1</sup>, respectively. Table 7 shows the adsorption capacities of bio-nanocomposites for uranium.

Bio-nanocomposites have been used to extract and separate uranium from uranium-contaminated solutions. Extraction with this class of nanomaterials is economical and highly efficient for very dilute solutions, and generates a low volume of hazardous waste. However, in the practical treatment of contaminated environmental water samples, serious problems such as post-separation, clogging, and washing out of the bio-nanocomposite are encountered.

The development of nanomaterials for uranium extraction from contaminated environmental water and nuclear waste in the last two decades is shown in Fig. 19.

#### 4. Nano-Ecology: Assessing environmental safety and impact of nanomaterials

Nano-ecology plays a crucial role in assessing the environmental safety and impact of nanomaterials used in uranium removal from water. As nanotechnology continues to advance, the need to understand the implications of introducing nanomaterials into the aquatic system and the environment becomes increasingly important. Nanomaterial-based separation has shown great promise in improving uranium separation and extraction from contaminated environmental water and nuclear industrial effluents by enhancing efficiency, reducing energy consumption, and removing contaminants effectively [220]. However, their potential environmental risks cannot be overlooked. Nanomaterials have the potential to infiltrate aquatic and terrestrial environments through multiple pathways, including direct industrial discharges, the release of wastewater treatment effluents, or surface runoff from soils. They can also enter indirectly through the application of land-applied wastewater treatment products such as sludges or biosolids. Once released into the environment, nanoparticles are subject to a range of potential transformations that are influenced by both their intrinsic properties and the characteristics of the receiving medium. These transformations primarily involve chemical and physical processes, such as aggregation, dissolution, and redox reactions [220]. The potential pathways through which nanomaterials may enter the environment are depicted in Fig. 20. This dynamic behavior in natural ecosystems underscores the complexity of predicting the fate and impact of nanomaterials in the environment.

Engineered nanocomposites employed for uranium separation and extraction from contaminated environmental water, while highly effective, carry the potential risk of introducing secondary pollution into aquatic systems. The fate and reactive transport of nanomaterials in aquatic ecosystems are influenced by biological processes, as well as physical processes (aggregation, agglomeration, sedimentation, and deposition) and chemical processes (photochemical reactions, dissolution, oxidation, and sulfidation). Key examples of these biological processes include microbial-mediated biodegradation and biomodification [221]. In natural aquatic systems, a rich array of organic matter ranging from small molecules to large macromolecules exists alongside inorganic clay minerals and natural colloids of various sizes. It is widely acknowledged that in these environments, the interaction of nanomaterials with surrounding substances is often associated with natural organic matter. As a ubiquitous element within aquatic ecosystems, natural organic matter plays a significant role in altering the aggregation and deposition behavior of NPs by affecting their surface chemistry and charge characteristics [222,223]. Redox processes and sulfidation are critical chemical transformations for many metal NPs, especially in environments with elevated sulfide concentrations, such as those found in certain areas of wastewater treatment plants [224]. These processes can lead to significant alterations not only in nanomaterial solubility but also surface charge and particle size. These modifications, in turn, influence the reactive transport, fate, bioaccumulation, and overall

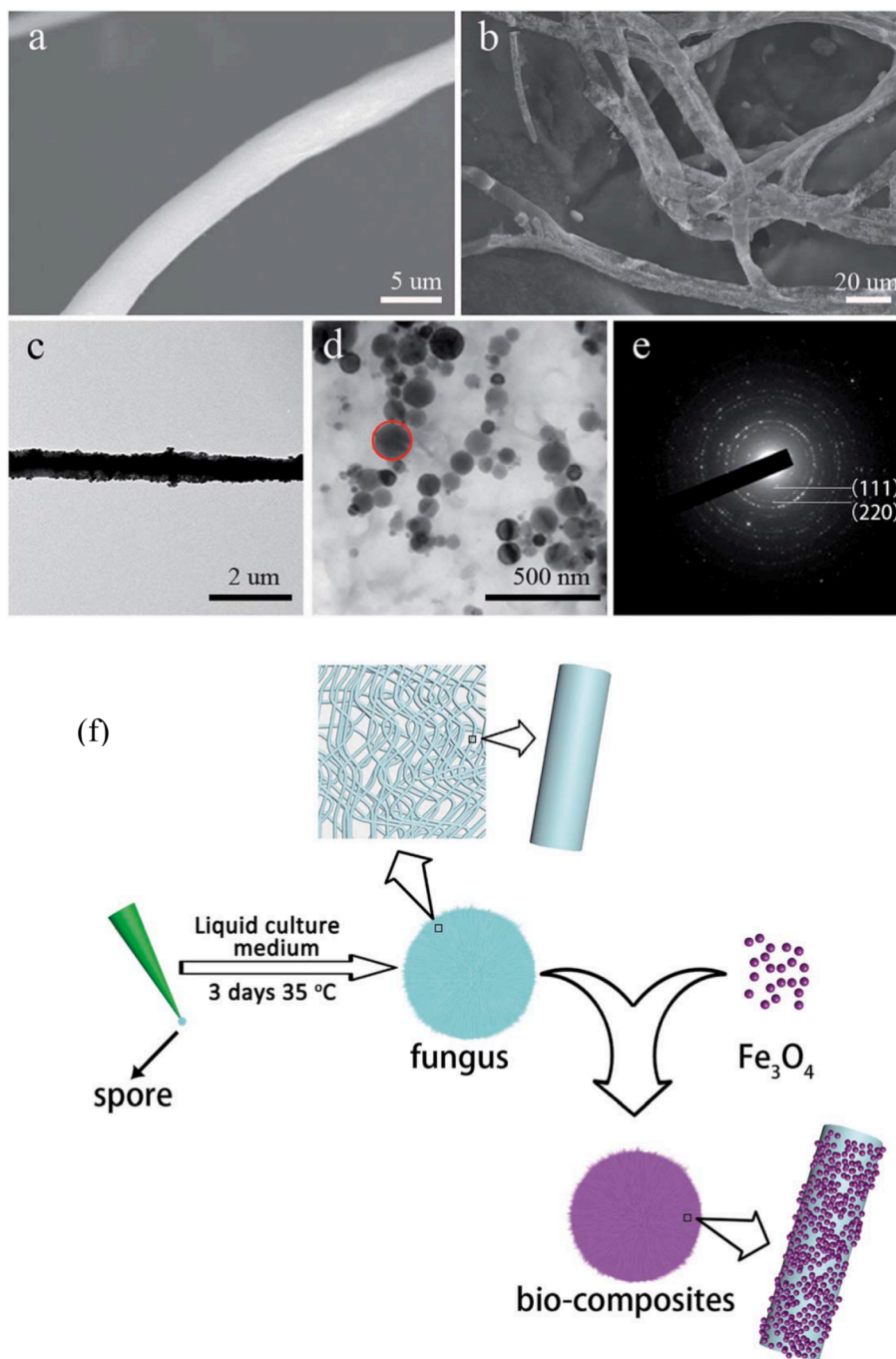


**Fig. 16.** Typical SEM images of (a) black *Aspergillus* and (b) fungus- $\text{Fe}_3\text{O}_4$  composites. (c and d) Typical TEM images at different magnifications of fungus- $\text{Fe}_3\text{O}_4$  composites. (e) SAED pattern of the  $\text{Fe}_3\text{O}_4$  NPs taken from the area marked in (d). (f) Synthesis of bio-nanocomposites (Reprinted with permission from ref. [[211]. Copyright 2015, Royal Society of Chemistry).

ecological impact of the nanomaterials. Notably, the sulfide form of these NPs tends to be more toxic to aquatic life [225]. On the other hand, oxidation, while not a primary transformation pathway for most NPs, plays a crucial role in the dissolution of metals like silver and in the redox transformations of metal oxides such as iron oxide and ceria. These oxidative processes are key parameters in determining the behavior and environmental interactions of NPs within aquatic systems [226]. The most common types of the numerous toxicity mechanisms associated with NPs are illustrated in Fig. 21. NPs are able to interact with a wide range of cellular components, including DNA, proteins, and mitochondria. These interactions can induce the formation of reactive oxygen species (ROS), thereby disrupting various cellular functions. This

disruption can manifest as DNA damage, alterations in lysosomal enzyme activity, increased ROS production, mitochondrial dysfunction, apoptosis, cell membrane disruption, and cytoplasmic impairment [227].

The cytotoxicity of NPs is influenced by several critical factors, including their surface area, shape and dimensionality, chemical composition, concentration or dosage, crystalline structure, solubility, hydrophilicity, surface charge, and degree of agglomeration. Smaller nanoparticles have a greater specific surface area, offering a more extensive interface for interactions with cellular components such as nucleic acids, proteins, fatty acids, and carbohydrates [228]. How living tissue alters its response to NPs depends on their shape and size. The

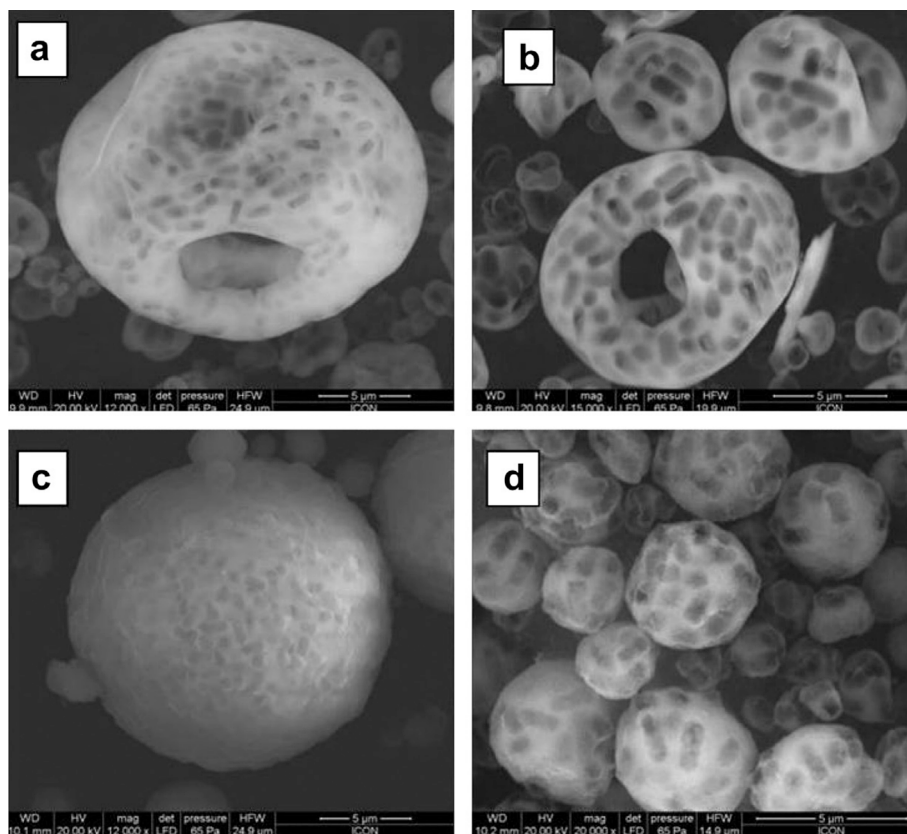


**Fig. 17.** SEM micrographs of microstructures: (a) spray-dried doughnut-shaped (SDSM), (b) calcined SDSM, (c) spray-dried spherical (SSSM), (d) calcined SSSM (Reprinted with permission from ref. [213]. Copyright 2014, Elsevier).

geometry and dimensions of NPs influence their interaction with cellular membranes and internal structures, which can impact their uptake and distribution within cells [229]. According to a study by Pan et al. [230], 15 nm-diameter gold NPs are approximately 60 times less toxic than 1.4 nm particles, particularly in macrophages, epithelial cells, melanoma cells, and fibroblasts. NPs with plate-like and needle-like morphologies are associated with markedly higher necrosis levels than spherical and rod-shaped NPs. This amplified impact arises from their enhanced ability to inflict physical damage on cells and tissues through direct interactions [231]. Beyond shape and size, metal solubility warrants critical consideration in the evaluation of the toxicological behavior of NPs. The potential release of metal ions into the cytoplasmic environment is intrinsically linked to the NP dissolution rate. Even with minimal dissolution, certain metallic ions can be extremely toxic in physiological environments. For instance, zinc oxide NPs, even at a concentration as low as  $10 \text{ mg L}^{-1}$  of dissolved zinc, are highly toxic due to their critical concentration and dose range [232]. On the other hand, experimental results further confirm that the surface charge of NPs exerts the most profound influence on their toxicological mechanisms. The interaction between cellular membranes and NPs is primarily driven by the NP surface charge [233]. Positively charged particles are more toxic, and variations in surface charge significantly influence cellular uptake. Notably, positively charged zinc oxide NPs are more toxic than their negatively charged counterparts [234].

### 5. Challenges in Transitioning from Lab-Scale Efficiency to Real-World Applications

The majority of published research on using nanomaterials for uranium separation from contaminated environmental water and nuclear waste has primarily focused on lab-scale experiments. Under laboratory conditions, the controlled environment allows for precise conditions

that enable nanomaterials to achieve optimal performance. However, transitioning from the lab to real-world scenarios introduces a host of complexities. These include varying concentrations of uranium and environmental factors such as temperature fluctuations, pH changes, and ionic strength, all of which can significantly impact the efficacy and selectivity of nanomaterials. These variations directly influence the adsorption capacity and affinity of nanomaterials for uranium ions, often reducing their effectiveness. Moreover, the practical deployment of nanomaterials in real contaminated environmental water and nuclear waste settings presents additional challenges related to their stability, reusability, and durability. Challenges like fouling, aggregation, and redox reactions can impair the effectiveness of NPs over time. Thus, it is crucial to develop robust nanomaterials that retain their stability and efficiency across various environmental conditions to ensure consistent performance in long-term applications. The high production costs associated with nanomaterials also present a significant barrier to their widespread use. Many synthesis methods, optimized for lab-scale production, are energy-intensive and rely on costly raw materials or reagents. As such, there is a pressing need to develop cost-effective and sustainable synthesis routes that can be scaled up without compromising the quality of the nanomaterials [235].

Evaluating the economic feasibility and ensuring regulatory compliance of nanomaterial-based separation techniques are crucial steps toward making these technologies viable for real-world applications. Overcoming the challenges of scaling up from lab research to practical applications requires a multidisciplinary approach. Advances in computational modeling and machine learning provide valuable tools for predicting the behavior of nanomaterials under diverse conditions, aiding in the optimization of their design and scalability. Moreover, collaboration among scientists, engineers, policymakers, and industry stakeholders is crucial for developing comprehensive strategies that address the entire lifecycle of nanomaterials, from production and

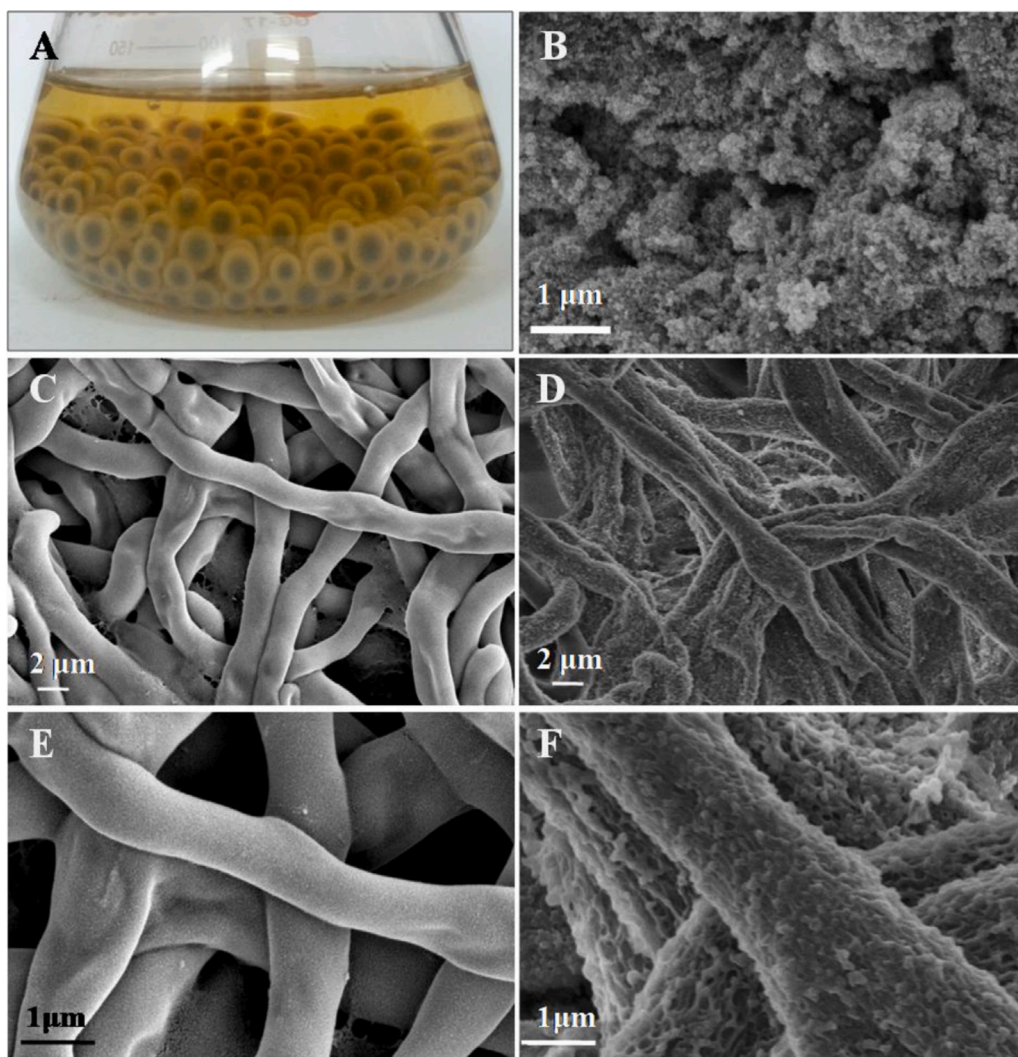


**Fig. 18.** Mycelium pellet of *Penicillium* sp. combined with nano-Fe<sub>3</sub>O<sub>4</sub> (A), SEM images of nano-Fe<sub>3</sub>O<sub>4</sub> (B), pure fungus of *Penicillium* sp. (C and E) and the bio-nanocomposites of fungus-Fe<sub>3</sub>O<sub>4</sub> (D and F) (Reprinted with permission from ref. [217]. Copyright 2015, Elsevier).

**Table 7**  
Adsorption capacities of bio-nanocomposites for uranium.

Bio-nanocomposites	Maximum adsorption capacity (mgU·g <sup>-1</sup> )	Reference
<i>Aspergillus</i> -Fe <sub>3</sub> O <sub>4</sub> NPs	171	[211]
Silica NPs- <i>Streptococcus lactis</i>	169.5	[213]
<i>Penicillium</i> sp.-nano-Fe <sub>3</sub> O <sub>4</sub>	223.9	[218]
CMC-FeS	430	[219]
Gelatin-FeS	556	[219]

deployment to disposal. These coordinated efforts are essential for harnessing the full potential of nanomaterials in uranium separation, ensuring both environmental and economic sustainability.

## 6. Uranium Quantification and Measurement

Uranium quantification and measurement has been developed to quantify dissolved uranium concentrations in environmental water, nuclear waste and contaminated solutions. These include Inductively Coupled Plasma Mass Spectrometry (ICP-MS), Fluorimetry, Inductively Coupled Plasma Optical Emission Spectrometry (ICP-OES), Instrumental Neutron Activation Analysis (INAA), Spectrophotometry, Graphite

Furnace Atomic Absorption Spectroscopy (GF-AAS), Voltammetry, Alpha Spectrometry, Raman Spectroscopy, and Ion-Selective Electrodes (ISEs). Among these, ICP-MS is widely regarded as the gold standard due to its exceptional sensitivity, low detection limits, and capability for rapid, high-precision isotopic analysis. Quadrupole ICP-MS has emerged as a preferred choice in uranium analysis because it combines rapid throughput with precise quantification, enabling detection limits down to parts-per-trillion (ppt) levels. It offers the flexibility to analyze both trace and bulk uranium concentrations, making it invaluable for environmental monitoring, nuclear forensics, and industrial applications. While laser fluorimetry is also frequently employed, particularly for field applications, its sensitivity is typically lower than that of ICP-MS [237].

Laser fluorimetry is a highly sensitive and well-established technique for uranium measurement, offering rapid analysis and broad applicability. This method relies on the excitation of uranyl ions (UO<sub>2</sub><sup>2+</sup>) by electromagnetic energy at specific wavelengths, followed by the measurement of uranium phosphorescence decay once the excitation source is turned off. Sensitivity is further enhanced through the use of fluorescence-enhancing reagents, which amplify the emitted signal. An innovative variation of this method, light-emitting diode (LED) fluorimetry, has been developed to reduce interference from matrix components, providing improved accuracy and portability for field applications [238]. Moreover, time-resolved laser fluorescence

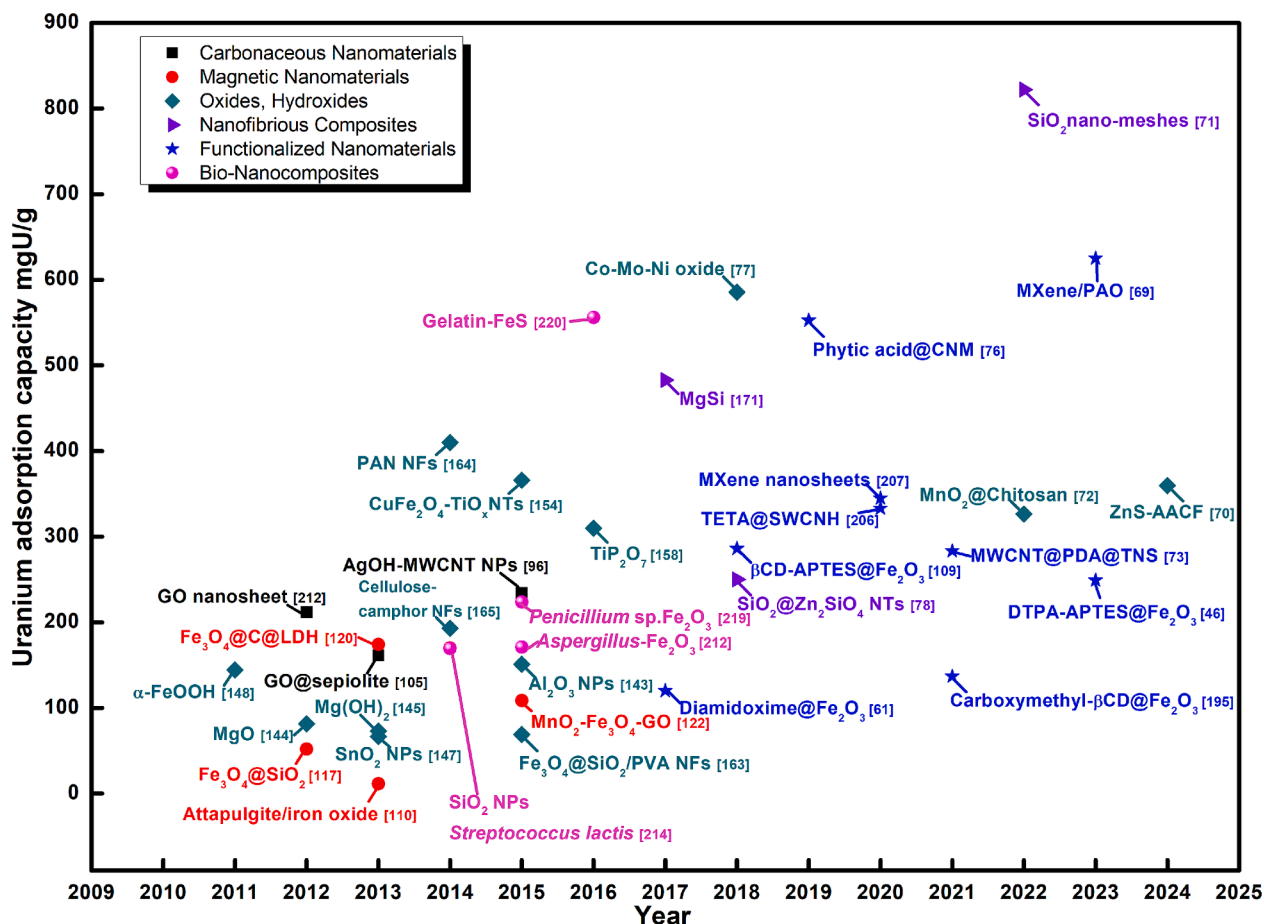


Fig. 19. Development of nanomaterials for uranium extraction from contaminated environmental water and nuclear waste in the last two decades.

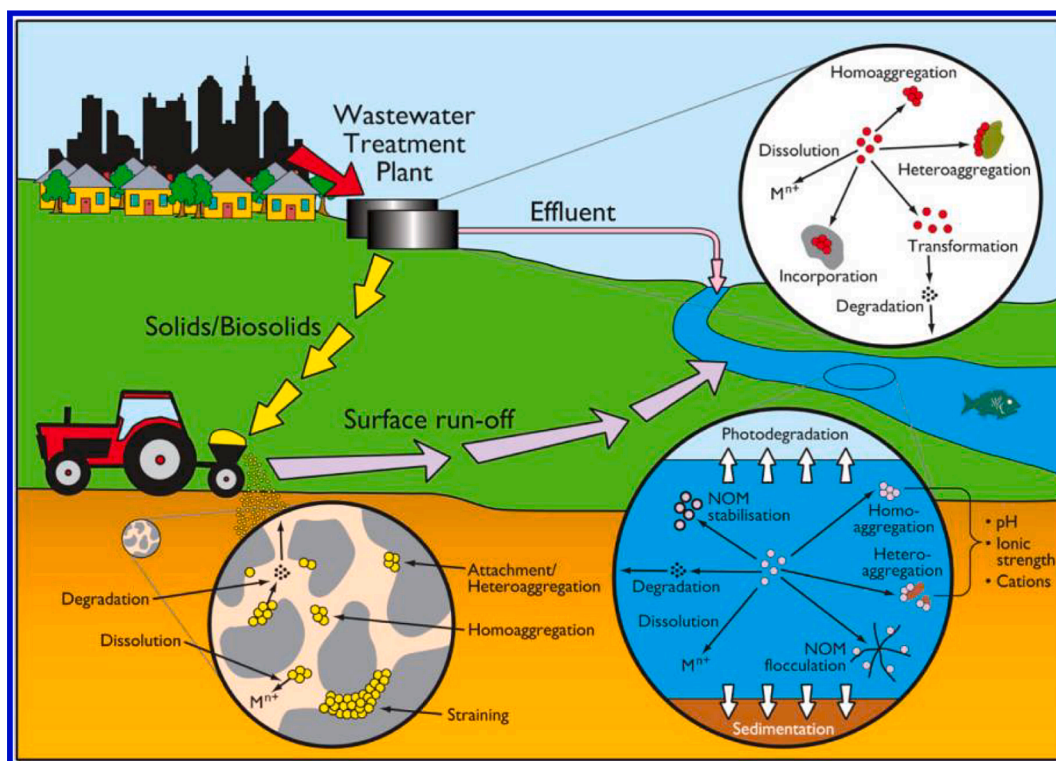


Fig. 20. Potential pathways through which nanomaterials enter the environment (Reprinted with permission from ref. [220]. Copyright 2013, ACS Publications).

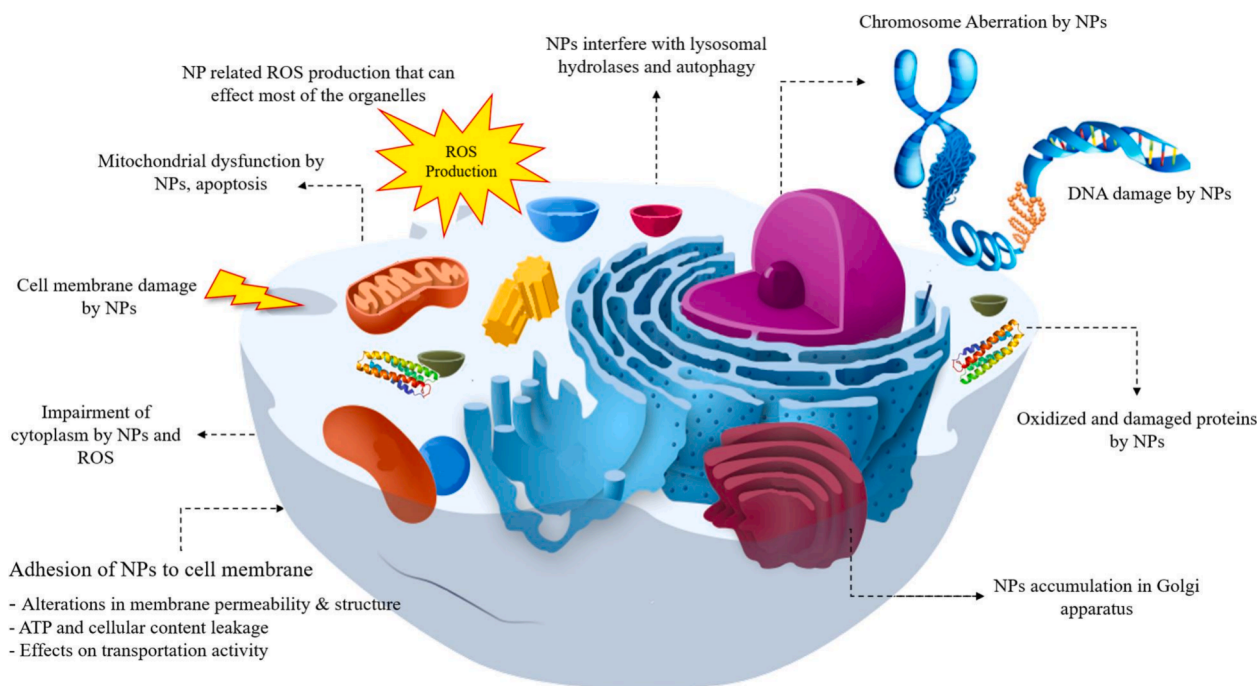


Fig. 21. Different mechanisms of nanotoxicity (Reprinted with permission from ref. [227]).

spectroscopy (TRLFS) improves sensitivity and specificity by isolating uranium fluorescence decay kinetics, effectively minimizing interference from organic compounds. Complexation of U(VI) with phosphoric acid is commonly employed in TRLFS to boost fluorescence intensity and detection efficiency [239]. Inductively Coupled Plasma Optical Emission Spectroscopy (ICP-OES) is another powerful technique for multi-element analysis, offering rapid throughput and robust performance. However, its typical uranium detection limit ( $\sim 20 \mu\text{g/L}$ ) is often insufficient for analyzing natural waters without preconcentration. Despite this limitation, Singhal et al. [240] demonstrated that optimization of emission lines and reduction of spectral interference could extend its detection range down to  $8 \mu\text{g/L}$ , eliminating the need for preconcentration. Similarly, Graphite Furnace Atomic Absorption Spectroscopy (GF-AAS) offers superior sensitivity compared to flame AAS and can detect trace uranium levels effectively. Sensitivity improvements, such as resin preconcentration, have been shown to significantly enhance its capabilities for uranium quantification in challenging matrices [241]. Raman spectroscopy serves as a versatile and non-invasive screening tool for uranium analysis. While its sensitivity is generally lower than that of other techniques, its ability to characterize the molecular structure of uranium compounds and its portability make it particularly useful for field applications and on-site environmental monitoring [242]. Each of these analytical methods has distinct strengths and limitations. Selection of the optimal technique depends on factors such as required sensitivity, sample matrix, portability, and the operational environment, emphasizing the need for a tailored approach to uranium quantification. For isotopic ratio analysis, thermal ionization mass spectrometry (TIMS) is recognized for its exceptional precision and accuracy, making it a standard tool in both geochemical and nuclear science applications. Similarly, magnetic sector ICP-MS is widely employed for uranium isotopic analysis due to its high sensitivity and isotopic resolution. Gamma spectrometry also plays a crucial role in uranium isotopic ratio determination, particularly for environmental and industrial applications. Its non-destructive nature enables rapid and reliable analysis without the need for extensive sample preparation, making it a valuable tool for real-time monitoring and on-site assessments [243].

Significant advancements have been made in the development of sensors and probes for uranium detection, utilizing its electrochemical

properties through techniques such as voltammetry, electrochemical impedance spectroscopy, and potentiometry. Among these, Ion-Selective Electrodes (ISEs) have emerged as a valuable addition to the arsenal of uranium measurement tools, particularly for on-site and real-time monitoring. ISEs operate by employing a uranyl-ion-sensitive membrane that directly interacts with uranium ions in the sample, enabling accurate quantification. These electrodes are prized for their portability, cost-effectiveness, and ease of use. However, their performance is significantly influenced by factors such as pH, ionic strength, and matrix composition [244,245]. The optimal operational pH range for Ion-Selective Electrodes (ISEs) is generally between 3 and 6, a range where uranyl ions ( $\text{UO}_2^{2+}$ ) are the most stable. At lower pH levels, the high concentration of competing hydrogen ions ( $\text{H}^+$ ) can significantly interfere with the electrode's sensitivity and response, diminishing its accuracy. Conversely, at higher pH levels, uranium tends to form carbonate or hydroxide complexes, thereby reducing the concentration of free uranyl ions available for detection. This behavior is consistent with the uranium Pourbaix diagram, as illustrated in Fig. 22 [246], which highlights the speciation and stability of uranium species under varying pH and potential conditions. Understanding these factors is critical for optimizing the performance and reliability of ISEs in uranium quantification. Additionally, the ionic strength of the sample can alter the activity coefficients, affecting the accuracy of the measurement. Matrix composition also plays a critical role, as the presence of interfering ions or complexing agents can degrade the selectivity and sensitivity of the electrode.

Table 8 provides a comprehensive summary of uranium detection techniques, offering a detailed comparison in terms of detection limits, sensitivity, key advantages, and inherent limitations.

The selection of an optimal technique for uranium detection in environmental water hinges on several critical factors, including sensitivity requirements, matrix complexity, operational constraints, and cost-effectiveness. Among the available methods, Inductively Coupled Plasma Mass Spectrometry (ICP-MS) stands as the premier choice due to its unmatched sensitivity, precision, and versatility. Capable of detecting uranium concentrations in the parts-per-trillion (ppt) range, ICP-MS is indispensable for trace-level analysis. Additionally, its ability to conduct isotopic analysis makes it invaluable for environmental tracing,

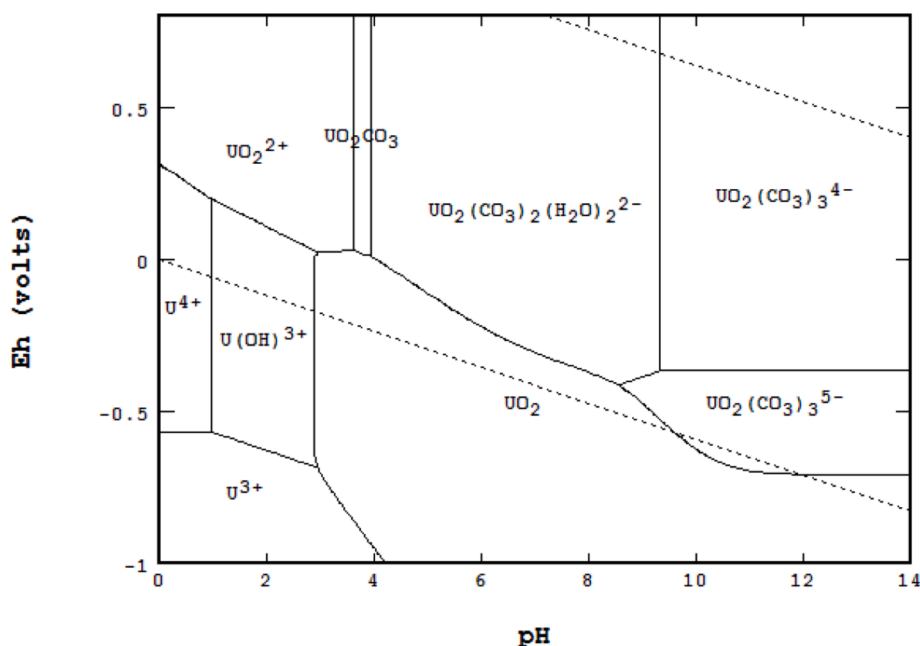


Fig. 22. The Eh-pH diagram of U with  $\log\Sigma\text{CO}_2 = -1$  [246].

**Table 8**  
Different techniques for uranium quantification in environmental water and nuclear waste.

Technique	Sensitivity	Key Advantages	Disadvantages	Detection Limit	References
ICP-MS	Ultra-high	high sensitivity; isotopic analysis; rapid throughput, wide dynamic range	expensive; matrix interferences; sample preparation	$0.4\text{--}2\text{ ng L}^{-1}$	[247,248]
ICP – OES	High	robustness; good sensitivity	high cost and maintenance; complex sample preparation	$8\text{ }\mu\text{g L}^{-1}$ , $2\text{ }\mu\text{g L}^{-1}$ with separation	[251]
Time-resolved laser fluorescence spectroscopy (TRLFS)	Ultra-High	highly selective; minimal sample preparation; portability	matrix interferences; limited to uranium (VI)	$4\text{--}5\text{ ng L}^{-1}$	[239]
Gamma Spectrometry	Moderate	non-destructive; minimal sample preparation	limited to gamma emitters	N/A	[243]
Laser Fluorimetry	High	high sensitivity and precision	expensive; quenching effects; complex operation	$0.2\text{ }\mu\text{g L}^{-1}$ (water), $0.01\text{ Ng L}^{-1}$ (coprecipitate)	[249,250]
LED Fluorimetry	High	cost effective; portability	limited selectivity; dependence on reagents	$0.2\text{ }\mu\text{g L}^{-1}$	[238]
Graphite-furnace AAS	Moderate	direct analysis; cost effective	low throughput; low detection limit; limited dynamic range	$0.2\text{ }\mu\text{g L}^{-1}$	[252]
Electrochemical (Ion Selective Electrode)	Moderate	portability; cost-effective; real-time	pH- and matrix- dependent; moderate accuracy	$0.05\text{ to }5\text{ }\mu\text{mol L}^{-1}$	[253]
Thermal Ionization Mass Spectrometry (TIMS)	Ultra-high	high precision and accuracy; exceptional sensitivity, isotopic analysis	low throughput; complex sample preparation; sample loss; high cost	$0.1\text{ pg mL}^{-1}$	[254,255]
Spectrophotometry	Moderate	no plasma requirement; ease of use	limited sensitivity; interferences; narrow applicability	$16\text{ }\mu\text{g L}^{-1}$	[256]
Alpha spectrometry	High	minimal interference; direct measurement	limited throughput; matrix-dependent sensitivity	$0.22\text{ mBq L}^{-1}$	[257]

contamination assessments, and nuclear forensics. With its capacity to handle complex matrices with minimal interference, ICP-MS excels as the benchmark for laboratory-based, high-precision uranium detection.

For scenarios requiring rapid, on-site assessments, techniques such as laser fluorimetry and Ion-Selective Electrodes (ISEs) provide compelling alternatives. Laser fluorimetry is highly sensitive, portable, and cost-effective, relying on the excitation of uranyl ions to measure fluorescence decay, often enhanced by time-resolved laser fluorescence spectroscopy (TRLFS). This method is ideal for field applications where quick

yet reliable results are paramount. Similarly, ISEs offer real-time monitoring by detecting free uranyl ions through a specialized selective membrane. These electrodes are most effective in a pH range of 3–6, where uranyl ions are most abundant. Outside this range, interference from hydrogen ions at low pH or carbonate complexes at high pH can compromise accuracy. While ISEs are less sensitive than ICP-MS, their portability and simplicity make them practical for routine monitoring. Ultimately, the choice of technique depends on the specific requirements of the application, such as the detection limits, the need for

isotopic analysis, and logistical factors. ICP-MS dominates where precision and ultra-trace detection are required, but its high cost and dependence on advanced instrumentation may limit accessibility. Conversely, laser fluorimetry and ISEs are more practical for rapid, cost-efficient, and field-deployable solutions. The selection process must also consider environmental factors like sample pH, ionic strength, and the presence of interfering species, all of which can impact the performance of methods like ISEs and electrochemical techniques. A thoughtful alignment of analytical needs with the strengths of each technique ensures accurate, efficient, and context-appropriate uranium detection in environmental waters.

## 7. Future Research Directions

To advance the practical applications of nanomaterials in uranium extraction, several research avenues should be pursued. Firstly, increasing the affinity of nanomaterials for uranium separation by enhancing their physicochemical properties, active site density, and ligand density (in the case of ligand-functionalized nanomaterials) is important. Secondly, further investigation into the mechanism of uranium complexation reactions in different environments and conditions is necessary to fabricate highly selective nano-adsorbents with high adsorption rates. Thirdly, developing efficient and non-destructive elution methods to enable recycling and reuse of nanomaterials, which will decrease the capital costs. Fourthly, large-scale studies are needed to validate promising laboratory-scale results. Fifthly, a thorough assessment of the toxicity and environmental hazards of nanomaterials is crucial. Sixthly, direct ligand design can be employed to synthesize more efficient ligands with higher affinity for uranyl ions, even in the presence of competing anions and cations. Furthermore, attention should be given to the stability (chemical, thermal, and mechanical) of nanomaterials-based uranium sorbents. Highly stable nanomaterials are required for uranium decontamination from drinking water, and issues such as core leaching or dissolution should be considered. Thermal stability is a critical factor limiting the application of nanomaterials in the treatment of high-level nuclear waste, while mechanical stability is necessary for shaping nanomaterials for practical applications. Precise control over the structure of nanomaterials, including surface area, particle size, morphologies, and crystal structure, is important as they strongly influence uranium selectivity, adsorption capacity, and reusability.

The translation of nanomaterials for uranium extraction from laboratory research to real-world applications requires overcoming significant barriers. These challenges call for a unified approach that leverages machine learning (ML), computational modeling, and the collaboration of scientists, engineers, policymakers, and industry stakeholders. Together, these efforts can unlock innovative, scalable, and sustainable solutions for uranium remediation in real-world scenarios. ML and computational modeling stand at the forefront of advancing nanomaterial applications for uranium removal. ML algorithms can analyze large datasets of nanomaterial properties, uranium-binding efficiencies, and environmental factors to identify optimal materials tailored for specific conditions. Computational modeling, on the other hand, provides a molecular-level understanding of how uranium interacts with nanomaterials under diverse conditions, such as varying pH, ionic strength, and the presence of competing ions. These tools reduce the reliance on time-consuming experimental processes, enabling researchers to predict the most efficient and durable nanomaterials for field applications. Furthermore, ML can optimize operational parameters, such as adsorption kinetics and flow dynamics, ensuring nanomaterials perform efficiently in large-scale systems while maintaining their structural integrity over extended use. Collaboration between scientists and engineers is crucial to bridging the gap between theoretical innovation and practical application. Scientists contribute fundamental knowledge on the design and functionalization of nanomaterials, such as surface modifications that enhance uranium adsorption or increase

resistance to environmental degradation. Engineers then translate these findings into real-world solutions by developing scalable synthesis methods and integrating nanomaterials into advanced filtration systems, such as adsorption columns, membrane reactors, or hybrid technologies. These collaborative efforts must focus on addressing key real-world challenges, including the cost-effectiveness of nanomaterials, their recyclability, and their long-term durability under extreme environmental conditions. The success of these efforts also hinges on the active involvement of policymakers and industry stakeholders. Policymakers must create an enabling environment by establishing regulatory frameworks that promote the safe development and deployment of nanomaterials while minimizing ecological risks. Incentivizing innovation through grants, public-private partnerships, and tax benefits can accelerate progress. Industry stakeholders bring expertise in scaling up production and deploying nanomaterial-based systems in diverse settings, ranging from municipal water treatment facilities to remote and resource-limited areas.

## 8. Summary and Concluding Remarks

The chemistry of uranium extraction and processing is highly complex, involving various aspects of fundamental physical and inorganic chemistry. Parameters such as complexation, thermodynamics, reaction kinetics, hydrolysis, acid-base equilibria, and the type of ligands all play crucial roles in the extraction process.

Nanomaterials have emerged as promising uranium nano-adsorbents, offering several advantages. Carbonaceous, magnetic, functionalized, and silicon-based nanomaterials, as well as metallic oxide or hydroxide NPs, nanostructured mixed oxides, and bio-nanocomposites, have been used for uranium extraction from various aqueous streams. Carbonaceous nanomaterials, for example, exhibit higher thermal and radiation resistance than organic ion-exchange resins and greater chemical stability than many inorganic sorbents in highly acidic nuclear waste streams. Magnetic nanomaterials show improved adsorption capacity and efficiency for uranium removal. Nano-bioremediation strategies that use microorganisms for the reductive immobilization of U(IV) are considered promising, less expensive alternatives to traditional techniques. Functionalized magnetic nanomaterials are the most promising category due to: (1) the easy separation of the adsorbent from the medium by means of a magnetic field, which makes solid-liquid phase separation fast and simple, as well as highly effective; (2) lower cost and lower consumption of reagents; (3) greater safety; (4) higher selectivity and capacity, and easy automation; (5) high preconcentration factors and eco-friendliness; (6) reusability of the adsorbent (7) the introduction of suitable ligands or functional groups on the surface of MNPs overcomes some disadvantages, such as strong dipole-dipole attractions between particles and their tendency to agglomerate.

## CRedit authorship contribution statement

**Ahmed S. Helal:** Writing – review & editing, Writing – original draft, Visualization, Supervision, Project administration, Methodology, Investigation, Conceptualization. **Miryana Hemadi:** Writing – review & editing, Visualization, Validation, Methodology, Investigation, Conceptualization. **John S. Lomas:** Writing – review & editing. **Souad Ammar:** Visualization, Methodology, Investigation. **Ali Abdelhafiz:** Writing – review & editing, Methodology, Investigation. **Said M. El-Sheikh:** Visualization, Validation. **Sheta M. Sheta:** Visualization, Validation. **Mitchell Galanek:** Writing – review & editing, Visualization, Methodology, Investigation. **Mohamed H. Hassan:** Writing – review & editing, Visualization, Validation, Methodology, Investigation. **Jeng-Kuei Chang:** Writing – review & editing, Visualization, Validation, Methodology, Investigation, Conceptualization. **Ju Li:** Writing – review & editing, Visualization, Validation, Supervision, Conceptualization.

## Declaration of competing interest

The authors declare that they have no known competing financial interests or personal relationships that could have appeared to influence the work reported in this paper.

## Acknowledgments

JL acknowledges support by DTRA, United States (Award No. HDTRA1-20-2-0002) Interaction of Ionizing Radiation with Matter (IIRM, United States) University Research Alliance (URA, United States). MH, JSL and SA acknowledge support by Campus France, France, by the ANR (Agence Nationale de la Recherche, France) and the CGI (Commissariat à l'Investissement d'Avenir, France) through IDEX and Labex SEAM (Science and Engineering for Advanced Materials and devices, France): ANR-13-SECU-0001 (Program DECRET), ANR 11 LABX 086, and ANR 11 IDEX 05 02.

## Data availability

No data was used for the research described in the article.

## References

- [1] M.Z. Jacobson, Review of solutions to global warming, air pollution, and energy security, *Energy Environ. Sci.* 2 (2009) 148–173, <https://doi.org/10.1039/B809990C>.
- [2] Y. Ye, J. Jin, W. Han, S. Miao, Y. Feng, Z. Qin, X. Tang, C. Li, Y. Chen, F. Chen, Y. Wang, Spontaneous electrochemical uranium extraction from wastewater with net electrical energy production, *Nat. Water* 1 (2023) 887–898, <https://doi.org/10.1038/s44221-023-00134-0>.
- [3] Y. Yuan, Q. Yu, M. Cao, L. Feng, S. Feng, T. Liu, T. Feng, B. Yan, Z. Guo, N. Wang, Selective extraction of uranium from seawater with biofouling-resistant polymeric peptide, *Nat. Sustain.* 4 (2021) 708–714, <https://doi.org/10.1038/s41893-021-00709-3>.
- [4] L. Yang, H. Xiao, Y. Qian, X. Zhao, X. Kong, P. Liu, W. Xin, L. Fu, L. Jiang, L. Wen, Bioinspired hierarchical porous membrane for efficient uranium extraction from seawater, *Nat. Sustain.* 5 (2022) 71–80, <https://doi.org/10.1038/s41893-021-00792-6>.
- [5] W. Cui, C. Zhang, W. Jiang, F. Li, R. Liang, J. Liu, J. Qiu, Regenerable and stable sp<sup>2</sup> carbon-conjugated covalent organic frameworks for selective detection and extraction of uranium, *Nat. Commun.* 11 (2020) 436, <https://doi.org/10.1038/s41467-020-14289-x>.
- [6] M. Keener, C. Hunt, T.G. Carroll, V. Kampel, R. Dobrovetsky, T.W. Hayton, G. Ménard, Redox-switchable carboranes for uranium capture and release, *Nature* 577 (2020) 652–655, <https://doi.org/10.1038/s41586-019-1926-4>.
- [7] H. Yang, X. Liu, M. Hao, Y. Xie, X. Wang, H. Tian, G.I.N. Waterhouse, P.E. Kruger, S.G. Telfer, S. Ma, Functionalized Iron–Nitrogen–Carbon Electrocatalyst Provides a Reversible Electron Transfer Platform for Efficient Uranium Extraction from Seawater, *Adv. Mater.* 33 (2021) 2106621, <https://doi.org/10.1002/adma.202106621>.
- [8] W. Zhang, C. Xu, X. Che, T. Wang, S. Willför, M. Li, C. Li, Encapsulating Amidoximated Nanofibrous Aerogels within Wood Cell Tracheids for Efficient Cascading Adsorption of Uranium Ions, *ACS Nano* 16 (2022) 13144–13151, <https://doi.org/10.1021/acsnano.2c06173>.
- [9] Y. Ying, A.M. Pourrahimi, Z. Sofer, S. Matějčková, M. Pumera, Radioactive Uranium Preconcentration via Self-Propelled Autonomous Microrobots Based on Metal–Organic Frameworks, *ACS Nano* 13 (2019) 11477–11487, <https://doi.org/10.1021/acsnano.9b04960>.
- [10] L. Tan, Y. Wang, Q. Liu, J. Wang, X. Jing, L. Liu, J. Liu, D. Song, Enhanced adsorption of uranium (VI) using a three-dimensional layered double hydroxide/graphene hybrid material, *Chem. Eng. J.* 259 (2015) 752–760, <https://doi.org/10.1016/j.cej.2014.08.015>.
- [11] D. Chen, Y. Li, X. Zhao, M. Shi, X. Shi, R. Zhao, G. Zhu, Self-Standing Porous Aromatic Framework Electrodes for Efficient Electrochemical Uranium Extraction, *ACS Cent. Sci.* 9 (2023) 2326–2332, <https://doi.org/10.1021/acscentsci.3c01291>.
- [12] C. Gupta, H. Singh, *Uranium Resource Processing: Secondary Resources*, Springer-Verlag, Berlin, 2003.
- [13] <http://environmentalprogress.org/big-news/2018/10/25/open-letter-to-heads-of-state-of-the-g-20-from-scientists-and-scholars-on-nuclear-for-climate-change> (accessed December, 2024). (n.d.).
- [14] International Atomic Energy Agency (IAEA). Uranium 2016: Resources, Production and Demand; Organisation for Economic Co-operation and Development (OECD) Publishing: 2016, NEA No. 7301.
- [15] J. Pizarro, B. Sainsbury, J.H. Hodgkinson, B. Loechel, Climate change vulnerability assessment for the uranium supply chain in Australia, *Prog. Nucl. Energy* 109 (2018) 53–65, <https://doi.org/10.1016/j.pnucene.2018.07.009>.
- [16] World nuclear association. Plans for New Reactors Worldwide. <http://www.world-nuclear.org/information-library/current-and-future-generation/plans-for-new-reactors-worldwide.aspx> (accessed December, 2024). (n.d.).
- [17] Uranium report 2018, [https://www.resource-capital.ch/fileadmin/reports/2017/Doppelseiten\\_Uran\\_en.pdf](https://www.resource-capital.ch/fileadmin/reports/2017/Doppelseiten_Uran_en.pdf) (accessed December, 2024). (n.d.).
- [18] <https://www.yellowcakeplc.com/uranium-market/#> (accessed December, 2024). (n.d.).
- [19] Outlook for the nuclear fuel, <https://www.neimagazine.com/advanced-reactorsfusion/outlook-for-nuclear-fuel-5946092/?cf-view> (accessed December, 2024). (n.d.).
- [20] Stages of the Nuclear Fuel Cycle. 2018, <https://www.nrc.gov/materials/fuel-cycle-fac/stages-fuel-cycle.html>. (accessed December, 2024). (n.d.).
- [21] C. Rivasseau, E. Farhi, A. Atteia, A. Couté, M. Gromova, D. de Gouvion Saint, A.-M. Cyr, A.-S. Boisson, E. Féré, R.B. Compagnon, An extremely radioresistant green eukaryote for radionuclide bio-decontamination in the nuclear industry, *Energy Environ. Sci.* 6 (2013) 1230–1239, <https://doi.org/10.1039/c2ee23129h>.
- [22] T.M. Morsi, A.M. Elbarbary, M.M. Ghobashy, S.H. Othman, Surface decontamination in fuel manufacture plants by chelating solution of nanoparticles, *Radiochim. Acta* 106 (2018) 383–392, <https://doi.org/10.1515/ract-2017-2849>.
- [23] N. Perlova, Y. Dzyazko, O. Perlova, A. Palchik, V. Sazonova, Formation of Zirconium Hydrophosphate Nanoparticles and Their Effect on Sorption of Uranyl Cations, *Nanoscale Res. Lett.* 12 (2017) 209–217, <https://doi.org/10.1186/s11671-017-1987-y>.
- [24] M.L. Zamora, B.L. Tracy, J.M. Zielinski, D.P. Meyerhof, M.A. Mossf, Chronic Ingestion of Uranium in Drinking Water: A Study of Kidney Bioeffects in Humans Chronic Ingestion of Uranium in Drinking Water A Study of Kidney Bioeffects in Humans, *Toxicol. Sci. Toxicol. Sci.* 43 (1998) 68–77, <https://doi.org/10.1006/toxs.1998.2426>.
- [25] K. Buesseler, M. Aoyama, M. Fukasawa, Impacts of the Fukushima nuclear power plants on marine radioactivity, *Environ. Sci. Technol.* 45 (2011) 9931–9935, <https://doi.org/10.1021/es202816c>.
- [26] M.E. Ibrahim, T.A. Lasheen, H.B. Hassib, A.S. Helal, Separation and Extraction of Uranium from Leach Liquor Containing Uranium and Molybdenum by Solvent Extraction with LIX 622N, *J. Dispers. Sci. Technol.* 35 (2014) 599–606, <https://doi.org/10.1080/01932691.2013.811685>.
- [27] R. Khamirchi, A. Hosseini-Bandegharai, A. Alahabadi, S. Sivamani, A. Rahmani-Sani, T. Shahryari, I. Anastopoulos, M. Miri, H.N. Tran, Adsorption property of BR-PADAP-impregnated multiwall carbon nanotubes towards uranium and its performance in the selective separation and determination of uranium in different environmental samples, *Ecotoxicol. Environ. Saf.* 150 (2018) 136–143, <https://doi.org/10.1016/j.ecoenv.2017.12.039>.
- [28] R. Zarrougui, R. Mdimagh, N. Raouafi, Highly efficient extraction and selective separation of uranium (VI) from transition metals using new class of undiluted ionic liquids based on H-phosphonate anions, *J. Hazard. Mater.* 342 (2018) 464–476, <https://doi.org/10.1016/j.jhazmat.2017.08.057>.
- [29] S. Wu, L. Wang, P. Zhang, H. El-Shall, B. Moudgil, X. Huang, L. Zhao, L. Zhang, Z. Feng, Simultaneous recovery of rare earths and uranium from wet process phosphoric acid using solvent extraction with D2EHPA, *Hydrometall.* 175 (2018) 109–116, <https://doi.org/10.1016/j.hydromet.2017.10.025>.
- [30] R. Selvakumar, G. Ramadoss, M.P. Menon, K. Rajendran, P. Thavamani, R. Naidu, M. Megharaj, Challenges and complexities in remediation of uranium contaminated soils: A review, *J. Environ. Radioact.* 192 (2018) 592–603, <https://doi.org/10.1016/j.jenvrad.2018.02.018>.
- [31] J. Rydberg, M. Cox, C. Musikas, G.R. Choppin (Eds.), *Solvent Extraction Principles and Practice*, CRC Press, Boca Raton, FL, USA, 2004.
- [32] K.L. Nash, G.J. Lumetta, *Advanced separation techniques for nuclear fuel reprocessing and radioactive waste treatment*, Woodhead Publishing Limited, Cambridge, UK, 2011.
- [33] T. Lin, T. Chen, C. Jiao, H. Zhang, K. Hou, H. Jin, Y. Liu, W. Zhu, R. He, Ion pair sites for efficient electrochemical extraction of uranium in real nuclear wastewater, *Nat. Commun.* 15 (2024) 4149, <https://doi.org/10.1038/s41467-024-48564-y>.
- [34] Q. Xin, Q. Wang, K. Luo, Z. Lei, F. Hu, F. Liang, E. Hu, H. Wang, Mechanism of selective uranium adsorption using polyvinyl alcohol/Cyphos IL-101 / reduced graphene oxide composites, *Chem. Eng. J.* 500 (2024) 157256, <https://doi.org/10.1016/j.cej.2024.157256>.
- [35] D. Shen, Q. Du, P. Wang, X. Tian, Y. Wang, R. Feng, J. Pan, Spatially confined conjugation of enzyme immobilized magnetic nanochains with poly(vinylphosphonic acid) polymers using droplet reactors for uranium extraction, *Chem. Eng. J.* 494 (2024) 152970, <https://doi.org/10.1016/j.cej.2024.152970>.
- [36] J. Zhao, Q. Cao, L. Zhao, F. Li, Y. Xin, Y. Liu, W. Zhang, X. Shi, M. Wu, Y. Zhao, Y. Fa, H. Liu, Optimisation of extraction performance for uranium with covalent organic frameworks of  $\beta$ -ketoenamines with different functional groups, *Chem. Eng. J.* 500 (2024) 156246, <https://doi.org/10.1016/j.cej.2024.156246>.
- [37] F. Wang, Z. Chen, Y. Wu, Y. Peng, T. Li, L. Xia, The amidoxime-functionalized magnetic dendritic fibrous nano-silica with a core-shell structure for the efficient capture of U(VI), *Appl. Surf. Sci.* 680 (2025) 161491, <https://doi.org/10.1016/j.apsusc.2024.161491>.
- [38] C. Jin, X. Yang, D. Fang, S. Ni, S. Wang, A. Ding, P. Cen, C. Xiao, Selective separation of radioactive thorium and uranium from scandium using N-heterocyclic carboxamide ligands, *Sep. Purif. Technol.* 328 (2024) 125028, <https://doi.org/10.1016/j.seppur.2023.125028>.
- [39] L.R. Morss, N.M. Edelman, J. Fuger, *The Chemistry of the Actinide and Transactinide Elements (set Vol. 1–6)* (2001), <https://doi.org/10.1007/978-94-007-0211-0>.

- [40] S. Gordon, W. Mulac, K.H. Schmidt, R.K. Sjoblom, J.C. Sullivan, Pulse-radiolysis studies of americium ions in aqueous perchlorate media, *Inorg. Chem.* 17 (1978) 294–296, <https://doi.org/10.1021/ic50180a021>.
- [41] T.E. Albrecht-Schmitt, Organometallic and coordination chemistry of the actinides, *Struct Bond* 127 (2008) 1–85, <https://doi.org/10.1007/978-3-540-77837-0>.
- [42] J.E. Gindler The Radiochemistry of Uranium. National Academy of Sciences, National Research Council 1962 Washington, DC, USA 10.17226/21563.
- [43] T.J. Sorg, P.A. Rebers, Removal of uranium from drinking water by conventional treatment methods, Lewis Publishers Inc, USA, 1991.
- [44] K. Muller, V. Brendler, H. Foerstendorf, Aqueous Uranium(VI) Hydrolysis Species Characterized by Attenuated Total Reflection Fourier-Transform Infrared Spectroscopy, *Inorg. Chem.* 47 (2008) 10127–10134, <https://doi.org/10.1021/ic8005103>.
- [45] C. Degueldre, Uranium as a renewable for nuclear energy, *Prog. Nucl. Energy* 94 (2017) 174–186, <https://doi.org/10.1016/j.pnucene.2016.03.031>.
- [46] Y. Xiao, A.S. Helal, E. Mazario, A. Mayoral, A. Chevillot-Biraud, P. Decorse, R. Losno, F. Maurel, S. Ammar, J.S. Lomas, M. Hémadi, Functionalized maghemite nanoparticles for enhanced adsorption of uranium from simulated wastewater and magnetic harvesting, *Environ. Res.* 216 (2023) 114569, <https://doi.org/10.1016/j.envres.2022.114569>.
- [47] B.F. Parker, Uranium and vanadium binding studies for the selective extraction of uranium from seawater, UC Berkeley. (2017) ProQuest ID: Parker\_berkeley\_0028E\_17236. Merritt ID: ark:/13030/m5vm9876. <https://escholarship.org/uc/item/2mj1f7fp>.
- [48] C.W. Abney, R.T. Mayes, T. Saito, S. Dai, Materials for the Recovery of Uranium from Seawater, *Chem. Rev.* 117 (2017) 13935–14013, <https://doi.org/10.1021/acs.chemrev.7b00355>.
- [49] F. Endrizzi, C.J. Leggett, L. Rao, Scientific Basis for Efficient Extraction of Uranium from Seawater. I: Understanding the Chemical Speciation of Uranium under Seawater Conditions, *Ind. Eng. Chem. Res.* 55 (2016) 4249–4256, <https://doi.org/10.1021/acs.iecr.5b03679>.
- [50] J. Wang, S. Zhuang, Extraction and adsorption of U(VI) from aqueous solution using affinity ligand-based technologies : an overview, *Rev. Environ. Sci. Bio/technology* 18 (2019) 437–452, <https://doi.org/10.1007/s11157-019-09507-y>.
- [51] S. Eldin, M. Babiker, Geochemistry of natural radionuclides in uranium-enriched river catchments, Ph.D thesis (2013) University of Manchester, UK. <https://research.manchester.ac.uk/en/studentTheses/geochemistry-of-natural-radionuclides-in-uranium-enriched-river-c>.
- [52] R. Guillaumont, T. Fanghänel, J. Fuger, I. Grenthe, V. Neck, D.A. Palmer, M. H. Rand, Update on the Chemical Thermodynamics of Uranium, Neptunium, Plutonium, Americium and Technetium, in: *Chemical Thermodynamics, Vol. 5, Elsevier Science Publishers, Amsterdam, Netherlands*, 2003.
- [53] M. Altmaier, E. Yalçintas, X. Gaona, V. Neck, R. Müller, M. Schlieker, T. Fanghänel, Solubility of U (VI) in chloride solutions. I. The stable oxides / hydroxides in NaCl systems, solubility products, hydrolysis constants and SIT coefficients, *J. Chem. Thermodyn.* 114 (2017) 2–13, <https://doi.org/10.1016/j.jct.2017.05.039>.
- [54] V. Neck, J.I. Kim, Solubility and hydrolysis of tetravalent actinides, *Radiochim. Acta* 89 (2001) 1–16, <https://doi.org/10.1524/ract.2001.89.1.001>.
- [55] N. Çevirim-Papaioannou, E. Yalçintas, X. Gaona, K. Dardenne, M. Altmaier, H. Geckeis, Redox chemistry of uranium in reducing, dilute to concentrated NaCl solutions, *Appl. Geochemistry* 98 (2018) 286–300, <https://doi.org/10.1016/j.apgeochem.2018.07.006>.
- [56] M. Khajeh, S. Laurent, K. Dastafkan, Nanoadsorbents : Classification , Preparation, and Applications (with Emphasis on Aqueous Media), *Chem. Rev.* 113 (2013) 7728–7768, <https://doi.org/10.1021/cr400086v>.
- [57] S.A. Cybart, E.Y. Cho, T.J. Wong, B.H. Wehlin, M.K. Ma, C. Huynh, R.C. Dynes, Nano Josephson superconducting tunnel junctions in YBa2Cu3O7- $\delta$  directly patterned with a focused helium ion beam, *Nat. Nanotechnol.* 10 (2015) 598–602, <https://doi.org/10.1038/nnano.2015.76>.
- [58] G. Sahay, W. Querbes, C. Alabi, A. Eltouky, S. Sarkar, C. Zurenko, E. Karagiannis, K. Love, D. Chen, R. Zoncu, Y. Buganin, A. Schroeder, R. Langer, D.G. Anderson, Efficiency of siRNA delivery by lipid nanoparticles is limited by endocytic recycling, *Nat. Biotechnol.* 13 (2013) 653–658, <https://doi.org/10.1038/nbt.2614>.
- [59] J. Liu, N.P. Wickramaratne, S.Z. Qiao, M. Jaroniec, Molecular-based design and emerging applications of nanoporous carbon spheres, *Nat. Mater.* 14 (2015) 763–774, <https://doi.org/10.1038/nmat4317>.
- [60] E. Vunain, A.K. Mishra, B.B. Mamba, Dendrimers, mesoporous silicas and chitosan-based nanosorbents for the removal of heavy-metal ions: A review, *Int. J. Biol. Macromol.* 86 (2016) 570–586, <https://doi.org/10.1016/j.ijbiomac.2016.02.005>.
- [61] E. Mazario, A.S. Helal, J. Stemper, A. Mayoral, P. Decorse, A. Chevillot-Biraud, S. Novak, C. Perruchot, C. Lion, R. Losno, T. Le Gall, S. Ammar, J.M. El Hage Chahine, M. Hémadi, Maghemite nanoparticles bearing di(amidoxime) groups for the extraction of uranium from wastewaters, *AIP Adv.* 7 (2017) 056702, <https://doi.org/10.1063/1.4973436>.
- [62] C. Li, Z. Zhuang, F. Huang, Z. Wu, Y. Hong, Z. Lin, Recycling Rare Earth Elements from Industrial Wastewater with Flowerlike Nano-Mg(OH)2, *ACS Appl. Mater. Interfaces* 5 (2013) 9719–9725, <https://doi.org/10.1021/am4027967>.
- [63] Q. Cao, F. Huang, Z. Zhuang, Z. Lin, A study of the potential application of nano-Mg(OH)2 in adsorbing low concentrations of uranyl tricarbonate from water, *Nanoscale* 4 (2012) 2423, <https://doi.org/10.1039/c2nr11993e>.
- [64] X. Tan, Q. Fan, X. Wang, B. Grambow, Eu(III) Sorption to TiO2 (Anatase and Rutile): Batch, XPS, and EXAFS Studies, *Environ. Sci. Technol.* 43 (2009) 3115–3121, <https://doi.org/10.1021/es803431c>.
- [65] A.S. Helal, P. Decorse, C. Perruchot, S. Novak, C. Lion, S. Ammar, J.M. El Hage Chahine, M. Hémadi, Functionalized magnetic nanoparticles for the decontamination of water polluted with cesium, *AIP Adv.* 6 (2016) 056601, <https://doi.org/10.1063/1.4942825>.
- [66] P. Singhal, S.K. Jha, S.P. Pandey, S. Neogy, Rapid extraction of uranium from sea water using Fe3O4 and humic acid coated Fe3O4 nanoparticles, *J. Hazard. Mater.* 335 (2017) 152–161, <https://doi.org/10.1016/j.jhazmat.2017.04.043>.
- [67] C. Jing, S. Landsberger, Y.L. Li, The application of illite supported nanoscale zero valent iron for the treatment of uranium contaminated groundwater, *J. Environ. Radioact.* 175–176 (2017) 1–6, <https://doi.org/10.1016/j.jenvrad.2017.04.003>.
- [68] W. Li, L.D. Troyer, S.S. Lee, J. Wu, C. Kim, B.J. Lafferty, J.G. Catalano, J. D. Fortner, Engineering Nanoscale Iron Oxides for Uranyl Sorption and Separation: Optimization of Particle Core Size and Bilayer Surface Coatings, *ACS Appl. Mater. Interfaces* 9 (2017) 13163–13172, <https://doi.org/10.1021/acsaami.7b01042>.
- [69] Y. Zhou, J. Yang, N. Zhou, H. Hao, X. Jiang, F. Lei, K. Shi, Y. Zhao, G. Zhou, T. Liu, S. Xing, Amidoxime-Functionalized MXene beads for the effective capture of uranium from wastewater with high fluoride concentrations, *Chem. Eng. J.* 471 (2023) 144647, <https://doi.org/10.1016/j.cej.2023.144647>.
- [70] L. Yang, X. Zeng, J. Tang, H. Sun, J. Liu, Y. Guo, W. Liu, M. Feng, X. Huang, Rapid and selective uranium adsorption by a low-cost, eco-friendly, and in-situ prepared nano-ZnS/alkali-activated collagen fiber composite, *Sep. Purif. Technol.* 333 (2024) 125856, <https://doi.org/10.1016/j.seppur.2023.125856>.
- [71] Q. Chen, X. Xue, Y. Liu, A. Guo, K. Chen, J. Yin, F. Yu, H. Zhu, X. Guo, Shear-induced fabrication of SiO2 nano-meshes for efficient uranium capture, *J. Hazard. Mater.* 438 (2022) 129524, <https://doi.org/10.1016/j.jhazmat.2022.129524>.
- [72] S. Wang, J. Ma, C. Wang, W. Xi, Y. Bai, W. Lu, J. Wang, Elimination of radionuclide uranium (VI) from aqueous solutions using an  $\alpha$ -MnO2@CTS composite adsorbent, *J. Mol. Liq.* 360 (2022) 119448, <https://doi.org/10.1016/j.molliq.2022.119448>.
- [73] Y. Zhou, Y. Li, D. Liu, D. Liu, L. Xu, C. Liu, Adsorption optimization of uranium (VI) onto polydopamine and sodium titanate co-functionalized MWCNTs using response surface methodology and a modeling approach, *Colloids Surf.* 627 (2021) 127145, <https://doi.org/10.1016/j.colsurfa.2021.127145>.
- [74] J. Xiong, J. Chen, Y. Han, J. Ma, S. Liu, Z. Xu, X. Liu, X. Tong, J. Luo, Graphene oxide sheathed cobalt vanadate porous nanospheres for enhanced uranium extraction, *J. Solid State Chem.* 322 (2023) 123972, <https://doi.org/10.1016/j.jssc.2023.123972>.
- [75] J. Zhao, P. Lu, T. He, Q. Zhang, J. Huang, Y. Liu, X. Zhao, Y. Wang, Z. Liu, D. Yuan, Synthesis of core-shell magnetic nanocomposite bearing phosphonic acid ligand for uranium extraction from strong HNO3 solution, *Chem. Eng. J.* 468 (2023) 143398, <https://doi.org/10.1016/j.cej.2023.143398>.
- [76] L. Li, R. Ma, T. Wen, P. Gu, S. Zhang, M. Zheng, X. Wu, X. Zhang, T. Hayat, X. Wang, Functionalization of carbon nanomaterials by means of phytic acid for uranium enrichment, *Sci. Total Env.* 694 (2019) 13369, <https://doi.org/10.1016/j.scitotenv.2019.133697>.
- [77] S. Yu, L. Yin, H. Pang, Y. Wu, X. Wang, P. Zhang, B. Hu, Z. Chen, X. Wang, Constructing sphere-like cobalt-molybdenum-nickel ternary hydroxide and calcined ternary oxide nanocomposites for efficient removal of U(VI) from aqueous solutions, *Chem. Eng. J.* 352 (2018) 360–370, <https://doi.org/10.1016/j.cej.2018.07.033>.
- [78] S. Tripathi, A. Roy, S. Nair, S. Durani, R. Bose, Removal of U(VI) from aqueous solution by adsorption onto synthesized silica and zinc silicate nanotubes: Equilibrium and kinetic aspects with application to real samples, *Environ. Nanotechnol. Monit. Manag.* 10 (2018) 127–139, <https://doi.org/10.1016/j.enmm.2018.05.003>.
- [79] S. Ijima, Helicoidal microtubules of graphitic carbon, *Nature* 354 (1991) 56–58, <https://doi.org/10.1038/354056a0>.
- [80] C. Herrero-Latorre, J. Álvarez-Méndez, J. Barciela-García, S. García-Martín, R. M. Peña-Creciente, Characterization of carbon nanotubes and analytical methods for their determination in environmental and biological samples: A review, *Anal. Chim. Acta* 853 (2015) 77–94, <https://doi.org/10.1016/j.aca.2014.10.008>.
- [81] R.B. Rakhi, K. Sethupathi, S. Ramaprabhu, Synthesis and hydrogen storage properties of carbon nanotubes, *Int. J. Hydrogen Energy* 33 (2008) 381–386, <https://doi.org/10.1016/j.ijhydene.2007.07.037>.
- [82] L. Niu, Y. Luo, Z. Li, A highly selective chemical gas sensor based on functionalization of multi-walled carbon nanotubes with poly(ethylene glycol), *Sensors Actuators B Chem.* 126 (2007) 361–367, <https://doi.org/10.1016/j.snb.2007.03.018>.
- [83] A. Schierz, H. Zänker, Aqueous suspensions of carbon nanotubes: Surface oxidation, colloidal stability and uranium sorption, *Environ. Pollut.* 157 (2009) 1088–1094, <https://doi.org/10.1016/j.envpol.2008.09.045>.
- [84] M.Y. Shao, D.Z. Jiang, X. Wang, J. Li, Plasma Induced Grafting Carboxymethyl Cellulose on Multiwalled Carbon Nanotubes for the Removal of UO22+ from Aqueous Solution, *J. Phys. Chem. B* 113 (2009) 860–864.
- [85] Y. Sun, S. Yang, G. Sheng, Z. Guo, X. Wang, The removal of U(VI) from aqueous solution by oxidized multiwalled carbon nanotube, *J. Environ. Radioact.* 105 (2012) 40–47, <https://doi.org/10.1016/j.jenvrad.2011.10.009>.
- [86] D. Shao, J. Hu, X. Wang, Plasma induced grafting multiwalled carbon nanotube with chitosan and its application for removal of UO2+2, Cu2+, and Pb2+ from aqueous solutions, *Plasma Process. Polym.* 7 (2010) 977–985, <https://doi.org/10.1002/ppap.201000062>.

- [87] M. Wang, J. Qiu, X. Tao, C. Wu, W. Cui, Q. Liu, S. Lu, Effect of pH and ionic strength on U(IV) sorption to oxidized multiwalled carbon nanotubes, *J. Radioanal. Nucl. Chem.* 288 (2011) 895–901, <https://doi.org/10.1007/s10967-011-1018-x>.
- [88] M. Song, Q. Wang, Y. Meng, Removal of UO<sub>2</sub><sup>2+</sup> from aqueous solution by plasma functionalized MWCNTs, *J. Radioanal. Nucl. Chem.* 293 (2012) 899–906, <https://doi.org/10.1007/s10967-012-1751-9>.
- [89] M. Xin, X. Dai, J. Han, M. Jin, C.A. Jimenez-Cruz, D. Ding, Z. Wang, R. Zhou, Carbon nanotubes adsorb U atoms differently in their inner and outer surfaces, *RSC Adv.* 4 (2014) 30074–30080, <https://doi.org/10.1039/C4RA02662D>.
- [90] A.C. do Lago, G. de F. Lima, M.G. Segatelli, C.R.T. Tarley, Highly sensitive ion preconcentration method based on flow sorbent extraction using multiwall carbon nanotubes, *Int. J. Environ. Anal. Chem.* 92 (2012) 767–782, <https://doi.org/10.1080/03067319.2010.548090>.
- [91] D. Peng, L. Yu, J. Yu, F. Jiao, Z. Peng, T. Zhang, Preparation of D-tartaric Acid Modified Multi-walled Carbon Nanotubes for Resolution of Propranolol Enantiomers, *Curr. Nanosci.* 9 (2013) 631–634, <https://doi.org/10.2174/15734137113099990061>.
- [92] I.I. Fasfous, J.N. Dawoud, Uranium (VI) sorption by multiwalled carbon nanotubes from aqueous solution, *Appl. Surf. Sci.* 259 (2012) 433–440, <https://doi.org/10.1016/j.apsusc.2012.07.062>.
- [93] P. Zong, J. Gou, Rapid and economical synthesis of magnetic multiwalled carbon nanotube/iron oxide composite and its application in preconcentration of U(VI), *J. Mol. Liq.* 195 (2014) 92–98, <https://doi.org/10.1016/j.molliq.2014.02.002>.
- [94] E. Zolfonoun, S.R. Yousefi, Sorption and preconcentration of uranium and thorium from aqueous solutions using multi-walled carbon nanotubes decorated with magnetic nanoparticles, *Radiochim. Acta* 103 (2015) 835–841, <https://doi.org/10.1515/ract-2015-2466>.
- [95] L. Tan, Q. Liu, X. Jing, J. Liu, D. Song, S. Hu, L. Liu, J. Wang, Removal of uranium (VI) ions from aqueous solution by magnetic cobalt ferrite/multiwalled carbon nanotubes composites, *Chem. Eng. J.* 273 (2015) 307–315, <https://doi.org/10.1016/j.cej.2015.01.110>.
- [96] F. Zare, M. Ghaedi, A. Daneshfar, S. Agarwal, I. Tyagi, T.A. Saleh, V.K. Gupta, Efficient removal of radioactive uranium from solvent phase using AgOH-MWCNTs nanoparticles: Kinetic and thermodynamic study, *Chem. Eng. J.* 273 (2015) 296–306, <https://doi.org/10.1016/j.cej.2015.03.002>.
- [97] A.K. Geim, K.S. Novoselov, The rise of graphene, *Nature Mater* 6 (2007) 183–191, <https://doi.org/10.1038/nmat1849>.
- [98] P. Lian, X. Zhu, S. Liang, Z. Li, W. Yang, H. Wang, Large reversible capacity of high quality graphene sheets as an anode material for lithium-ion batteries, *Electrochim. Acta* 55 (2010) 3909–3914, <https://doi.org/10.1016/j.electacta.2010.02.025>.
- [99] Z. Li, F. Chen, L. Yuan, Y. Liu, Y. Zhao, Z. Chai, W. Shi, Uranium(VI) adsorption on graphene oxide nanosheets from aqueous solutions, *Chem. Eng. J.* 210 (2012) 539–546, <https://doi.org/10.1016/j.cej.2012.09.030>.
- [100] Y. Shen, Q. Fang, B. Chen, Environmental applications of three-dimensional graphene-based macrostructures: Adsorption, transformation, and detection, *Environ. Sci. Technol.* 49 (2015) 67–84, <https://doi.org/10.1021/es504421y>.
- [101] S. Yu, X. Wang, X. Tan, X. Wang, Sorption of radionuclides from aqueous systems onto graphene oxide-based materials: a review, *Inorg. Chem. Front.* 2 (2015) 593–612, <https://doi.org/10.1039/C4QI00221K>.
- [102] Y. Guo, Y. Guo, X. Wang, P. Li, L. Kong, G. Wang, X. Li, Y. Liu, Enhanced photocatalytic reduction activity of uranium(VI) from aqueous solution using the Fe<sub>2</sub>O<sub>3</sub>-graphene oxide nanocomposite, *Dalt. Trans.* 46 (2017) 14762–14770, <https://doi.org/10.1039/C7DT02639K>.
- [103] T. Xinquan, Y. Xiaobo, L. Songsheng, W. Mingming, Efficient removal of radionuclide U(VI) from aqueous solutions by using graphene oxide nanosheets, *J. Radioanal. Nucl. Chem.* 303 (2015) 245–253, <https://doi.org/10.1007/s10967-014-3429-y>.
- [104] G. Zhao, T. Wen, X. Yang, S. Yang, J. Liao, J. Hu, D. Shao, X. Wang, Preconcentration of U(vi) ions on few-layered graphene oxide nanosheets from aqueous solutions, *Dalt. Trans.* 41 (2012) 6182–6188, <https://doi.org/10.1039/c2dt00054g>.
- [105] H. Cheng, K. Zeng, J. Yu, Adsorption of uranium from aqueous solution by graphene oxide nanosheets supported on sepiolite, *J. Radioanal. Nucl. Chem.* 298 (2013) 599–603, <https://doi.org/10.1007/s10967-012-2406-6>.
- [106] Z. Gu, Y. Wang, J. Tang, J. Yang, J. Liao, Y. Yang, N. Liu, The removal of uranium (VI) from aqueous solution by graphene oxide-carbon nanotubes hybrid aerogels, *J. Radioanal. Nucl. Chem.* 303 (2015) 1835–1842, <https://doi.org/10.1007/s10967-014-3795-5>.
- [107] Y. Liang, L. Yu, R. Yang, X. Li, L. Qu, J. Li, High sensitive and selective graphene oxide/molecularly imprinted polymer electrochemical sensor for 2,4-dichlorophenol in water, *Sensors Actuators, B Chem.* 240 (2017) 1330–1335, <https://doi.org/10.1016/j.snb.2016.08.137>.
- [108] S. Duan, X. Xu, X. Liu, Y. Wang, T. Hayat, A. Alsaedi, Y. Meng, J. Li, Highly enhanced adsorption performance of U(VI) by non-thermal plasma modified magnetic Fe<sub>3</sub>O<sub>4</sub> nanoparticles, *J. Colloid Interface Sci.* 513 (2018) 92–103, <https://doi.org/10.1016/j.jcis.2017.11.008>.
- [109] A.S. Helal, E. Mazario, A. Mayoral, P. Decorse, R. Losno, C. Lion, S. Ammar, M. Hémadi, Highly efficient and selective extraction of uranium from aqueous solution using a magnetic device: succinyl-β-cyclodextrin-APTES@maghemite nanoparticles, *Environ. Sci. Nano* 5 (2018) 158–168, <https://doi.org/10.1039/C7EN00902J>.
- [110] L. Chen, J. Xu, J. Hu, Removal of U(VI) from aqueous solutions by using attapulgite/iron oxide magnetic nanocomposites, *J. Radioanal. Nucl. Chem.* 297 (2013) 97–105, <https://doi.org/10.1007/s10967-012-2360-3>.
- [111] T. Madrakian, M. Rahimi, A. Afkhami, Removal, preconcentration and spectrophotometric determination of U(VI) from water samples using modified maghemite nanoparticles, *J. Radioanal. Nucl. Chem.* 291 (2012) 597–602, <https://doi.org/10.1007/s10967-011-1453-8>.
- [112] A. Etale, H. Tutu, D.C. Drake, Application of maghemite nanoparticles as sorbents for the removal of Cu(II), Mn(II) and U(VI) ions from aqueous solution in acid mine drainage conditions, *Appl. Water Sci.* 6 (2016) 187–197, <https://doi.org/10.1007/s13201-014-0217-3>.
- [113] D.M. Singer, S.M. Chatman, E.S. Ilton, K.M. Rosso, J.F. Banfield, G.A. Waychunas, Identification of simultaneous U(VI) sorption complexes and U(IV) nanoprecipitates on the magnetite (111) surface, *Environ. Sci. Technol.* 46 (2012) 3811–3820, <https://doi.org/10.1021/es203877x>.
- [114] E.K. Leshar, J.F. Ranville, B.D. Honeyman, Analysis of pH Dependent Uranium (VI) Sorption to Nanoparticulate Hematite by Flow Field-Flow Fractionation - Inductively Coupled Plasma Mass Spectrometry, *Environ. Sci. Technol.* 43 (2009) 5403–5409, <https://doi.org/10.1021/es900592r>.
- [115] Z. Dai, H. Zhang, Y. Sui, D. Ding, N. Hu, L. Li, Y. Wang, Synthesis and characterization of a novel core-shell magnetic nanocomposite via surface-initiated RAFT polymerization for highly efficient and selective adsorption of uranium (VI), *J. Radioanal. Nucl. Chem.* 9 (2018) 1–14, <https://doi.org/10.1007/s10967-018-5720-9>.
- [116] D. Das, M.K. Sureshkumar, S. Koley, N. Mithal, C.G.S. Pillai, Sorption of uranium on magnetite nanoparticles, *J. Radioanal. Nucl. Chem.* 285 (2010) 447–454, <https://doi.org/10.1007/s10967-010-0627-0>.
- [117] F.L. Fan, Z. Qin, J. Bai, W.D. Rong, F.Y. Fan, W. Tian, X.L. Wu, Y. Wang, L. Zhao, Rapid removal of uranium from aqueous solutions using magnetic Fe<sub>3</sub>O<sub>4</sub>@SiO<sub>2</sub> composite particles, *J. Environ. Radioact.* 106 (2012) 40–46, <https://doi.org/10.1016/j.jenvrad.2011.11.003>.
- [118] J. Wei, X. Zhang, Q. Liu, Z. Li, L. Liu, J. Wang, Magnetic separation of uranium by CoFe<sub>2</sub>O<sub>4</sub> hollow spheres, *Chem. Eng. J.* 241 (2014) 228–234, <https://doi.org/10.1016/j.cej.2013.12.035>.
- [119] X. Zhang, J. Wang, Preparation of carbon coated Fe<sub>3</sub>O<sub>4</sub> nanoparticles for magnetic separation of uranium, *Solid State Sci.* 75 (2018) 14–20, <https://doi.org/10.1016/j.solidstatesciences.2017.11.003>.
- [120] X. Zhang, J. Wang, R. Li, Q. Dai, Preparation of Fe<sub>3</sub>O<sub>4</sub>@C@Layered Double Hydroxide composite for magnetic separation of uranium, *Ind. Eng. Chem. Res.* 52 (2013) 10152–10159, <https://doi.org/10.1021/ie3024438>.
- [121] P. Zong, S. Wang, Y. Zhao, H. Wang, H. Pan, C. He, Synthesis and application of magnetic graphene/iron oxides composite for the removal of U(VI) from aqueous solutions, *Chem. Eng. J.* 220 (2013) 45–52, <https://doi.org/10.1016/j.cej.2013.01.038>.
- [122] L. Tan, J. Wang, Q. Liu, Y. Sun, X. Jing, L. Liu, J. Liu, D. Song, The synthesis of a manganese dioxide-iron oxide-graphene magnetic nanocomposite for enhanced uranium(VI) removal, *New J. Chem.* 39 (2015) 868–876, <https://doi.org/10.1039/C4NJ01256A>.
- [123] S. Yan, B. Hua, Z. Bao, J. Yang, C. Liu, B. Deng, Uranium(VI) removal by nanoscale zerovalent iron in anoxic batch systems, *Environ. Sci. Technol.* 44 (2010) 7783–7789, <https://doi.org/10.1021/es9036308>.
- [124] R.A. Crane, H. Pullin, T.B. Scott, The influence of calcium, sodium and bicarbonate on the uptake of uranium onto nanoscale zero-valent iron particles, *Chem. Eng. J.* 277 (2015) 252–259, <https://doi.org/10.1016/j.cej.2015.03.085>.
- [125] S. Klimkova, M. Cernik, L. Lacinova, J. Filip, D. Jancik, R. Zboril, Zero-valent iron nanoparticles in treatment of acid mine water from in situ uranium leaching, *Chemosphere* 82 (2011) 1178–1184, <https://doi.org/10.1016/j.chemosphere.2010.11.075>.
- [126] S. Yan, Y. Chen, W. Xiang, Z. Bao, C. Liu, B. Deng, Uranium(VI) reduction by nanoscale zero-valent iron in anoxic batch systems: The role of Fe(II) and Fe(III), *Chemosphere* 117 (2014) 625–630, <https://doi.org/10.1016/j.chemosphere.2014.09.087>.
- [127] Y. Sun, C. Ding, W. Cheng, X. Wang, Simultaneous adsorption and reduction of U(VI) on reduced graphene oxide-supported nanoscale zerovalent iron, *J. Hazard. Mater.* 280 (2014) 399–408, <https://doi.org/10.1016/j.jhazmat.2014.08.023>.
- [128] W.-X. Zhang, C.-B. Wang, Synthesizing Nanoscale Iron Particles for Rapid and Complete Dechlorination of TCE and PCBs, *Environ. Sci. Technol.* 31 (1997) 2154–2156, <https://doi.org/10.1021/es970039c>.
- [129] R.A. Crane, T.B. Scott, Nanoscale zero-valent iron: Future prospects for an emerging water treatment technology, *J. Hazard. Mater.* 211–212 (2012) 112–125, <https://doi.org/10.1016/j.jhazmat.2011.11.073>.
- [130] R.A. Crane, C. Noubactep, Elemental metals for environmental remediation: Lessons from hydrometallurgy, *Fresenius Environ. Bull.* 21 (2012) 1192–1196.
- [131] R.A. Crane, T. Scott, The removal of uranium onto carbon-supported nanoscale zero-valent iron particles, *J. Nanoparticle Res.* 16 (2014) 2813, <https://doi.org/10.1007/s11051-014-2813-4>.
- [132] R.A. Crane, M. Dickinson, T.B. Scott, Nanoscale zero-valent iron particles for the remediation of plutonium and uranium contaminated solutions, *Chem. Eng. J.* 262 (2015) 319–325, <https://doi.org/10.1016/j.cej.2014.09.084>.
- [133] Y. Shin, S. Bae, W. Lee, Formation of surface mediated iron colloids during U(VI) and nZVI interaction, *Adv. Environ. Res.* 2 (2013) 167–177, <https://doi.org/10.12989/aer.2013.2.3.167>.
- [134] R.A. Crane, M. Dickinson, I.C. Popescu, T.B. Scott, Magnetite and zero-valent iron nanoparticles for the remediation of uranium contaminated environmental water, *Water Res.* 45 (2011) 2931–2942, <https://doi.org/10.1016/j.watres.2011.03.012>.
- [135] O. Riba, T.B. Scott, K.V. Ragnarsdottir, G.C. Allen, Reaction mechanism of uranyl in the presence of zero-valent iron nanoparticles, *Geochim. Cosmochim. Acta* 72 (2008) 4047–4057, <https://doi.org/10.1016/j.gca.2008.04.041>.

- [136] M. Dickinson, T.B. Scott, The application of zero-valent iron nanoparticles for the remediation of a uranium-contaminated waste effluent, *J. Hazard. Mater.* 178 (2010) 171–179, <https://doi.org/10.1016/j.jhazmat.2010.01.060>.
- [137] Z.J. Li, L. Wang, L.Y. Yuan, C.L. Xiao, L. Mei, L.R. Zheng, J. Zhang, J.H. Yang, Y. L. Zhao, Z.T. Zhu, Z.F. Chai, W.Q. Shi, Efficient removal of uranium from aqueous solution by zero-valent iron nanoparticle and its graphene composite, *J. Hazard. Mater.* 290 (2015) 26–33, <https://doi.org/10.1016/j.jhazmat.2015.02.028>.
- [138] G. Sheng, X. Shao, Y. Li, J. Li, H. Dong, W. Cheng, X. Gao, Y. Huang, Enhanced removal of uranium(VI) by nanoscale zerovalent iron supported on Na-bentonite and an investigation of mechanism, *J. Phys. Chem. A* 118 (2014) 2952–2958, <https://doi.org/10.1021/jp412404w>.
- [139] L. Ling, W.X. Zhang, Enrichment and Encapsulation of Uranium with Iron Nanoparticle, *J. Am. Chem. Soc.* 137 (2015) 2788–2791, <https://doi.org/10.1021/ja510488r>.
- [140] M.J. Comarmond, T.E. Payne, J.J. Harrison, S. Thiruvoth, H.K. Wong, R. D. Aughterson, G.R. Lumpkin, K. Müller, H. Foersterdorf, Uranium sorption on various forms of titanium dioxide - Influence of surface area, surface charge, and impurities, *Environ. Sci. Technol.* 45 (2011) 5536–5542, <https://doi.org/10.1021/es201046x>.
- [141] Y. Sun, S. Yang, G. Sheng, Z. Guo, X. Tan, J. Xu, X. Wang, Comparison of U(VI) removal from contaminated groundwater by nanoporous alumina and non-nanoporous alumina, *Sep. Purif. Technol.* 83 (2011) 196–203, <https://doi.org/10.1016/j.seppur.2011.09.050>.
- [142] H.B. Jung, M.I. Boyanov, H. Konishi, Y. Sun, B. Mishra, K.M. Kemner, E.E. Roden, H. Xu, Redox behavior of uranium at the nanoporous aluminum oxide-water interface: Implications for uranium remediation, *Environ. Sci. Technol.* 46 (2012) 7301–7309, <https://doi.org/10.1021/es2044163>.
- [143] L. Qian, M. Ma, D. Cheng, Adsorption and desorption of uranium on nano goethite and nano alumina, *J. Radioanal. Nucl. Chem.* 303 (2015) 161–170, <https://doi.org/10.1007/s10967-014-3352-2>.
- [144] Z. Camtakan, S. Erenturk, S. Yusan, Magnesium Oxide Nanoparticles: Preparation, Characterization, and Uranium Sorption Properties, *Environ. Prog. Sustain. Energy* 31 (2012) 536–543, <https://doi.org/10.1002/ep.10575>.
- [145] Z. Chen, Z. Zhuang, Q. Cao, X. Pan, X. Guan, Z. Lin, Adsorption-Induced Crystallization of U-Rich Nanocrystals on Nano-Mg(OH)<sub>2</sub> and the Aqueous Uranyl Enrichment, *ACS Appl. Mater. Interfaces* 6 (2013) 1301–1305, <https://doi.org/10.1021/am405306j>.
- [146] L. Tan, X. Zhang, Q. Liu, X. Jing, J. Liu, D. Song, S. Hu, L. Liu, J. Wang, Synthesis of Fe<sub>3</sub>O<sub>4</sub>@TiO<sub>2</sub> core-shell magnetic composites for highly efficient sorption of uranium (VI), *Colloids Surfaces A Physicochem. Eng. Asp.* 469 (2015) 279–286, <https://doi.org/10.1016/j.colsurfa.2015.01.040>.
- [147] A. Nilchi, T.S. Dehaghan, S.R. Garmarodi, Kinetics, isotherm and thermodynamics for uranium and thorium ions adsorption from aqueous solutions by crystalline tin oxide nanoparticles, *Desalination* 321 (2013) 67–71, <https://doi.org/10.1016/j.desal.2012.06.022>.
- [148] S.D. Yusan, S.A. Erenturk, Sorption behaviors of uranium (VI) ions on  $\alpha$ -FeOOH, *Desalination* 269 (2011) 58–66, <https://doi.org/10.1016/j.desal.2010.10.042>.
- [149] T. Yousefi, A.R. Khanchi, S.J. Ahmadi, M.K. Rofouei, R. Yavari, R. Davarkhah, B. Myanji, Cerium(III) molybdate nanoparticles: Synthesis, characterization and radionuclides adsorption studies, *J. Hazard. Mater.* 215–216 (2012) 266–271, <https://doi.org/10.1016/j.jhazmat.2012.02.064>.
- [150] C. Banerjee, N. Dudwadkar, S.C. Tripathi, P.M. Gandhi, V. Grover, C.P. Kaushik, A.K. Tyagi, Nano-cerium vanadate: A novel inorganic ion exchanger for removal of americium and uranium from simulated aqueous nuclear waste, *J. Hazard. Mater.* 280 (2014) 63–70, <https://doi.org/10.1016/j.jhazmat.2014.07.026>.
- [151] Ü.H. Kaynar, M. Ayvacikli, S.Ç. Kaynar, Ü. Hiçsönmez, Removal of uranium(VI) from aqueous solutions using nanoporous ZnO prepared with microwave-assisted combustion synthesis, *J. Radioanal. Nucl. Chem.* 299 (2014) 1469–1477, <https://doi.org/10.1007/s10967-014-2919-2>.
- [152] M.R. Abdi, H.R. Shakur, K.R.E. Sarae, M. Sadeghi, Effective removal of uranium ions from drinking water using CuO/X zeolite based nanocomposites: Effects of nano concentration and cation exchange, *J. Radioanal. Nucl. Chem.* 300 (2014) 1217–1225, <https://doi.org/10.1007/s10967-014-3092-3>.
- [153] H.R. Shakur, K.R.E. Sarae, M.R. Abdi, G. Azimi, Highly selective and effective removal of uranium from contaminated drinking water using a novel PAN/AgX/ZnO nanocomposite, *Microporous Mesoporous Mater.* 234 (2016) 257–266, <https://doi.org/10.1016/j.micromeso.2016.07.034>.
- [154] W.I. Mortada, A.F. Moustafa, A.M. Ismail, M.M. Hassanien, A.A. Aboud, Microwave assisted decoration of titanium oxide nanotubes with CuFe<sub>2</sub>O<sub>4</sub> quantum dots for solid phase extraction of uranium, *RSC Adv.* 5 (2015) 62414–62423, <https://doi.org/10.1039/C5RA10304E>.
- [155] Y.Y. Chen, S.H. Yu, Q.Z. Yao, S.Q. Fu, G.T. Zhou, One-step synthesis of Ag<sub>2</sub>O/Mg(OH)<sub>2</sub> nanocomposite as an efficient scavenger for iodine and uranium, *J. Colloid Interface Sci.* 510 (2018) 280–291, <https://doi.org/10.1016/j.jcis.2017.09.073>.
- [156] G. Sheng, P. Yang, Y. Tang, Q. Hu, H. Li, X. Ren, B. Hu, X. Wang, Y. Huang, New insights into the primary roles of diatomite in the enhanced sequestration of UO<sub>2</sub><sup>2+</sup> by zerovalent iron nanoparticles: An advanced approach utilizing XPS and EXAFS, *Appl. Catal. B Environ.* 193 (2016) 189–197, <https://doi.org/10.1016/j.apcatb.2016.04.035>.
- [157] P. Tang, J. Shen, Z. Hu, G. Bai, M. Wang, B. Peng, R. Shen, W. Linghu, High-efficient scavenging of U(VI) by magnetic Fe<sub>3</sub>O<sub>4</sub>@gelatin composite, *J. Mol. Liq.* 221 (2016) 497–506, <https://doi.org/10.1016/j.molliq.2016.06.008>.
- [158] R. Wang, J. Ye, A. Rauf, X. Wu, H. Liu, G. Ning, H. Jiang, Microwave-induced synthesis of pyrophosphate Zr<sub>1-x</sub>Ti<sub>x</sub>P<sub>2</sub>O<sub>7</sub> and TiP<sub>2</sub>O<sub>7</sub> with enhanced sorption capacity for uranium (VI), *J. Hazard. Mater.* 315 (2016) 76–85, <https://doi.org/10.1016/j.jhazmat.2016.03.092>.
- [159] W. Chouyyok, C.L. Warner, K.E. Mackie, M.G. Warner, G.A. Gill, R.S. Addleman, Nanostructured metal oxide sorbents for the collection and recovery of uranium from seawater, *Ind. Eng. Chem. Res.* 55 (2016) 4195–4207, <https://doi.org/10.1021/acs.iecr.5b03650>.
- [160] I.S. Chronakis, Novel nanocomposites and nanoceramics based on polymer nanofibers using electrospinning process—A review, *J. Mater. Process. Technol.* 167 (2005) 283–293, <https://doi.org/10.1016/j.jmatprotec.2005.06.053>.
- [161] L. Hu, X.W. Yan, X.J. Zhang, D. Shan, Integration of adsorption and reduction for uranium uptake based on SrTiO<sub>3</sub>/TiO<sub>2</sub> electrospun nanofibers, *Appl. Surf. Sci.* 428 (2018) 819–824, <https://doi.org/10.1016/j.apsusc.2017.09.216>.
- [162] S. Wang, C. Wang, B. Zhang, Z. Sun, Z. Li, X. Jiang, X. Bai, Preparation of Fe<sub>3</sub>O<sub>4</sub>/PVA nanofibers via combining in-situ composite with electrospinning, *Mater. Lett.* 64 (2010) 9–11, <https://doi.org/10.1016/j.matlet.2009.09.043>.
- [163] G.H. Mirzabe, A.R. Keshtkar, Selective sorption of U(VI) from aqueous solutions using a novel aminated Fe<sub>3</sub>O<sub>4</sub>@SiO<sub>2</sub>/PVA nanofiber adsorbent prepared by electrospinning method, *J. Radioanal. Nucl. Chem.* 303 (2015) 561–576, <https://doi.org/10.1007/s10967-014-3478-2>.
- [164] A. Dastbaz, A.R. Keshtkar, Adsorption of Th<sup>4+</sup>, U<sup>6+</sup>, Cd<sup>2+</sup>, and Ni<sup>2+</sup> from aqueous solution by a novel modified polyacrylonitrile composite nanofiber adsorbent prepared by electrospinning, *Appl. Surf. Sci.* 293 (2014) 336–344, <https://doi.org/10.1016/j.apsusc.2013.12.164>.
- [165] N. Singh, K. Balasubramanian, An effective technique for removal and recovery of uranium(VI) from aqueous solution using cellulose-campohr soot nanofibers, *RSC Adv.* 4 (2014) 27691–27701, <https://doi.org/10.1039/C4RA01751J>.
- [166] S. Xie, X. Liu, B. Zhang, H. Ma, C. Ling, M. Yu, L. Li, J. Li, Electrospun nanofibrous adsorbents for uranium extraction from seawater, *J. Mater. Chem. A* 3 (2015) 2552–2558, <https://doi.org/10.1039/C4TA06120A>.
- [167] B. Wang, Y. Zhou, L. Li, Y. Wang, Preparation of amidoxime-functionalized mesoporous silica nanospheres (ami-MSN) from coal fly ash for the removal of U(VI), *Sci. Total Environ.* 626 (2018) 219–227, <https://doi.org/10.1016/j.scitotenv.2018.01.057>.
- [168] J. Qu, W. Li, C.-Y. Cao, X.-J. Yin, L. Zhao, J. Bai, Z. Qin, W.-G. Song, Metal silicate nanotubes with nanostructured walls as superb adsorbents for uranyl ions and lead ions in water, *J. Mater. Chem.* 22 (2012) 17222–17226, <https://doi.org/10.1039/c2jm33178k>.
- [169] H. Sepehrian, M. Samadfam, Z. Asadi, Studies on the recovery of uranium from nuclear industrial effluent using nanoporous silica adsorbent, *Int. J. Environ. Sci. Technol.* 9 (2012) 629–636, <https://doi.org/10.1007/s13762-012-0065-3>.
- [170] Z. Shiri-Yekta, M.R. Yaftian, A. Nilchi, Silica nanoparticles modified with a Schiff base ligand: An efficient adsorbent for Th(IV), U(VI) and Eu(III) ions, *Korean J. Chem. Eng.* 30 (2013) 1644–1651, <https://doi.org/10.1007/s11814-013-0077-9>.
- [171] S. Zhang, H. Gao, J. Li, Y. Huang, A. Alsaedi, T. Hayat, X. Xu, X. Wang, Rice husks as a sustainable silica source for hierarchical flower-like metal silicate architectures assembled into ultrathin nanosheets for adsorption and catalysis, *J. Hazard. Mater.* 321 (2017) 92–102, <https://doi.org/10.1016/j.jhazmat.2016.09.004>.
- [172] E. Cail, J. Qi, O. Preedy, S. Chen, D. Boldrin, W.R. Branford, L. Vandeperre, M. P. Ryan, Functionalised magnetic nanoparticles for uranium adsorption with ultra-high capacity and selectivity, *J. Mater. Chem. A* (2018) 3063–3073, <https://doi.org/10.1039/C7TA09240G>.
- [173] M. Xu, X. Han, D. Hua, Polyoxime-functionalized magnetic nanoparticles for uranium adsorption with high selectivity over vanadium, *J. Mater. Chem. A* 5 (2017) 12278–12284, <https://doi.org/10.1039/C7TA02684F>.
- [174] S. Sayin, M. Yilmaz, Preparation and uranyl ion extraction studies of calix[4] arene-based magnetite nanoparticles, *Desalination* 276 (2011) 328–335, <https://doi.org/10.1016/j.desal.2011.03.073>.
- [175] S. Abbasizadeh, A.R. Keshtkar, M.A. Mousavian, Preparation of a novel electrospun polyvinyl alcohol/titanium oxide nanofiber adsorbent modified with mercapto groups for uranium(VI) and thorium(IV) removal from aqueous solution, *Chem. Eng. J.* 220 (2013) 161–171, <https://doi.org/10.1016/j.cej.2013.01.029>.
- [176] R. Banerjee, Y. Katsenovich, L. Lagos, M. Senn, M. Naja, V. Balsamo, K.H. Pannell, C.Z. Li, Functional magnetic nanoshells integrated nanosensor for trace analysis of environmental uranium contamination, *Electrochim. Acta* 55 (2010) 7897–7902, <https://doi.org/10.1016/j.electacta.2010.05.060>.
- [177] O.A. Elhefnawy, W.I. Zidan, M.M. Abo-Aly, E.M. Bakier, G.A. Elsayed, Synthesis and characterization of a new surface modified Amberlite-7HP resin by nano-iron oxide (Fe<sub>3</sub>O<sub>4</sub>) and its application for uranyl ions separation, *J. Radioanal. Nucl. Chem.* 299 (2014) 1821–1832, <https://doi.org/10.1007/s10967-013-2879-y>.
- [178] S. Sayin, M. Yilmaz, Synthesis of a new calixarene derivative and its immobilization onto magnetic nanoparticle surfaces for excellent extractants toward Cr(VI), As(V), and U(VI), *J. Chem. Eng. Data* 56 (2011) 2020–2029, <https://doi.org/10.1021/je1010328>.
- [179] M. Sundararajan, Designing Novel Nanomaterials through Functionalization of Carbon Nanotubes with Supramolecules for Application in Nuclear Waste Management, *Sep. Sci. Technol.* 48 (2013) 2391–2396, <https://doi.org/10.1080/01496395.2013.807829>.
- [180] Y. Wang, Z. Gu, J. Yang, J. Liao, Y. Yang, N. Liu, J. Tang, Amidoxime-grafted multiwalled carbon nanotubes by plasma techniques for efficient removal of uranium(VI), *Appl. Surf. Sci.* 320 (2014) 10–20, <https://doi.org/10.1016/j.apsusc.2014.08.182>.
- [181] X. Zhao, S. Zhang, C. Bai, B. Li, Y. Li, L. Wang, R. Wen, M. Zhang, L. Ma, S. Li, Nano-diamond particles functionalized with single/double-arm amide-thiourea ligands for adsorption of metal ions, *J. Colloid Interface Sci.* 469 (2016) 109–119, <https://doi.org/10.1016/j.jcis.2016.02.017>.

- [182] W. Song, D. Shao, S. Lu, X. Wang, Simultaneous removal of uranium and humic acid by cyclodextrin modified graphene oxide nanosheets, *Sci. China Chem.* 57 (2014) 1291–1299, <https://doi.org/10.1007/s11426-014-5119-6>.
- [183] D. Dupont, W. Brullot, M. Bloemen, T. Verbiest, Selective Uptake of Rare Earths from Aqueous Solutions by EDTA-Functionalized Magnetic and Nonmagnetic Nanoparticles, *ACS Appl. Mater. Interfaces* 6 (2014) 4980–4988.
- [184] L. Wang, Z. Yang, J. Gao, K. Xu, H. Gu, B. Zhang, X. Zhang, B. Xu, A biocompatible method of decorporation: Bisphosphonate-modified magnetite nanoparticles to remove uranyl ions from blood, *J. Am. Chem. Soc.* 128 (2006) 13358–13359, <https://doi.org/10.1021/ja0651355>.
- [185] M.G. Mahfouz, A.A. Galhoum, N.A. Gomaa, S.S. Abdel-Rehem, A.A. Atia, T. Vincent, E. Guibal, Uranium extraction using magnetic nano-based particles of diethylenetriamine-functionalized chitosan: Equilibrium and kinetic studies, *Chem. Eng. J.* 262 (2015) 198–209, <https://doi.org/10.1016/j.cej.2014.09.061>.
- [186] S. Sadeghia, H. Azhdaria, H. Arabib, Surface modified magnetic Fe3O4 nanoparticles as a selective sorbent for solid phase extraction of uranyl ions from water samples, *J. Hazard. Mater.* 215 (2012) 208–216.
- [187] C. Wang, A.S. Helal, Z. Wang, J. Zhou, X. Yao, Z. Shi, Y. Ren, J. Lee, J. Chang, B. Fugetsu, J. Li, Uranium In Situ Electrolytic Deposition with a Reusable Functional Graphene-Foam Electrode, *Adv. Mater.* 33 (2021) 2102633, <https://doi.org/10.1002/adma.202102633>.
- [188] L. Tan, J. Wang, Q. Liu, Y. Sun, H. Zhang, Y. Wang, X. Jing, J. Liu, D. Song, Facile preparation of oxine functionalized magnetic Fe3O4 particles for enhanced uranium (VI) adsorption, *Colloids Surfaces A Physicochem. Eng. Asp.* 466 (2015) 85–91, <https://doi.org/10.1016/j.colsurfa.2014.11.020>.
- [189] I.C. Popescu, P. Filip, D. Humelnicu, I. Humelnicu, T.B. Scott, R.A. Crane, Removal of uranium (VI) from aqueous systems by nanoscale zero-valent iron particles suspended in carboxy-methyl cellulose, *J. Nucl. Mater.* 443 (2013) 250–255, <https://doi.org/10.1016/j.jnucmat.2013.07.018>.
- [190] G.W. Peng, D.X. Ding, F.Z. Xiao, X.L. Wang, N. Hun, Y.D. Wang, Y.M. Dai, Z. Cao, Adsorption of uranium ions from aqueous solution by amine-group functionalized magnetic Fe3O4 nanoparticle, *J. Radioanal. Nucl. Chem.* 301 (2014) 781–788, <https://doi.org/10.1007/s10967-014-3278-8>.
- [191] L. Huang, L. Zhang, D. Hua, Synthesis of polyamidoxime-functionalized nanoparticles for uranium(VI) removal from neutral aqueous solutions, *J. Radioanal. Nucl. Chem.* 305 (2015) 445–453, <https://doi.org/10.1007/s10967-015-3988-6>.
- [192] L. Li, F. Huang, Y. Yuan, J. Hu, Q. Tang, S. Tang, Preparation and sorption performance of magnetic 18-crown-6/Fe3O4 nanocomposite for uranium(VI) in solution, *J. Radioanal. Nucl. Chem.* 298 (2013) 227–235, <https://doi.org/10.1007/s10967-013-2443-9>.
- [193] S. Yang, P. Zong, J. Hu, G. Sheng, Q. Wang, X. Wang, Fabrication of  $\beta$ -cyclodextrin conjugated magnetic HNT/iron oxide composite for high-efficient decontamination of U(VI), *Chem. Eng. J.* 214 (2013) 376–385, <https://doi.org/10.1016/j.cej.2012.10.030>.
- [194] P. Zong, X. Xu, M. Shao, D. Cao, S. Wang, H. Zhang, Efficient elimination of uranium by carboxymethyl- $\beta$ -cyclodextrin nanoparticles decorated iron oxides: Water chemistry influences and mechanism researches, *Int. J. Hydrogen Energy* 46 (2021) 1370–1384, <https://doi.org/10.1016/j.ijhydene.2020.09.238>.
- [195] A.A. Galhoum, M.G. Mahfouz, A.A. Atia, S.T. Abdel-Rehem, N.A. Gomaa, T. Vincent, E. Guibal, Amfouin Acid Functionalized Chitosan Magnetic Nanobased Particles for Uranyl Sorption, *Ind. Eng. Chem. Res.* 54 (2015) 12374–12385, <https://doi.org/10.1021/acs.iecr.5b03331>.
- [196] A.A. Galhoum, M.G. Mahfouz, N.A. Gomaa, S.S. Abdel-Rehem, A.A. Atia, T. Vincent, Cysteine-Functionalized Chitosan Magnetic Nano-Based Particles for the Recovery of Uranium(VI): Uptake Kinetics and Sorption Isotherms, *Sep. Sci. Technol.* 50 (2015) 2776–2789, <https://doi.org/10.3390/nano5010154>.
- [197] H. Shehzad, L. Zhou, Z. Li, Q. Chen, Y. Wang, Z. Liu, A.A. Adesina, Effective adsorption of U(VI) from aqueous solution using magnetic chitosan nanoparticles grafted with maleic anhydride: equilibrium, kinetic and thermodynamic studies, *J. Radioanal. Nucl. Chem.* 315 (2017) 1–12, <https://doi.org/10.1007/s10967-017-5647-6>.
- [198] S.S. Lee, W. Li, C. Kim, M. Cho, B.J. Lafferty, J.D. Fortner, Surface functionalized manganese ferrite nanocrystals for enhanced uranium sorption and separation in water, *J. Mater. Chem. A* 3 (2015) 21930–21939, <https://doi.org/10.1039/C5TA04406E>.
- [199] S.S. Lee, W. Li, C. Kim, M. Cho, J.G. Catalano, B.J. Lafferty, P. Decuzzi, J. D. Fortner, Engineered manganese oxide nanocrystals for enhanced uranyl sorption and separation, *Environ. Sci. Nano* 2 (2015) 500–508, <https://doi.org/10.1039/C5EN00010F>.
- [200] X.T. Chen, L.F. He, R.Z. Liu, C. Zhang, B. Liu, Y.P. Tang, Effective uranium(VI) sorption from alkaline media using bi-functionalized silica-coated magnetic nanoparticles, *RSC Adv.* 5 (2015) 56658–56665, <https://doi.org/10.1039/C5RA07436C>.
- [201] W. Guo, C. Nie, L. Wang, Z. Li, L. Zhu, L. Zhu, Z. Zhu, W. Shi, L. Yuan, Easily prepared and stable functionalized magnetic ordered mesoporous silica for efficient uranium extraction, *Sci. China Chem.* 59 (2016) 629–636, <https://doi.org/10.1007/s11426-016-5561-8>.
- [202] M.A. Mahmoud, Preparation of magnetic nanomaterial for U (VI) uptake from the aqueous solution, *J. Saudi Chem. Soc.* 25 (2021) 101214, <https://doi.org/10.1016/j.jscs.2021.101214>.
- [203] Y. Xu, K. Zhang, C. Wang, Q. Zhu, J. Luo, F. Chen, F. Xiao, G. Peng, Fabrication of magnetic functionalized m-carboxyphenyl azo calix [4] arene amine oxime derivatives for highly efficient and selective adsorption of uranium (VI), *J. Radioanal. Nucl. Chem.* 323 (2020) 1145–1155, <https://doi.org/10.1007/s10967-020-07029-4>.
- [204] J. Luo, Y. Xu, Q. Zhu, K. Zhang, F. Chen, X. Yu, Z. Huang, F. Xiao, A novel magnetic functionalized m-carboxyphenyl azo calix [4] arene symmetric sulfide derivative: synthesis and application as a selective adsorbent for removal of U (VI), *J. Radioanal. Nucl. Chem.* 327 (2021) 175–188, <https://doi.org/10.1007/s10967-020-07472-3>.
- [205] C. Wang, D. Huang, F. He, T. Jin, B. Huang, J. Xu, Y. Qian, Efficient Removal of Uranium (VI) from Aqueous Solutions by Triethylenetetramine-Functionalized Single-Walled Carbon Nanohorns, *ACS Omega* 5 (2020) 27789–27799, <https://doi.org/10.1021/acsomega.0c02715>.
- [206] P. Zhang, L. Wang, K. Du, S. Wang, Z. Huang, L. Yuan, Z. Li, H. Wang, L. Zheng, Z. Chai, W. Shi, Effective removal of U (VI) and Eu (III) by carboxyl functionalized MXene nanosheets, *J. Hazard. Mater.* 396 (2020) 122731, <https://doi.org/10.1016/j.jhazmat.2020.122731>.
- [207] D.R. Lovley, E.J.P. Phillips, Y. Gorby, E.R. Landa, Microbial reduction of uranium, *Nature* 350 (1991) 413–416, <https://doi.org/10.1038/350413a0>.
- [208] S.A. Davis, S.L. Burkett, N.H. Mendelson, S. Mann, Bacterial templating of ordered macrostructures in silica and silica-surfactant mesophases, *Nature* 385 (1997) 420–423, <https://doi.org/10.1038/385420a0>.
- [209] Z. Li, S. Chung, J. Nam, D.S. Ginger, C.A. Mirkin, Living Template for the Hierarchical Assembly of Gold Nanoparticles, *Angew. Chem. Int. Ed. Engl.* 115 (2003) 2408–2411, <https://doi.org/10.1002/ange.200351231>.
- [210] M. Xu, G. Wei, N. Liu, L. Zhou, C. Fu, M. Chubik, A. Gromov, W. Han, Novel fungus-titanate bio-nanocomposites as high performance adsorbents for the efficient removal of radioactive ions from wastewater, *Nanoscale* 6 (2014) 722–725, <https://doi.org/10.1039/C3NR03467D>.
- [211] L. Li, M. Xu, M. Chubik, M. Chubik, A. Gromov, G. Wei, W. Han, Entrapment of radioactive uranium from wastewater by using fungus-Fe<sub>3</sub>O<sub>4</sub> bio-nanocomposites, *RSC Adv.* 5 (2015) 41611–41616, <https://doi.org/10.1039/C5RA03643G>.
- [212] S. Handley-Sidhu, J.A. Hriljac, M.O. Cuthbert, J.C. Renshaw, R.A.D. Patrick, J. M. Charnock, B. Stolpe, J.R. Lead, S. Baker, L.E. Macaskie, Bacterially produced calcium phosphate nanobiomaterials: Sorption capacity, site preferences, and stability of captured radionuclides, *Environ. Sci. Technol.* 48 (2014) 6891–6898, <https://doi.org/10.1021/es500734n>.
- [213] A. Mishra, J.S. Melo, D. Sen, S.F. D'Souza, Evaporation induced self assembled microstructures of silica nanoparticles and *Streptococcus lactis* cells as sorbent for uranium (VI), *J. Colloid Interface Sci.* 414 (2014) 33–40, <https://doi.org/10.1016/j.jcis.2013.09.046>.
- [214] M. Baiget, M. Constantí, M.T. López, F. Medina, Uranium removal from a contaminated effluent using a combined microbial and nanoparticle system, *N. Biotechnol.* 30 (2013) 788–792, <https://doi.org/10.1016/j.nbt.2013.05.003>.
- [215] W. Wang, Y. Feng, X. Tang, H. Li, Z. Du, A. Yi, X. Zhang, Enhanced U(VI) bioreduction by alginate-immobilized uranium-reducing bacteria in the presence of carbon nanotubes and anthraquinone-2,6-disulfonate, *J. Environ. Sci. (china)* 31 (2015) 68–73, <https://doi.org/10.1016/j.jes.2014.11.005>.
- [216] J. Bai, X. Wu, F.F. Fan, W. Tian, X. Yin, L. Zhao, F.F. Fan, Z. Li, L. Tian, Z. Qin, J. Guo, Biosorption of uranium by magnetically modified *Rhodotorula glutinis*, *Enzyme Microb. Technol.* 51 (2012) 382–387, <https://doi.org/10.1016/j.enzmictec.2012.08.007>.
- [217] C. Ding, W. Cheng, Y. Sun, X. Wang, Novel fungus-Fe3O4 bio-nanocomposites as high performance adsorbents for the removal of radionuclides, *J. Hazard. Mater.* 295 (2015) 127–137, <https://doi.org/10.1016/j.jhazmat.2015.04.032>.
- [218] M. Seder-Colomina, G. Morin, J. Brest, G. Ona-Nguema, N. Gordien, J.J. Pernelle, D. Banerjee, O. Mathon, G. Esposito, E.D. Van Hullebusch, Uranium(VI) Scavenging by Amorphous Iron Phosphate Encrusting Sphaerotilus natans Filaments, *Environ. Sci. Technol.* 49 (2015) 14065–14075, <https://doi.org/10.1021/acs.est.5b03148>.
- [219] D. Shao, X. Ren, J. Wen, S. Hu, J. Xiong, T. Jiang, X. Wang, X. Wang, Immobilization of uranium by biomaterial stabilized FeS nanoparticles: Effects of stabilizer and enrichment mechanism, *J. Hazard. Mater.* 302 (2016) 1–9, <https://doi.org/10.1016/j.jhazmat.2015.09.043>.
- [220] G.E. Batley, J.K. Kirby, M.J. McLaughlin, Fate and Risks of Nanomaterials in Aquatic and Terrestrial Environments, *Acc. Chem. Res.* 46 (2013) 854–862, <https://doi.org/10.1021/ar2003368>.
- [221] S. Singh, S. Mohan, P. Gausiya, Fate and toxicity of nanoparticles in aquatic systems, *Acta Geochim* 42 (2023) 63–76, <https://doi.org/10.1007/s11631-022-00572-9>.
- [222] J.A. Gallego-Urrea, J. Tuoriniemi, T. Pallander, M. Hasselöf, Measurements of nanoparticle number concentrations and size distributions in contrasting aquatic environments using nanoparticle tracking analysis, *Environ. Chem.* 7 (2009) 67–81.
- [223] R. Arvidsson, S. Molander, Impacts of a Silver-Coated Future Particle Flow Analysis of Silver Nanoparticles, *J. Ind. Ecol.* 15 (2011) 844, <https://doi.org/10.1111/j.1530-9290.2011.00400.x>.
- [224] R. Kaegi, A. Voegelin, B. Sinnet, S. Zuleeg, H. Hagendorfer, M. Burkhardt, H. Siegrist, Behavior of Metallic Silver Nanoparticles in a Pilot Wastewater Treatment Plant, *Environ. Sci. Technol.* 45 (2011) 3902–3908, <https://doi.org/10.1021/es1041892>.
- [225] L. Li, L. Hu, Q. Zhou, C. Huang, Y. Wang, C. Sun, G. Jiang, Sulfidation as a Natural Antidote to Metallic Nanoparticles Is Overestimated: CuO Sulfidation Yields CuS Nanoparticles with Increased Toxicity in Medaka (*Oryzias latipes*) Embryos, *Environ. Sci. Technol.* 49 (2015) 2486–2495, <https://doi.org/10.1021/es505878f>.
- [226] J.R. Lead, G.E. Batley, P.J.J. Alvarez, R.D. Handy, M.J. McLaughlin, Nanomaterials in the Environment: Behavior, Fate, Bioavailability, and Effects — An Updated Review, *Environ. Toxicol. Chem.* 37 (2018) 2029–2063, <https://doi.org/10.1002/etc.4147>.

- [227] S. Attarilar, J. Yang, M. Ebrahimi, Q. Wang, J. Liu, The Toxicity Phenomenon and the Related Occurrence in Metal and Metal Oxide Nanoparticles : A Brief Review From the Biomedical Perspective, *Front. Bioeng. Biotechnol.* 8 (2020) 822, <https://doi.org/10.3389/fbioe.2020.00822>.
- [228] Y. Huang, The Toxicity of Nanoparticles Depends on Multiple Molecular and Physicochemical Mechanisms, *Int. J. Mol. Sci.* 18 (2019) 2702, <https://doi.org/10.3390/ijms18122702>.
- [229] M.A. Zoroddu, S. Medici, A. Ledda, V.M. Nurchi, J.I. Lachowicz, M. Peana, Recent progress on the discovery of anti-moebic agents, *Curr. Med. Chem.* 21 (2014) 3837.
- [230] Y. Pan, S. Neuss, A. Leifert, M. Fischler, F. Wen, U. Simon, G. Schmid, W. Brandau, W. Jahnen-dechent, Size-Dependent Cytotoxicity of Gold Nanoparticles, *Small* 3 (2007) 1941–1949, <https://doi.org/10.1002/sml.200700378>.
- [231] X. Zhao, S. Ng, B. Chin, H. Jun, L. Ma, T. Thatt, Y. Tan, K. Woei, N. Say, C. Joachim, Cytotoxicity of hydroxyapatite nanoparticles is shape and cell dependent, *Arch Toxicol* 87 (2013) 1037–1052, <https://doi.org/10.1007/s00204-012-0827-1>.
- [232] S.A. Khan, *Metal Nanoparticles Toxicity: Role of Physicochemical Aspects*, Elsevier Inc, Amsterdam, 2020.
- [233] A.M. El Badawy, R.G. Silva, B. Morris, K.G. Scheckel, M.T. Suidan, T.M. Tolaymat, Surface Charge-Dependent Toxicity of Silver Nanoparticles, *Environ. Sci. Technol.* 45 (2011) 283.
- [234] H. Nguyen, R.M. Ignacio, J. Kim, H. Cho, Y. Kim, M. Kim, B. Park, S. Kim, Immunotoxicity of zinc oxide nanoparticles with different size and electrostatic charge, *Int. J. Nanomedicine* 9 (2014) 195–205.
- [235] I. Khan, K. Saeed, I. Khan, Nanoparticles: Properties, applications and toxicities, *Arab. J. Chem.* 12 (2019) 908–931.
- [236] S. Sayin, M. Yilmaz, M. Tavasli, Syntheses of two diamine substituted 1,3-distal calix[4]arene-based magnetite nanoparticles for extraction of dichromate, arsenate and uranyl ions, *Tetrahedron* 67 (2011) 3743–3753, <https://doi.org/10.1016/j.tet.2011.03.012>.
- [237] P.L. Smedley, D.G. Kinniburgh, Uranium in natural waters and the environment: Distribution, speciation and impact, *Appl. Geochem.* 148 (2023) 105534, <https://doi.org/10.1016/j.apgeochem.2022.105534>.
- [238] V. Balaran, A. Rani, D.P.S. Rathore, Uranium in groundwater in parts of India and world: A comprehensive review of sources, impact to the environment and human health, analytical techniques, and mitigation technologies, *Geosystems and Geoenvironment* 1 (2022) 100043, <https://doi.org/10.1016/j.geogeo.2022.100043>.
- [239] C. Moulin, C. Beaucaire, P. Decambox, P. Mauchien, Determination of uranium in solution at the ng l<sup>-1</sup> level by time-resolved laser-induced spectrofluorimetry: application to geological samples, *Anal. Chim. Acta* 238 (1990) 291–296, [https://doi.org/10.1016/S0003-2670\(00\)80550-4](https://doi.org/10.1016/S0003-2670(00)80550-4).
- [240] M. Singh, K. Tapadia, D. Jhariya, P. Sahu, Evaluation of uranium containing ground water quality and non-carcinogenic risk assessment in inhabitant of Bijapur District of Chhattisgarh, Central India, *J. Radioanal. Nucl. Chem.* 327 (2021) 939–947, <https://doi.org/10.1007/s10967-020-07572-0>.
- [241] S.K. Gupta, S.K. Thulasidas, N. Goyal, S.v., Godbole A modular-type atomic absorption instrument with the graphite furnace in a glove box for nuclear applications, *Instrum Sci. Technol.* 42 (2014) 161–172, <https://doi.org/10.1080/10739149.2013.845848>.
- [242] C. Ruan, W. Luo, W. Wang, B. Gu, Surface-enhanced Raman spectroscopy for uranium detection and analysis in environmental samples, *Anal. Chim. Acta* 605 (2007) 80–86, <https://doi.org/10.1016/j.aca.2007.10.024>.
- [243] J. Zsigrai, T.C. Nguyen, A. Berlizov, Gamma-spectrometric determination of <sup>232</sup>U in uranium-bearing materials, *Nucl. Instrum. Methods Phys. Res., Sect. B* 359 (2015) 137–144, <https://doi.org/10.1016/j.nimb.2015.07.047>.
- [244] X. Tang, H. Han, L. Li, H. Wang, Electrodes functionalized with advanced recognition materials for trace electrochemical sensing of uranyl ion, *Microchem. J.* 199 (2024) 109924, <https://doi.org/10.1016/j.microc.2024.109924>.
- [245] X. Wu, Q. Huang, Y. Mao, X. Wang, Y. Wang, Q. Hu, H. Wang, X. Wang, Sensors for determination of uranium: A review, *TrAC Trends Anal. Chem.* 118 (2019) 89–111, <https://doi.org/10.1016/j.trac.2019.04.026>.
- [246] H.-H. Huang, The Eh-pH Diagram and Its Advances, *Metals* 6 (2016) 23, <https://doi.org/10.3390/met6010023>.
- [247] L. Rován, M. Strok, Optimization of the sample preparation and measurement protocol for the analysis of uranium isotopes by MC-ICP-MS without spike addition, *J. Anal. at. Spectrom.* 34 (2019) 1882–1891, <https://doi.org/10.1039/C9JA00144A>.
- [248] S.C. Metzger, K.T. Rogers, D.A. Bostick, E.H. McBay, B.W. Ticknor, B.T. Manard, C.R. Hexel, Optimization of uranium and plutonium separations using TEVA and UTEVA cartridges for MC-ICP-MS analysis of environmental swipe samples, *Talanta* 198 (2019) 257–262, <https://doi.org/10.1016/j.talanta.2019.02.034>.
- [249] S. Ganesh, F. Khan, M. Ahmed, P. Velavendan, N. Pandey, U. Mudali, S. Pandey, Determination of ultra traces amount of uranium in raffinates of Purex process by laser fluorimetry, *J. Rad. Nucl. Chem.* 292 (2012) 331–334, <https://doi.org/10.1007/s10967-011-1431-1>.
- [250] D.P.S. Rathore, Advances in technologies for the measurement of uranium in diverse matrices, *Talanta* 77 (2008) 9–20, <https://doi.org/10.1016/j.talanta.2008.06.019>.
- [251] K. Chandrasekaran, D. Karunasagar, J. Arunachalam, Dispersive liquid-liquid micro extraction of uranium(VI) from groundwater and seawater samples and determination by inductively coupled plasma–optical emission spectrometry and flow injection–inductively coupled plasma mass spectrometry, *Anal. Meth.* 3 (2011) 2140–2147, <https://doi.org/10.1039/C1AY05329A>.
- [252] R. Ziolkowski, Ł. Górski, E. Malinowska, Carboxylated graphene as a sensing material for electrochemical uranyl ion detection, *Sens. Actuators B* 238 (2017) 540–547, <https://doi.org/10.1016/j.snb.2016.07.119>.
- [253] A. Quemet, A. Ruas, V. Dalier, C. Rivier, Development and comparison of high accuracy thermal ionization mass spectrometry methods for uranium isotope ratios determination in nuclear fuel, *Int. J. Mass Spectrom.* 438 (2019) 166–174, <https://doi.org/10.1016/j.ijms.2019.01.008>.
- [254] M. Penkin, S. Boulyga, B. Dabbs, D. Fischer, M. Humphrey, A. Kochetkov, A. Koepf, M. Sturm, Isotopic composition of commercially available uranium chemicals and elemental analysis standards, *J. Radioanal. Nucl. Chem.* 316 (2018) 791–798, <https://doi.org/10.1007/s10967-018-5740-5>.
- [255] N. Hassan, A.S. Amin, Membrane optode for uranium (VI) preconcentration and colorimetric determination in real samples, *RSC. Adv.* 7 (2017) 46566–46574, <https://doi.org/10.1039/C7RA08942B>.
- [256] G. Jia, M. Belli, U. Sansone, S. Rosamilia, R. Ocone, S. Gaudino, Determination of uranium isotopes in environmental samples by alpha-spectrometry, *J. Radioanal. Nucl. Chem.* 253 (2002) 395–406, <https://doi.org/10.1023/A:1020413302019>.